Indoor Localization using Augmented UHF RFID System for the Internet-of-Things

by

Jing Wang

A thesis submitted to the
Faculty of Graduate and Postdoctoral Studies
in partial fulfillment of the requirements for the degree of

Doctor of Philosophy in
Electrical and Computer Engineering

School of Electrical Engineering and Computer Science
University of Ottawa
Ottawa, Ontario
April, 2017

The undersigned hereby recommends to the
Faculty of Graduate and Postdoctoral Studies
acceptance of the thesis

Indoor Localization using Augmented UHF RFID System for the Internet-of-Things

Professor Kevin Bouchard, External Examiner

Professor Miodrag Bolić, Thesis Supervisor

Professor Amiya Nayak, Internal Examiner

Professor Tet Yeap, Internal Examiner

Professor Richard M. Dansereau, Internal Examiner

School of Electrical Engineering and Computer Science
University of Ottawa
April, 2017

Abstract

Indoor localization with proximity information in ultra-high-frequency (UHF) radio-frequency-identification (RFID) is widely considered as a potential candidate of locating items in Internet-of-Things (IoT) paradigm. First, the proximity-based methods are less affected by multipath distortion and dynamic changes of the indoor environment compared to the traditional range-based localization methods. The objective of this dissertation is to use tag-to-tag backscattering communication link in augmented UHF RFID system (AURIS) for proximity-based indoor localization solution. Tag-to-tag backscattering communication in AURIS has an obvious advantage over the conventional reader-to-tag link for proximity-based indoor localization by keeping both landmark and mobile tags simple and inexpensive. This work is the very first thesis evaluating proximity-based localization solution using tag-to-tag backscattering communication.

Our research makes the contributions in terms of phase cancellation effect, the improved mathematical models and localization algorithm. First, we investigate the phase cancellation effect in the tag-to-tag backscattering communication, which has a significant effect on proximity-based localization. We then present a solution to counter such destructive effect by exploiting the spatial diversity of dual antennas. Second, a novel and realistic detection probability model of ST-to-tag detection is proposed. In AURIS, a large set of passive tags are placed at known locations as landmarks, and STs are attached mobile targets of interest. We identify two technical roadblocks of AURIS and existing localization algorithms as false synchronous detection assumption and state evolution model constraints. With the new and more realistic detection probability model we explore the use of particle filtering methodology for localizing ST, which overcomes the aforementioned roadblocks. Last, we propose a landmark-based sequential localization and mapping framework (SQLAM)

for AURIS to locate STs and passive tags with unknown locations, which leverages a set of passive landmark tags to localize ST, and sequentially constructs a geographical map of passive tags with unknown locations while ST is moving in the environment. Mapping passive tags with unknown locations accurately leads to practical advantages. First, the localization capability of AURIS is not confined to the objects carrying STs. Second, the problem of failed landmark tags is addressed by including passive tags with resolved locations into landmark set.

Each of the contributions is supported by extensive computer simulation to demonstrate the performance of enhancements.

Acknowledgments

First and foremost, I would like to express my deeply gratitude to my supervisor, examiner and mentor Prof. Miodrag Bolic. Thank you for countless discussions, suggestions and guidance regarding the content and direction of my research over the past four years.

I would like to cordialy thank Prof. Amiya Nayak, Prof. Richard Dansereau, Prof. Tet Yeap and Prof. Kevin Bouchard for serving as my committee members and providing important advice and suggestion on my research. I would also like to thank Dr. Vytas Kezys from Teslonix Inc. for the technical advice. My gratitude also goes to my mentors in Blackberry Inc. Lijun Chen and Varughese George for the support. Special thanks also go to Dr. Daniel Arnitz, who develops PARIS simulator and makes it open-source. My gratitude also goes to China Scholarship Council, which provides funding for my thesis.

I would like to thank my colleagues and friends in Identigo research lab and University of Ottawa, Hassan Roshan, Yu Wang, Majed Rostamian, Hala As'Ad, Deliang Guo, Chao Li, Ziyang Wang, Jingwen Feng, Qiyin Zhang, Licheng Peng and Huan Huang, who have been supportive in every way.

Finally, I would like to offer my sincere gratitude to my family, Jinglong Wang, Zhiheng Wu, Shulin Fang, Haiyun Zhang, Jieqiong Wang, Xu Zhang and Mengyuan Zhang. It was their support and encouragement that made my study possible. Special and heartfelt thanks to my wife Rui Fang for the unconditional love, encouragement and support, also for a thorough proof-reading of the thesis.

Table of Contents

Abstract **iii**

Acknowledgments **v**

Table of Contents **vi**

List of Tables **ix**

List of Figures **x**

Nomenclature **xiv**

1 Introduction **1**

1.1 Motivation 1
1.2 Contributions 5
1.3 Limitations and boundaries 8
1.4 Thesis organization 9

2 Background and related work **11**

2.1 Internet of Things 11
2.2 UHF RFID technology 13
2.2.1 UHF RFID system 13
2.2.2 Backscattering communication 14
2.2.3 EPCglobal Class1 Generation 2 (Gen2) protocol 16
2.3 Indoor localization 22
2.3.1 Triangulation 23
2.3.2 Scene analysis 28

2.3.3 Proximity 28
2.3.4 The challenges of indoor localization 28
2.4 State-of-art proximity-based localization with UHF RFID 29
2.4.1 Overview of existing approaches 30
2.4.2 Inference algorithm 32
2.4.3 Literature review on existing approaches 39
2.4.4 PASS simulation framework 51

3 Phase cancellation in AURIS **58**
3.1 Problem formulation 59
3.1.1 ASK modulated tag's backscattering signal 60
3.1.2 PSK modulated tag's backscattering signal 63
3.2 Dual-antenna technique 67
3.2.1 Simple combination technique 68
3.2.2 Receiving path selection technique 73
3.2.3 Simulation results 77
3.3 Summary 85

4 Indoor localization with AURIS **86**
4.1 The detection probability model 86
4.1.1 ST-to-tag link budget 87
4.1.2 Model description 90
4.1.3 Model evaluation 92
4.2 Particle filter-based localization method with AURIS 98
4.2.1 Problem formulation 98
4.2.2 PF-AA algorithm 102
4.2.3 Performance evaluation 107
4.3 Landmark-based sequential localization and mapping framework using AURIS 112
4.3.1 Framework overview 115
4.3.2 The SQLAM Framework 117
4.3.3 Performance Evaluation 125
4.4 Summary 136

5 Research directions and future work 138
5.1 ST-to-ST backscattering network 138
5.2 Reducing phase cancellation effect in ST-to-ST backscattering network 142
5.3 Future directions related to AURIS 147

6 Conclusion 150

List of References 153

Appendix A The PASS Simulation Framework 162
A.1 Component models 163

List of Tables

2.1 Summary of terms and their definitions in SLAM 38
2.2 Comparison table of the analyzed solutions 55
3.1 The values of physical quantities and phase cancellation condition calculation 80
3.2 The values of physical quantities at dual antennas of ST 83
3.3 The physical quantities of simple combined signal 84
4.1 ST locator protocol 99
4.2 Summary of terms and their definitions related to SQLAM 118

List of Figures

1.1 Research problems, and their effects on the localization performance of AURIS, as well as the contributions of the thesis. 8
2.1 IoT technology roadmap. (Courtesy: Strategic Business Insights) . . 12
2.2 Standard RFID system 14
2.3 Backscatter coupling mechanism 15
2.4 PIE symbols (figure adapted from [1]) 17
2.5 FM0 basis function, generator state diagram and symbols (figure adapted from [1]) 18
2.6 Miller basis function, state diagram and encoding sequences (figure adapted from [1]) 19
2.7 Reader-to-tag link preamble and frame-sync (figure adapted from [1]) 20
2.8 Tag-to-reader link preamble with optional pilot tone, and ending of FM0 transmission(figure adapted from [1]) 20
2.9 Tag-to-reader link preamble with optional pilot tone and ending of MMS transmission (figure adapted from [1]) 21
2.10 Slots with successful read, collision and empty reply (figure adapted from [1]) 22
2.11 Q algorithm for tag anti-collision (figure adapted from [1]) 23
2.12 UHF RFID localization method taxonomy 24
2.13 Localization with AoA technique 25
2.14 Localization with range-based method 27
2.15 Existing proximity-based approaches 30
2.16 The block diagram of ST 31
2.17 Localization infrastructure 42
2.18 Synchronous and asynchronous measurements. 46

2.19 CDF of location errors for three inference algorithms. 48
2.20 The hierarchical structure of PASS 52
3.1 Schematic depiction of ST-to-tag backscatter link 59
3.2 Phasor diagram that shows superimposed signal at the ST antenna when the tag transmits logic zero and logic one with ASK modulation. 62
3.3 Variations of amplitude difference $|A_1 - A_2|$ with varying θ ($A_R = 1$) 63
3.4 Phasor diagram that shows superimposed signal at the ST antenna when the tag transmits logic zero and logic one with PSK modulation. 66
3.5 Variations of amplitude difference $|A_1 - A_2|$ with varying θ ($A_R = 1, A_T = 0.4$) 67
3.6 Phasor diagram that shows superimposed signal at the ST antenna when the tag transmits logic zero and logic one. 72
3.7 Block diagram of the ST model with receiving path selection technique 73
3.8 The pattern of amplitude difference $|A_1 - A_2|$ at ST's antenna for the case when reader is at $(0, 0)$ and the tag is at $(2, 0)$. 76
3.9 The structure and functions of ST 77
3.10 Experiment setup. 78
3.11 Simulation setup in PASS (1, 3, 5 cells). 79
3.12 With phase cancellation. 81
3.13 Without phase cancellation. 82
3.14 Experiment setup for the second experiment. 83
3.15 Measurements of amplitude difference. 84
3.16 Probability of phase cancellation. 85
4.1 Block diagram of passive tag 90
4.2 Representation of detection probability model parameters. 91
4.3 Antenna radiation pattern 93
4.4 Simulation setup 94
4.5 The estimated detection probability versus (a) D and d with $\theta = 0$, $\phi = 0$ (b) θ and ϕ with $D = 2\ m$, $d = 0.5\ m$ for RTS model 95
4.6 The detection probability versus d for TS model 96
4.7 The detection probability versus (a) D with data from region $d \in [0.4, 1]$ (b) d with data from region $D \in [2, 4]$ 97
4.8 The deployment of AURIS 99

4.9 Representation of a set of queries Q_T and Q_S with $N = 4$ 101
4.10 Experiment setup with landmark tags deployment, and ST trajectories. 109
4.11 The performance of PF-AA bias compensation technique. 109
4.12 The performance of PF-AA and PF-BIN with ST speed 0.5 m/s. . . . 110
4.13 The performance of PF-AA and PF-BIN with ST speed 2.5 m/s. . . . 111
4.14 The CDFs of position erros of PF-AA and PF-BIN. 111
4.15 The performance of PF-AA and WCL with random walk trajectory. . 113
4.16 Cpation of 114
4.17 The SQLAM framework architecture (the blue box represents the algorithm that will be performed, the light red shape represents the data that will be stored). 116
4.18 Experiment setup with landmark tag, unknown tag and ST. 125
4.19 The performance of PF and WCL with random walk trajectory (the RMSE of ST location estimation against time). 127
4.20 The performance of temporal WCL with different N_{tmp} (the RMSE of unknown tag location estimation against the number of N_{tmp}). 127
4.21 The performance of temporal WCL for 42 unknown tags (the mapping accuracy of 42 unknown tags against time). 128
4.22 The estimation error of unknown tag versus (a) variance of observations in *Constraint* 2 (b) summation of read rates in vector OV in *Constraint* 2*. 129
4.23 ST Localization performance with three methods: parametric-based method, Monte Carlo-based method and PF without replacement method. 130
4.24 ST localization accuracy for different percentage of failed landmark tags (ST localization accuracy is measured by ℓ^2-norm operation of the difference between estimation and true location). 131
4.25 The floor plan of uOttawa SITE 5130 research lab. 132
4.26 Simulation setup following the deployment scenario in SITE 5130 (the square represents landmark tag, the hexagon represents unknown tag, and the red line represents the boundary). 133
4.27 The heat map of location estimation error associated with coordinates when all landmark tags are available (each block is 0.5 $m \times 0.5$ m). . 134

4.28 The mapping accuracy of 55 unknown tags in research lab scenario against time. 135
4.29 Simulation setup (the 14 darker passive tags are landmarks). 136
4.30 The heat map of location estimation error associated with coordinates when all landmark tags are not available, and 14 passive tags with resolved locations are used as substitutes of landmarks (each block is 0.5 $m \times 0.5$ m). 137
5.1 The infrastructure of AURIS on the left and ST-to-ST backscattering network on the right. 139
5.2 Schematic depiction of ST-to-ST backscatter link 140
5.3 Backscatter modulator scheme 143
5.4 Model of ST reflection coefficients 143
5.5 Phasor diagram that shows superimposed signals at receiving ST antenna for ASK-PSK backscatter modulation 144
5.6 Experiment setup for ASK-PSK modulated stamp technique. 145
5.7 The format of ASK-PSK modulated stamp in test. 146
5.8 Anti-phase cancellation performance. 147
A.1 Signal flow and component model graph for the simulator 162
A.2 Basic structure and functions of reader model 163
A.3 The structure and functions of tag 164
A.4 The structure and functions of ST 165
A.5 The structure and functions of channel model 166

Nomenclature

A/D	Analog to Digital
AoA	Arrival of Angle
APDP	Average Power-Delay-Profile
ASK	Amplitude Shift Keying
AR	Auto-regressive
AURIS	Augmented UHF RFID System
AWGN	Additional White Gaussian Noise
BLF	Backscatter Link Frequency
CL	Centroid Localization
CSI	Channel State Information
CW	Carrier Wave
DC	Direct Current
EM	Electromagnetic
EPC	Electronic Product Code
FET	Field-effect Transistor
FPGA	Field Programmable Gate Array
FSM	Finite State Machine
ICT	Information and Communication Technology

IoT	Internet of Things
ISO	International Organization for Standardization
KNN	K Nearest Neighbor
MMS	Miller modulated subcarrier
NLoS	None Line-of-Sight
OFDM	Orthogonal Frequency Division Multiplexing
PASS	Proximity-detection-based Augmented UHF RFID System Simulator
PF	Particle Filter
PIE	Pulse Interval Encoding
PSK	Phase Shift Keying
QAM	Quadrature Amplitude Modulation
RCS	Radar Cross Section
RF	Radio Frequency
RFID	Radio Frequency Identification
RSS	Received Signal Strength
RSSI	Received Signal Strength Index
SLAM	Simultaneous Localization and Mapping
SNR	Signal Noise Ratio
SoC	System on Chip
SQLAM	Sequential Localization and Mapping
ST	Sense-a-Tag
TDoA	Time Difference of Arrival
ToA	Time of Arrival
ToF	Time of Flight

UHF	Ultra-high Frequency
WCL	Weighted Centroid Localization
XPE	Xilinx Power Estimator

Chapter 1

Introduction

1.1 Motivation

It is widely recognized that the Internet of Things (IoT) will be the third innovation wave of Information and Communication Technology (ICT) world, following the computer and Internet [2]. The IoT conceptually means "who", "where" and "how" of physical objects, such as food packages in supermarkets, pharmaceutical boxes in stores and file folders in offices. It is anticipated that trillions of radio tags will be embedded into objects, monitoring their status, providing automation identification, as well as geographical location information. The popular satellite-based positioning services to date are restricted to relatively open and flat outdoor environment, since the signal from satellite is too weak to penetrate most construction materials [3]. Therefore, the provision of localization service for trillions of objects in indoor environment forms the major bottleneck preventing seamless localization. Due to its low cost, miniature size, easy deployment and ultra-low power consumption, ultra-high-frequency (UHF) radio-frequency-identification (RFID) continues to gain recognition both in industry and academia as a pivot enabler for IoT indoor localization application [4].

The majority of state-of-art UHF RFID localization methods are based on the fusion of multiple pieces of relevant information, which are either direction of arrival (AoA), time of arrival (ToA), time difference of arrival (TDoA), received signal strength (RSS) or certain other propagation characteristic obtained by single or multiple antenna points [4]. The major problem with the above methods is that they are easily affected by the non-line-of-sight (NLoS) conditions, severe multi-path distortions and fast temporal changes of indoor environment [5]. One direction to solve this problem is to apply proximity-based method, which relies on using binary measurements to determine whether a target is within the small range from the reference landmarks. Existing approaches are to deploy passive tags at fixed locations as landmarks and attach the RFID reader to the mobile target [6, 7] and vice versa [8]. However, these approaches are strictly constrained by energy, cost and size. For example, the former approach is limited to relatively large and expensive objects that justifying carrying the RFID reader, such as autonomous household robot. In the latter approach, it is not cost-efficient to densely deploy readers with tuned read range.

In order to keep both mobile targets and landmarks simple and inexpensive, a novel UHF RFID component, referred to as ST, is developed to augment the standard UHF RFID system [5]. In the same way as passive tag, ST applies envelope detection to extract baseband signal in the receiving path, and backscatter modulation to talk back to in the transmitting path respectively. The difference is that ST's receiving path does not only capture RFID reader's pulse-interval-encoding (PIE) command, but also passive tags' backscattering signal. Such unique functionality enables tag-to-tag backscattering communication link, which could keep both mobile targets and landmarks simple and inexpensive. Therefore, by adding ST to the standard UHF RFID system, the augmented UHF RFID system (AURIS) can offer fine-grained proximity-based localization in indoor environment.

Indoor localization with AURIS provides several advantages over the conventional

UHF RFID proximity-based localization solutions. Compared with tag localization with readers as landmarks, localization with AURIS reduces infrastructure cost by using cheap passive tags instead of expensive readers as landmarks. And the grid of densely deployed passive tags can improve the localization accuracy of mobile targets. On the other hand, compared with reader localization with passive tags as landmarks, ST outperforms reader in terms of size, power efficiency and cost. The off-the-shelf handhold UHF RFID readers cost at least 500 CAD [9]. For rapid prototyping the current implementation of ST is a semi-passive component, which includes FPGA Xilinx Spartan 3AN and alkaline 9V2100 mAh battery. ST is $3'2'' \times 3'2''$, which costs about 50 CAD, and can continuously work up to 10 days [10]. Our group is working on migrating from FPGA design to low-power miccontroller that can reduce the size and cost, and increase the battery lifetime to one year. The ultimate version of ST would be a passive UHF RFID component. Therefore, localization with AURIS is a promising approach for proximity-based UHF RFID indoor localization, in particular for the vision of locating trillions of small items indoor in IoT paradigm.

Using tag-to-tag backscattering communication link for proximity-based indoor localization is still in its infancy. Available works are mostly feasibility study and provide only a high-level view [5, 10, 11]. To use the tag-to-tag backscattering communication in AURIS for indoor localization, certain challenges need to be addressed. In tag-to-tag backscattering communication scheme, the RFID reader must transmit CW for the tag to backscatter. Consequently, the signal at the ST's antenna is the superposition of reader's CW and the tag's backscattering signal. Unfortunately, due to the relative phase difference between them, the modulation depth of tag's backscattering signal at ST's envelope detector could be significantly attenuated or even cancelled out. We refer such effect to as *phase cancellation effect*. Since the proximity-based localization method purely depends on the detection of proximal tags by ST, handling the challenge of phase cancellation is the critical step for indoor localization utilizing tag-to-tag backscattering communication link. The first research problem is "*What is phase cancellation effect in AURIS, and how could we counter such effect?*".

It is demonstrated that the CW from RFID reader has a major effect on ST-to-tag detection probability, such as the aforementioned phase cancellation effect. Besides that, the sensing range of ST-to-tag depends on the amount of energy that passive tag backscatters from impinging RFID reader CW. Therefore, the detection of ST-to-tag depends on numerous factors such as the distance between tag to reader, the distance between the ST and the tag, as well as the relative orientation of the reader, tag and ST antennas. The traditional detection probability model used in RFID system, which simply depends on the distance between two communication participants, is far from realistic for ST-to-tag communication. Current model-based localization algorithms [11] take into account only the distance between the tag and the ST which can result in inaccurate localization. The second research problem is "*How could the detection probability model of ST-to-tag be improved based on the investigation of tag-to-tag backscattering communication link?*"

To address the localization problem in AURIS, we consider N passive tags as landmarks in the environment with the target attached with ST collecting ST-to-tag detections. The successful target localization comes from the effective extraction of useful information about target's state from ST-to-tag detections. With the proposed detection probability model of ST-to-tag, we introduce particle filter algorithm to localize ST. To this end, we identify two technical roadblocks of AURIS and existing inference algorithms as false synchronous detection assumption and state evolution model constraints. The third research problem is "*How to design the particle filter-based algorithm to localize ST accurately?*"

ST has the capability to capture the backscattering communication between passive landmark tags and RFID reader. The location of ST could be inferred from the aggregated detection information and prior known landmark map. On the other hand, unknown tags[1] are mapped based on the uncertain ST location estimation rather than landmark map, since there is no direct communication link between unknown tags and landmarks. In AURIS system ST is attached to mobile target which is always moving, while passive tags are attached to static objects. Along with more aggregated detection information collected by ST, the mapping accuracy of unknown tags is improved gradually. Landmark tags will fail to respond to RFID readers due to temporary electromagnetic blockage or permanent hardware failure, which is fatal to proximity-based localization method. Therefore, it is anticipated that ST localization would benefit from compensating the failure of landmark tags by including mapped unknown tags into landmark set. The last research problem is "*How to bring the landmark-based sequential localization and mapping framework to AURIS?*"

1.2 Contributions

In this thesis, we aim to use tag-to-tag backscattering communication link in AURIS for indoor localization towards the IoT. This thesis makes the following four contributions according to the research problems raised in previous section.

First, we analyze the phase cancellation effect in detail and propose solutions to counter such effect. The phase cancellation effect originates from the very nature of tag-to-tag backscattering communication. Destructive superposition takes place at the receiving tag (ST) antenna, which makes the system being unaware of its occurrence. We model the superposition of the passive tag's backscattering signal and reader's CW at the ST antenna for both ASK and PSK modulation. For the design of phase cancellation effect-reducing techniques, there are certain constraints to follow:

[1] In this thesis, unknown tag means passive tag with unknown location.

- Minimal increase of the cost of ST, which means that envelope detection in downlink and backscattering modulator in uplink should be preserved.
- ST should be compliant with the established RFID protocol (EPCglobal Class1 Gen2).

Therefore, we propose solutions to counter such effect by exploiting spatial diversity of dual antennas. Two ST antennas offer two reference points for the reception of the superimposed signal. Signals from two antennas are combined using simple combination and selection scheme. The simple combination technique combines the received signal from two ST antennas together. On the contrary, the receiving path selection technique depends on two parallel co-operating receiving path in ST. The simulation demonstrates that the dual-antenna based implementation of ST performs better than the original single antenna implementation. In particular, the overall probability of phase cancellation for the receiving path selection technique is below 1%.

Second, one new and realistic probability detection model is proposed, which is better suited to ST-to-tag communication link. The probability detection model of ST-to-tag integrates the distance and relative angle between tag and reader's antenna in addition to the distance between tag to ST. It also takes into consideration phase cancellation effect and ST implementation of receiving path selection technique.

Third, some previous work dealing with particle filter-based RFID indoor localization possesses strong assumption and constraints on the target state-space model, such as exact knowledge of the initial position of moving object, linear target motion model or exteroceptive sensor information [7, 8, 11, 12]. Additionally, in AURIS the host computer controls RFID reader to send out a fixed number of successive query rounds to the reference tags. Then the location inference algorithm localizes ST using aggregated binary information reported by ST. Existing inference algorithms rely on false synchronous detection assumption, which assumes that the detection measurements are received by ST synchronously [10, 11]. Our newly proposed PF-AA introduces current measurements into constraint-free auto-regressive (AR) state evolution model, and it also addresses the asynchronous measurements with a minor modification of ST locator protocol which is still EPCglobal Class1 Gen2 compliant.

Last, a novel landmark-based sequential localization and mapping (SQLAM) framework is proposed to allow for localization and mapping in proximity-based localization system. The framework expands the localization capability of AURIS to unknown tags. Furthermore, the unknown tags with resolved locations are utilized to localize ST. Through extensive computer simulation, we show that SQLAM enables the accurate mapping of unknown passive tags. In addition, when certain landmark tags are not available, the unknown tags with resolved locations assist in the localization of ST. Some work dealing with sequential or iterative localization can be found in the area of wireless sensor networks. In [13, 14], the localization of sensor nodes with unknown locations utilizes the characteristic of received signal, such as RSSI and ToA, from landmark nodes. Sensors with resolved locations are used to localize other unknown nodes together with available landmark nodes. Such sequential scheme achieves localization of unknown nodes for the entire network. However, in SQLAM there is no direct communication link between landmark tags and unknown tags. The localization of unknown objects, including unknown tags and ST, purely depends on the proximity information collected by ST. The major contribution of this section is the introduction of sequential localization and mapping framework to proximity-based localization system. To best of our knowledge, there is no previous work tackling such problem in RFID system. It is demonstrated that the higher localization accuracy is achieved in comparison with the situation where unknown tags with resolved locations are not included into the localization procedure.

Figure 1.1 depicts the research problems, their effects on the localization performance of AURIS, as well as the contributions of the thesis.

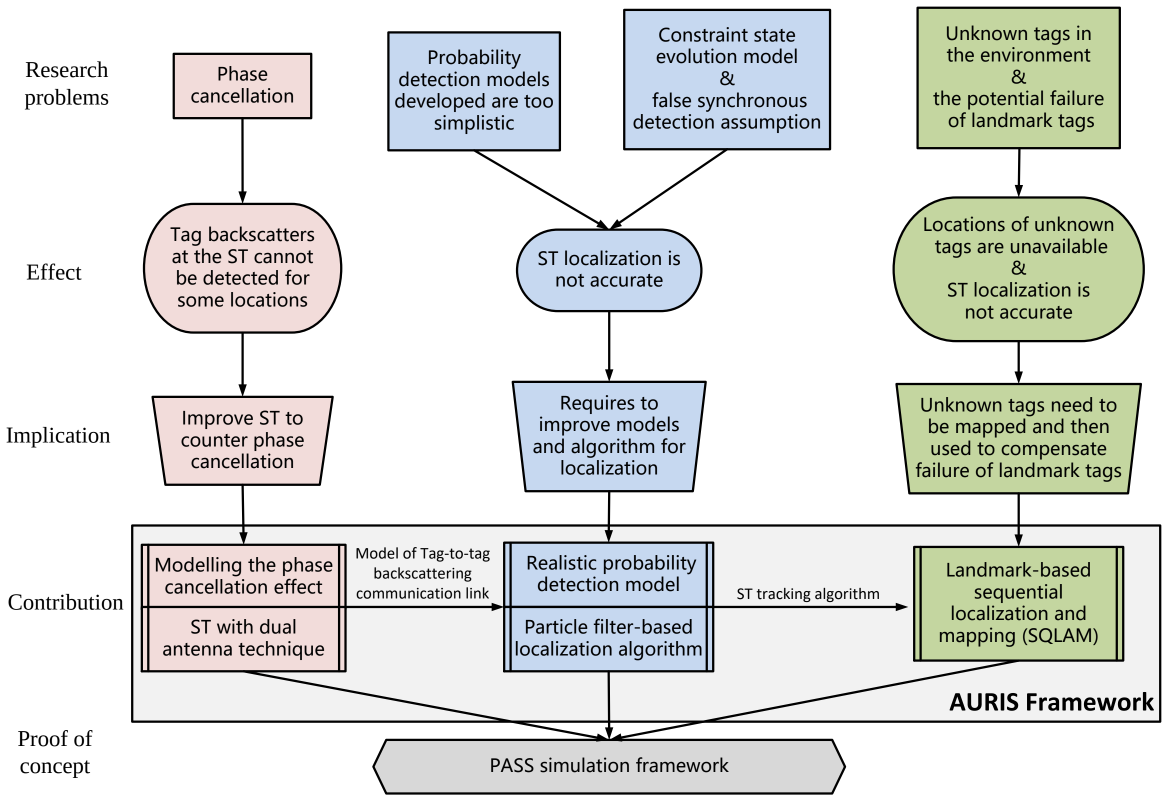

Figure 1.1: Research problems, and their effects on the localization performance of AURIS, as well as the contributions of the thesis.

1.3 Limitations and boundaries

This thesis is focused on addressing the research problems as phase cancellation, mathematical models and localization algorithm in AURIS. Even though the thesis is simulation-based, each component of AURIS system is validated by experiments. Experiments with FPGA-based ST have been performed by [5, 10, 15]. The ST is implemented in hardware as well as in simulation as a semi-passive device with the goal of being simple and inexpensive, and eventually to be implemented as a passive device in the future. In the simulation, every part of ST is implemented including RF, analog and digital sections. The physical models of passive tag and RFID reader used in the simulation are validated by the experiments in PARIS simulator [16]. The passive tag model is based on NXP UCODE G2XM passive UHF RFID tag, and the reader model is based on general-purpose UHF RFID reader. Wireless communication channel used in the simulation is based on the channel model from PARIS simulator, which includes large-scale path loss, antenna gain pattern, virtual transmitter for surface reflection, and statistical small-scale model [16]. The communication protocol that was used is EPCglobal Class1 Gen2 [1]. The idea behind using the protocol is to make the implementation of the results of the thesis applicable and easily developed in real system. The simulation in the thesis is developed in MATLAB. MATLAB has extensive functions and tools to establish accurate physical models, and support different types of arithmetic, array and matrix operations for complex algorithm [17]. Noteworthily, the Q selection algorithm in Gen2 protocol is not implemented in the simulator, since the simulation platform MATLAB is discommodious for scheduling algorithm and also slow for massive computation tasks. Besides that, PASS does not implement the interference between antennas for ST dual-antenna implementation. Although the channel model of PASS includes the NLoS components, which are from surface reflection and statistical multipath model, it does not consider the human or metal shielding effect, which are common in realistic scenario.

Having the whole system implemented in the simulator allows for much faster evaluation of the system and faster validation of the effectiveness of ideas.

1.4 Thesis organization

The remaining of this dissertation is organized as following. In Chapter 2, we provide a brief overview of UHF RIFD technology and indoor localization system in the context of IoT. We formulate the phase cancellation effect in AURIS and provide solutions to counter such effect in Chapter 3. In Chapter 4, the novel probability detection model of ST-to-tag is described with the investigation of the tag-to-tag backscattering communication link. With the newly proposed detection model, the particle filter-based location inference algorithm is proposed for AURIS. Besides that, we introduce the SQLAM framework with localization capability of ST and unknown tags. In Chapter 5, the thesis presents the research directions of future work. Finally, Chapter 6 closes the thesis with the main conclusions.

Chapter 2

Background and related work

In this chapter, we present the basics of Internet of Things and RFID technology, and introduce UHF RFID-based indoor localization technique taxonomy. Furthermore, we discuss the state-of-the-art in proximity-based approaches, location inference algorithms, and UHF RFID simulation framework specified for indoor localization research.

2.1 Internet of Things

The concept "Internet of Things", coined back in 1999 by Auto-ID center at Massachusetts Institute of Technology, is rapidly gaining ground in modern wireless telecommunication, with day-to-day continuously emerging in all context of our lives [18]. The concept is simple but powerful, which envisages the infrastructure of ubiquitous wireless sensing and identification with trillions of IoT nodes to connect anything from anywhere at anytime [19]. The IoT nodes such as radio tags-type micro devices can be embedded into objects, monitoring their status, monitoring surrounding environment as well as acquiring geographical information. These micro-devices are the fundamental elements for the context-aware energy-aware and location-aware computing for IoT. Unquestionably, IoT will make a huge impact on everyday-life

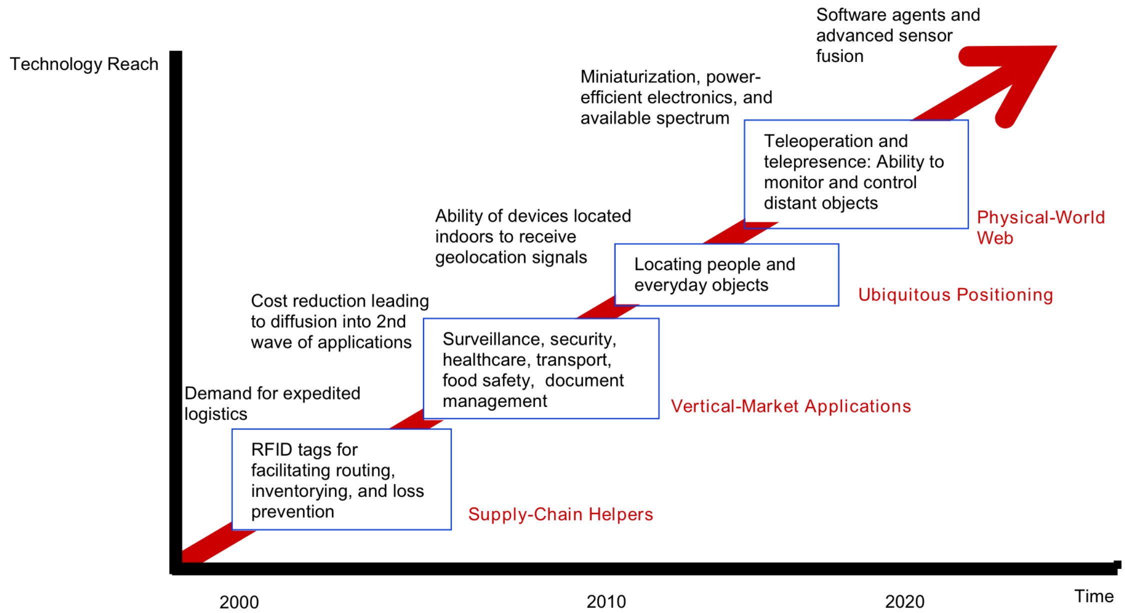

Figure 2.1: IoT technology roadmap. (Courtesy: Strategic Business Insights)

and also socio-economy with rewarding applications in domains such as [20]

- transportation and logistics,
- healthcare,
- smart environment,
- social domain.

Figure 2.1 presents the IoT technology roadmap [21]. RFID technology is used for tagging everyday objects since 2000. Everyday objects include not only the electronic devices, but the miscellany of commerce and culture. By 2015, smartphones will serve as “windows on everyday things” to enable people to interact electronically with everyday objects. Ubiquitous localization technology is the focus of research and development by 2020. Ubiquitous localization means locating objects that may reside indoors where satellite signals may be unavailable. Later after 2020, intelligent software agents may emerge that analyze the big data acquired from connected everyday objects to make unsupervised decisions and act on behalf of people.

2.2 UHF RFID technology

2.2.1 UHF RFID system

RFID is the use of radio waves to transfer data, for the purpose of identifying items. The first application of RFID-like technology can be traced back to World War II in discriminating friend aircrafts from foes [22]. Recently along with the development of radio antenna, ultra-low power chipsets as well as SoC integration and miniaturization, RFID becomes more practical and promising in business world. Recent applications can be seen in automated checkouts [23], anti-theft [24], streamline supply chain [25], animal tracking [26] and asset management [27]. Noteworthily, this is by no means an exhaustive list but it gives an indication of the many applications of RFID technology.

The archetypal RFID system shown in Figure 2.2 consists a transponder or a tag, which is affixed to the object of the interest, and a interrogator or a reader, which is the data capture device to perform the identification. The first distinction criteria for RFID systems is the presence or absence of radio transmitter and battery in tags. Active tags are full-fledged transceivers, and have their independent power source. Thus, active tag's lifetime is limited by the onboard battery. Passive tags, on the other hand, do not have any power supply and have no radio transmitter of their own. Passive tags depend on the minute electrical current induced in the antenna by the incoming magnetic or EM field from the reader to support the operation of their circuity. And passive tags transmit information to the reader by modifying their interaction with the impinging field from the reader (e.g. by load modulation

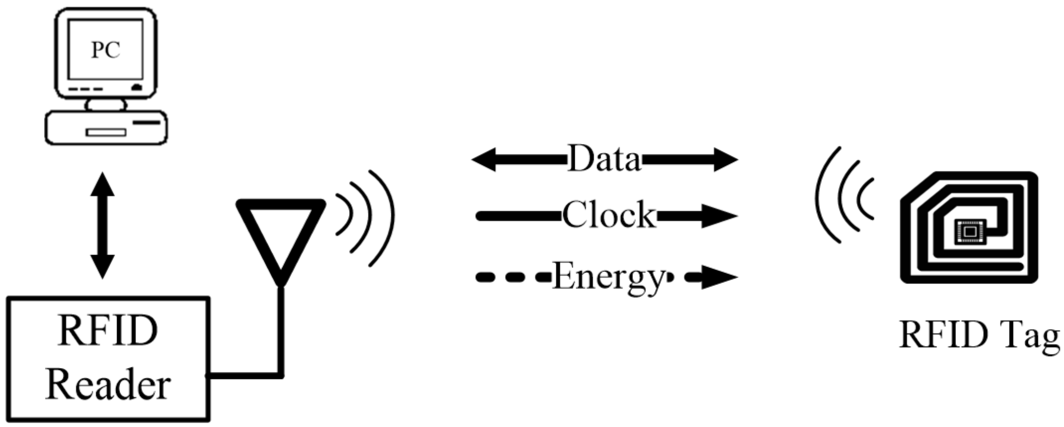

Figure 2.2: Standard RFID system

or backscatter modulation) [28].

Frequencies of RFID system varies from 100 KHz to over 5 GHz. Among them, low frequency (LF) system operates at 125 KHz, high frequency (HF) at 13.56 MHz, and UHF operates in the range of 860 – 960 MHz. UHF RFID allows high data rates, small antenna size and several meters of read range [3]. UHF RFID provides superior performance among passive RFID systems, and it is a potent candidate for localization in the context of IoT application.

2.2.2 Backscattering communication

Figure 2.3 illustrates the backscattering communication mechanism in UHF RFID system [2]. RFID reader generates a carrier wave (CW), which is transmitted by reader antenna to free space. RFID tag captures the incoming CW to power up its own circuitry. Then the tag sends data back to RFID reader. In this mechanism, RFID tag works as a reflector of impinging CW of RFID reader. The "reflection characteristic" (referred to as RCS) of RFID tag can be changed by altering the parallel load of the tag antenna. Therefore, the tag can reflect back more or less of impinging reader's transmitting signal corresponding to the pattern of data.

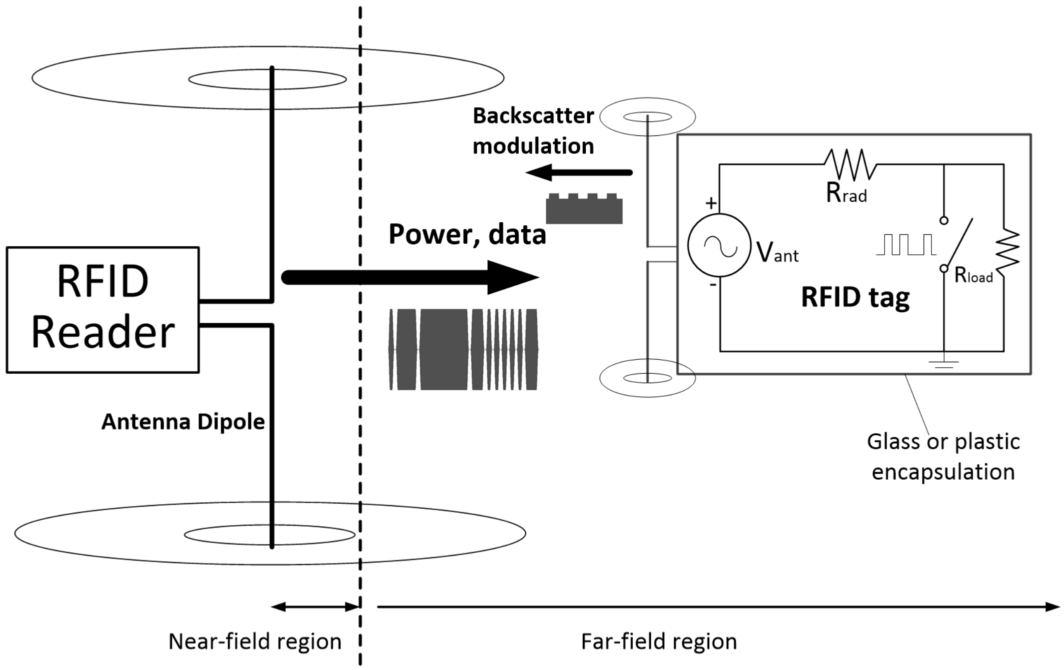

Figure 2.3: Backscatter coupling mechanism

The research on backscattering communication has grown drastically in recent years, which even extends to other technologies such as Bluetooth, WiFi etc. In [29], the author presents a design of the ambient backscatter that enables the backscattering communication between two devices using existing TV and cellular transmissions as the source of power. Ambient backscatter differs from the UHF RFID backscattering communication in the following aspects. Firstly, it takes advantages of existing RF source rather than a special-purpose power infrastructure. Secondly, it enables device-to-device communication. However, this work in [29] is a feasibility study, which simply investigates the one-hop device-to-device backscattering communication. Since the device is power hungry, and limited in computational capability, the devices could merely perform simple task such as card emulation and proximity detection. Since the communication between devices in ambient backscatter system is one-hop, there is no simple and cost efficient method to deliver the proximity information to the server.

In [30], the WiFi Backscatter is presented, which uses backscattering communication to bridge RF-powered devices with the Internet. WiFi Backscatter communicates by modulating the CSI and RSSI of WiFi channel as seen by WiFi-enabled mobile device. WiFi backscatter follows a request-response model, which is similar to EPC-global Class1 Gen2 protocol. In [31], the author shows that BLE advertising packets can be created by backscattering single incident CW carrier using a novel backscatter subcarrier modulation. Although the power sources of the previous systems are different, the general designs of tags are similar, which enables the conventional UHF RFID Reader-to-tag-like communication in WiFi and Bluetooth respectively.

2.2.3 EPCglobal Class1 Generation 2 (Gen2) protocol

To exchange data successfully every communication system should follow certain rules and protocols. EPCglobal® is a standardization organization aiming at both world-wide adoption of EPC technology and worldwide support standard for RFID. With EPCglobal®'s consistent standardization effort, today the commercial UHF RFID systems adhere to the single global standard EPCglobal Class 1 Generation 2 (Gen2).

Symbols and encoding

Gen 2 is reader-talk-first protocol. The modulation scheme of reader-to-tag link uses double sideband amplitude shift keying (DSB-ASK), single sideband amplitude shift keying (SSB-ASK), or phase-reversal amplitude shift keying (PR-ASK) [1]. The data encoding format is pulse-interval-encoding (PIE) as shown in Figure 2.4. High and low values represent CW and attenuated CW respectively. Data '0' consists of a high value interval followed by a low value interval with the same duration. The total length of data '0' is the reference time interval referred as *Tari*. The value of *Tari* is in the range from 6.25 μs to 25 μs. Data '1' can last as short as 1.5 *Tari* to as long

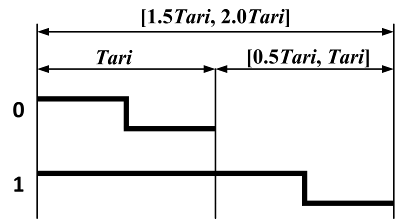

Figure 2.4: PIE symbols (figure adapted from [1])

as 2 *Tari*.

EPCglobal Class 1 Gen 2 tags use amplitude shift keying (ASK) or phase shift keying (PSK) to modulate the reader's RF carrier in tag-to-reader link. Gen 2 tags have two encoding formats. One is FM0 baseband, the other is Miller-modulated subcarrier (MMS) encoding. The reader command specifies the encoding format.

As shown in Figure 2.5, FM0 encoding is straightforward. FM0 inverts the baseband value at the edge of every symbol. Data '0' has an additional transition in the middle of symbol; data '1' does not. The generator state diagram maps a logical data sequence for FM0 basis functions.

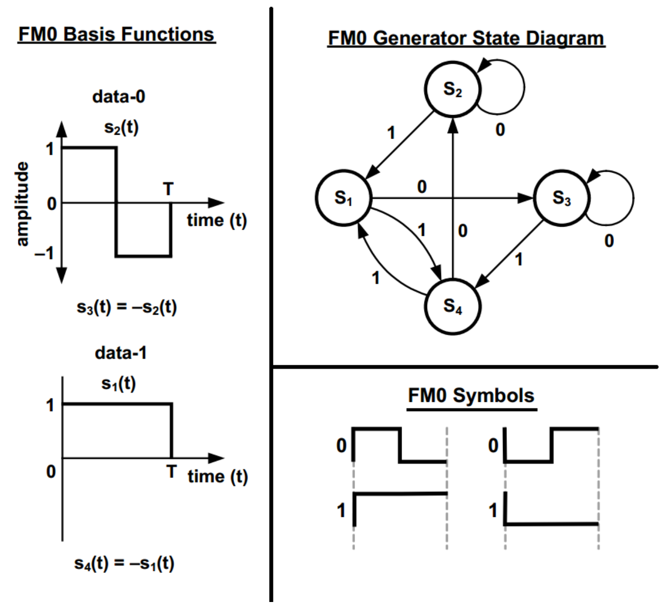

Figure 2.5: FM0 basis function, generator state diagram and symbols (figure adapted from [1])

However, FM0 depends on the accurate detection of single transition to discriminate data symbols. In addition, it is also vulnerable to co-channel reader interference. To provide more flexibility to counter noise and interference, EPCglobal Class 1 Gen 2 defines MMS encoding format. Figure 2.6 illustrates the Miller basis functions and generator state diagram. In the opposite fashion of FM0, data '1' has a state transition in the middle of the symbol; data '0' does not. In addition, baseband Miller places a state transition at the symbol edge between two data '0's in sequence. The baseband waveform then is multiplied by a square-wave whose sampling rate is M times higher, where M can be 2, 4 or 8. Simple examples with M = 2 and 4 are shown in Figure 2.6.

Framing

Both the forward-link and reverse-link in Gen 2 protocol are packetized. For reader-to-tag link the reader shall start with either a preamble or a frame-sync sequence

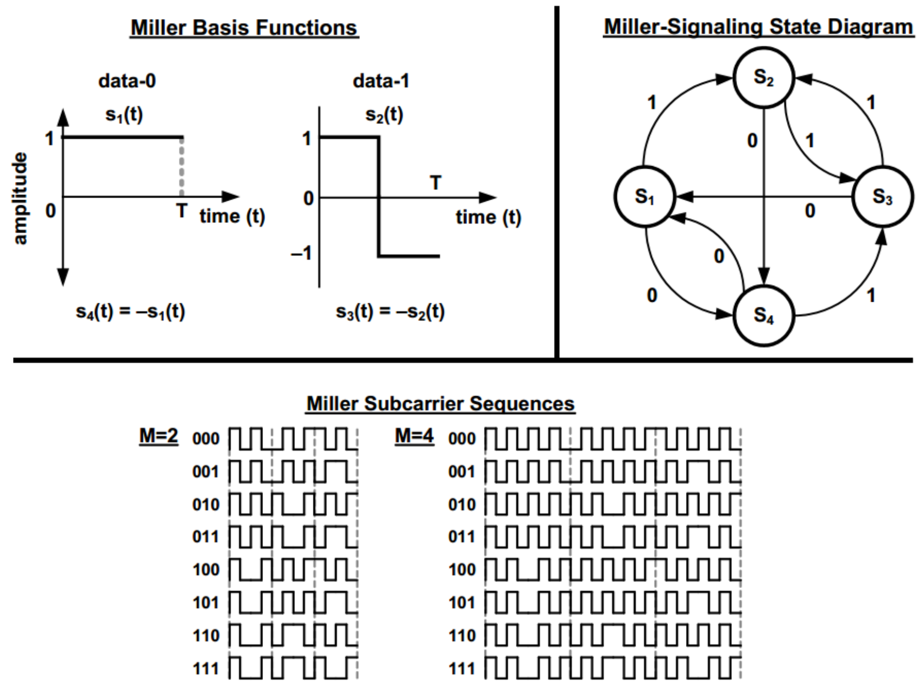

Figure 2.6: Miller basis function, state diagram and encoding sequences (figure adapted from [1])

as shown in Figure 2.7. Each of these sequences is preceded by a delimiter, which is always 12.5 μs long. After delimiter a preamble comprises a data '0' symbol, an $R => T$ calibration (RTcal), and a $T => R$ calibration (TRcal). The length of RTcal equals to the length of data '0' symbol plus the length of data '1' symbol. TRcal specifies tag's backscatter link frequency (BLF) with divide ratio (DR) in the payload. A frame-sync sequence is identical to a preamble, reducing the TRcal symbol.

For tag-to-reader link, tag replies begin with a preamble and optional pilot tone. In FM0 the preamble comprises a sequence of symbols 1-0-1-0 and a violation. The violation helps discriminating the preamble from regular data sequence. TRext value specified by reader command determines whether the pilot tone is used or not. These

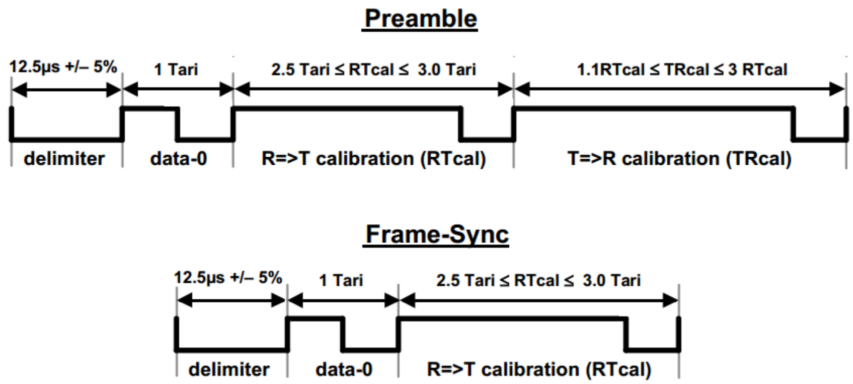

Figure 2.7: Reader-to-tag link preamble and frame-sync (figure adapted from [1])

two formats of preambles are shown in Figure 2.8. In MMS the default baseband preamble contains four consecutive data '0' symbols, followed by the sequence 0-1-0-1-1-1. If TRext is set to 1 by the reader command, the preamble of tag begins with sixteen consecutive data '0' symbols instead of four. For either FM0 or MMS the transmission ends with a 'dummy' data '1' and always ends on the low level as shown in Figure 2.8 and 2.9.

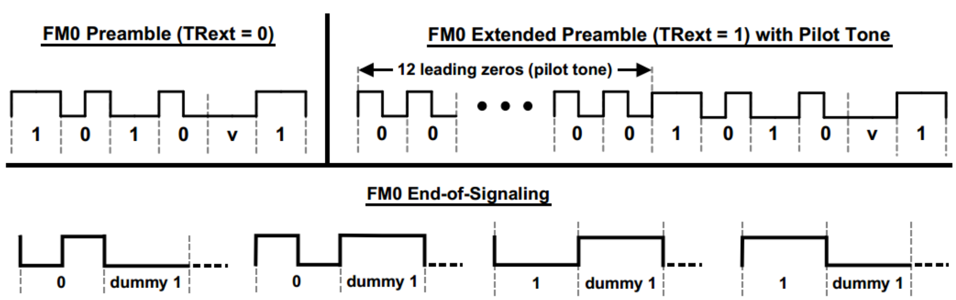

Figure 2.8: Tag-to-reader link preamble with optional pilot tone, and ending of FM0 transmission(figure adapted from [1])

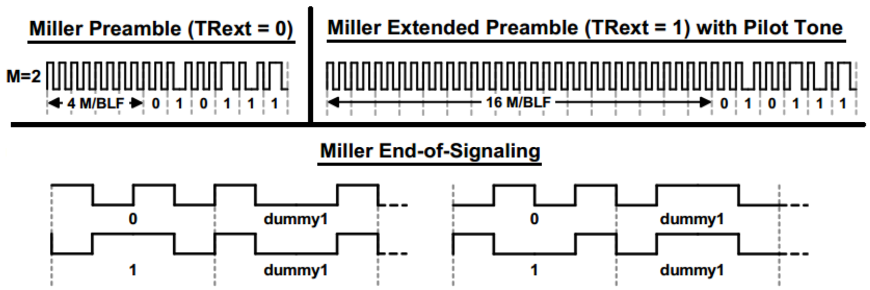

Figure 2.9: Tag-to-reader link preamble with optional pilot tone and ending of MMS transmission (figure adapted from [1])

Media access control

EPCglobal Class 1 Gen 2 MAC protocol adopts a adaptive slotted Aloha variant instead of the binary tree search in Gen 1. The protocol is known as Q protocol.

As in Figure 2.10, a reader issues a Query command to initiate an inventory. The Query command contains a numerical parameter Q. Q is four bit binary number, which takes value from 0 to 15. After receiving the Query command, each tag generates a random number in the range of $[0, 2^Q - 1]$. If a tag's slot count equals to 0, it responds with a new 16-bit random number RN16 in the slot. In a successful slot, reader sends back an acknowledge command ACK, containing the received RN16. If tag receives the ACK command and RN16 has the same value as it previously sent, it then replies with a longer packet containing its ID.

If the tags' IDs are what the reader needs, at this point the reader issues QueryRep to signal the end of a slot. Other tags decrease the slot count by 1 in response to QueryRep, and start the process again. If no tags replies in a slot, the reader issues another QueryRep. If there are multiple tags that replied, a collision occurs in this slot.

For the following inventory round, Q algorithm in Gen 2 protocol determines new value of Q based on the recorded number of empty and collision slots in the last

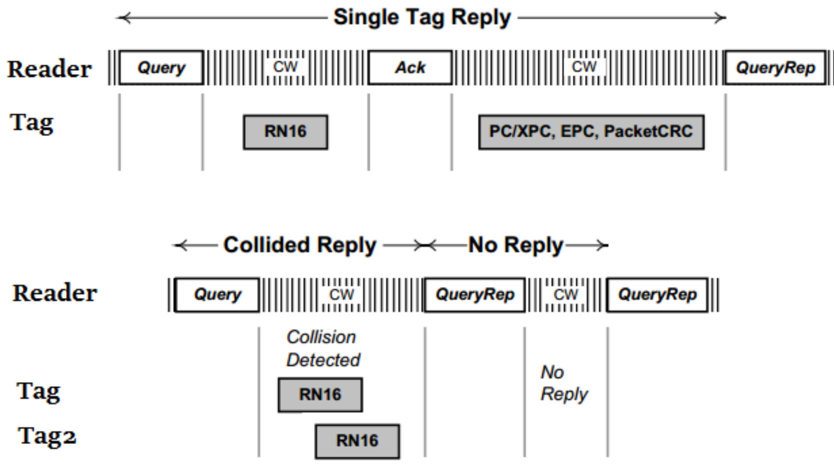

Figure 2.10: Slots with successful read, collision and empty reply (figure adapted from [1])

inventory round as shown in Figure 2.11. C is constant number. There is a wide area of research to obtain the optimal value of C for different scenarios.

2.3 Indoor localization

During the past decade, academic and industrial community has carried out intense research work to design and build indoor localization system to realize the vision of IoT. The availability of indoor localization system will facilitate the location-based IoT services and applications, which will subsequently benefit enormously to mankind welfare. For indoor location sensing, a number of technologies have been studied, such as camera, infrared, acoustic, WLAN/Wi-Fi, UWB, RFID and et al. [18]. Among these technologies, passive UHF RFID has been widely recognized as enabler technology for IoT location application due to its miniature size, easy deployment, low-cost and ultra-low power consumption [2].

State-of-art UHF RFID localization methods can be broadly classified into three categories: triangulation, scene-analysis and proximity [32]. Figure 2.12 provides the

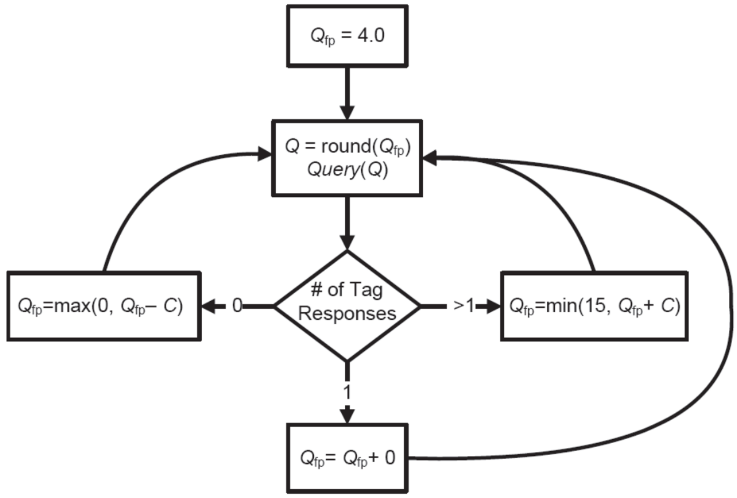

Figure 2.11: Q algorithm for tag anti-collision (figure adapted from [1])

taxonomy of the UHF RFID localization methods.

2.3.1 Triangulation

Triangulation localization method is the technique of determining the target location using the trigonometry and geometry with multiple reference points.

Direction-based method

The AoA technique determines the target location by the intersection of pairs of angle direction lines from multiple reference points to the target. AoA technique may use at least two reference points and measured angles to perform 2-D localization. The concept can be extended to 3-D with no pain. Measurements of AoA usually are accomplished by directional antennas, phased arrays or smart antennas [33]. A directional antenna can transmit energy to a small angular sector. Once the tag enters into the area covered by the directional antenna, the reader can sense it, thus obtain the angle-of-arrival [34]. Another approach to estimate the tag's direction uses phased arrays, in which the effective reception pattern is formulate by the relative

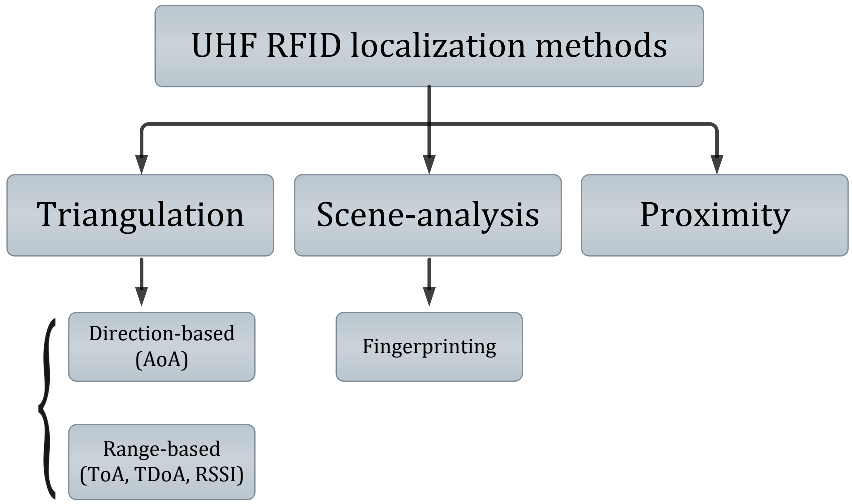

Figure 2.12: UHF RFID localization method taxonomy

phases of the respective signal feeding to a group of antennas [35].

The triangulation of the tag location is shown in Figure 2.13. The reference points are RFID reader 1 (x_1, y_1) and reader 2 (x_2, y_2). The AoAs measured at the two RFID readers are θ_1 and θ_2 respectively. The location of the tag is determined by the intersection of two rays.

$$\begin{cases} x = x_1 + Dcos(\theta_1 + \phi) \\ y = y_1 + Dcos(\theta_1 + \phi) \end{cases} \tag{2.1}$$

where

$$\begin{aligned} D &= \frac{sin(\theta_2)}{sin(\theta_1 + \theta_2)} \sqrt{(x_1 - x_2)^2 + (y_1 - y_2)^2} \\ \phi &= atan(\frac{y_1 - y_2}{x_1 - x_2}) \end{aligned}$$

The advantages of AoA include less quantity of reference points needed, no synchronization requirement, and overall sub-meter level resolutions compared to ToA

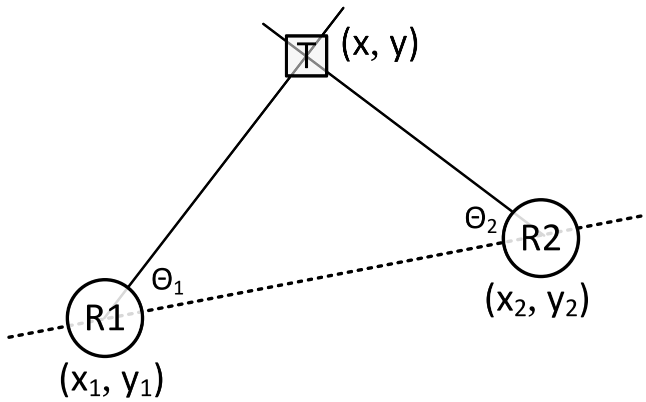

Figure 2.13: Localization with AoA technique

and TDoA-based methods [36]. The disadvantages are as following: first, it needs complex and custom designed hardware; second, localization accuracy degrades as the distance between target and reference points increasing; third, the angle measurements are influenced by misleading direction of signal reflection and also by measuring aperture orientation [37].

Range-based method

The range-based method estimates the coordinates of the target using its geometric distance from multiple reference points. The distance is derived from the strength attenuation level or propagation time of wireless signal.

ToA technique estimates the distance by measuring the absolute propagation time of signal from transmitter to receiver, requiring precise synchronization between two ends, as well as a timestamp in transmitting signal [38]. For example, the distance can be estimated by the measurement of round-trip time-of-flight (ToF) as [4]

$$\hat{d} = c \cdot \frac{ToF}{2} = \frac{c \cdot (ToP - T_p)}{2}$$

where ToP is the overall round trip delay, T_p is the signal processing time consumed by tag circuitry, and c is the speed of light.

TDoA technique examines arriving time difference of transmitting signal at multiple reference points, while avoiding synchronization between transmitter and receiver. However, due to common NLoS condition and the requirement of synchronization, ToA and TDoA are challenging for implementing realistic system [38].

Signal attenuation-based technique utilizes the attenuation level of transmitted signal strength to estimate distance between the target and reference point according to either theoretical or empirical propagation path-loss model [39]. For an UHF RFID system, a round-trip path loss of the wireless signal, which is transmitted from the reader and backscattered at the tag, is formulated as

$$P_{RX,reader} = P_{TX,reader} \eta G_{tag}^2 G_{reader}^2 (\frac{\lambda}{4\pi d})^{2n} \tag{2.2}$$

where $P_{TX,reader}$ is the transmit power from the reader, η is the power transfer efficiency of the tag, the typical value of η is $1/3$ or -5 dB. G_{tag} and G_{reader} are the antenna gains of the tag and reader respectively. λ is the wavelength, d is the range between the tag and the reader. n is the path loss exponent. The typical value of n is between 1.6 and 1.8 for line-of-sight indoor environment [4].

Consider a tag localization problem in 2-D scenario as shown in Figure 2.14. The range of the unknown tag to reference points (RFID reader) (x_1, y_1), (x_2, y_2) and (x_3, y_3) are estimated as d_1, d_2 and d_2 based on the aforementioned methods. The location of unknown tag, which denotes as (x, y), can be solved from the following system of equations

$$\begin{cases} (x - x_1)^2 + (y - y_1)^2 = d_1^2 \\ (x - x_2)^2 + (y - y_2)^2 = d_2^2 \\ (x - x_3)^2 + (y - y_3)^2 = d_3^2 \end{cases} \tag{2.3}$$

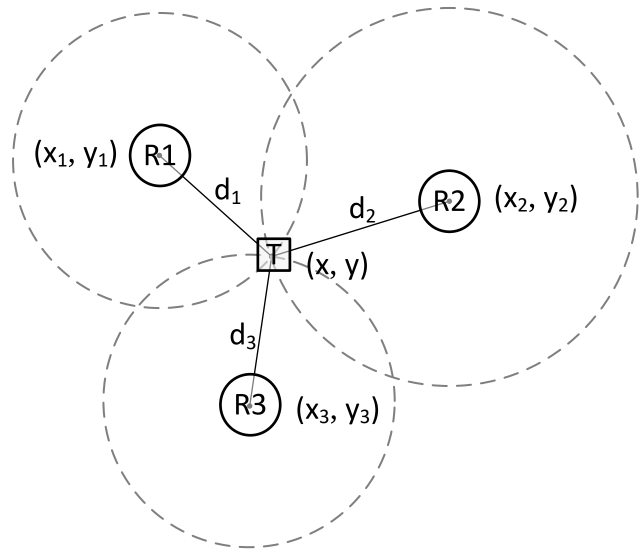

Figure 2.14: Localization with range-based method

One possible method to solve this problem is presented in [40]. We express the equations in vector form

$$\mathbf{A} \cdot \begin{pmatrix} x \\ y \end{pmatrix} = \mathbf{b} \tag{2.4}$$

where

$$\mathbf{A} = \begin{pmatrix} x_1 - x_2 & y_1 - y_2 \\ x_2 - x_3 & y_2 - y_3 \end{pmatrix} \qquad \mathbf{b} = \frac{1}{2} \begin{pmatrix} d_2^2 - d_1^2 + x_1^2 - x_2^2 + y_1^2 - y_2^2 \\ d_3^2 - d_2^2 + x_2^2 - x_3^2 + y_2^2 - y_3^2 \end{pmatrix}$$

The least-square solution of Equation 2.4 is

$$\begin{pmatrix} x \\ y \end{pmatrix} = (\mathbf{A}^T\mathbf{A})^{-1}\mathbf{A}^T\mathbf{b} \tag{2.5}$$

2.3.2 Scene analysis

Scene analysis technique collects RSSI fingerprints of an observed scene in off-line stage. The observed fingerprints are usually specific and unique, which are used to estimate target location through matching online measurements [41]. Approaches from pattern recognition field are commonly used such as k-nearest-neighbor (KNN) [42].

The main challenge of the technique is that RSSI is sensitive to shadowing, reflection, scattering and fast temporal change of indoor environment. Therefore, periodic renewing of coordinate-based RSSI database is necessary, which makes it impractical.

2.3.3 Proximity

Proximity-based techniques exploit symbolic relative location information related to the presence or absence of the target within a small range of reference points. These techniques do not require sophisticated hardware or propagation model, which makes it suitable for the low-cost RFID tags [5].

In proximity-based approach, each reference point has a limited coverage area around the antenna. Therefore, observing whether the target is within the coverage range of the antenna yields target's location information. For example, if a target is detected by more than one reference point, the location of target can be estimated by collocating with the reference point with the highest signal strength, or the intersection of the coverage area of these reference points. Thus the density of reference points heavily affects the localization resolution.

2.3.4 The challenges of indoor localization

Indoor environment are particularly challenging for localization due to a number of practical issues [16, 18, 43].

- Small-scale multipath fading can significantly reduce UHF RFID tag's read range and reliability. Severe small-scale fading is caused by waves scattered from the walls, furniture, objects and humans in indoor environment.
- In UHF RFID, the LoS from RFID reader to the tag is often blocked by the product on which the tag is attached to or other obstacles. Any localization system has to deal with the NLoS conditions.
- Indoor environment also suffers from the fast temporal changes due to the p-resence of people and opening windows or doors.
- The vision of ubiquitous localization requires using tiny, simple and inexpensive devices. These devices usually come with limited processing capabilities, low memory space and poor power supply.

2.4 State-of-art proximity-based localization with UHF RFID

In indoor environment, due to NLoS conditions, severe multipath distortions and fast temporal changes, the overall accuracy and robustness of techniques, which depend on extracting location information from propagation characteristics of RF signal returned to reference points from target, are low [44]. One direction to address this problem is to apply proximity-based method, which relies on using binary measurements related to whether a target is within small range of reference landmarks. This thesis emphasizes on utilizing proximity information for indoor localization in context of IoT application.

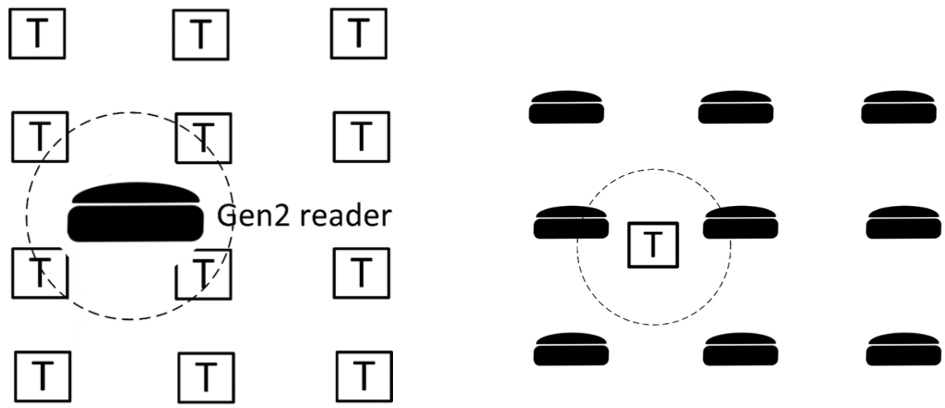

(a) Reader-based method (b) Tag-based method

Figure 2.15: Existing proximity-based approaches

2.4.1 Overview of existing approaches

Conventional approaches

Existing approaches are based on deploying passive tags at fixed locations as landmarks and attaching RFID reader to the mobile target and vice versa as shown in Figure 2.15. Usually, the former approach is referred to as reader-based method while the latter as tag-based method.

In [45] researchers deploy a grid of UHF RFID tags on the ceiling of the building. The read region of each tag is well defined, thus the floor environment is subdivided into a set of cells. When the target equipped with reader enters into the read region of UHF RFID tag, the tag ID or the equivalent tag coordinates are retrieved. The location of target is estimated according to retrieved data. Based on such reader-based technique, multiple indoor localization systems have been proposed [7, 46, 47].

In [8, 12] the area is covered by a mesh grid of a large set of RFID readers and associated antennas, whose locations are known. The objects with attached UHF RFID tags are localized and tracked using particle filter based inference algorithm.

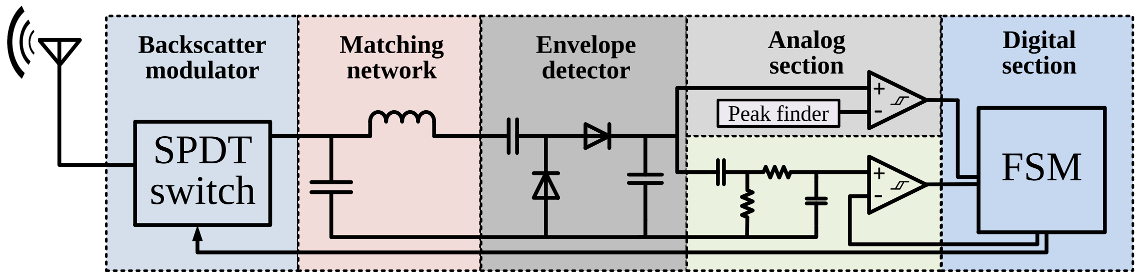

Figure 2.16: The block diagram of ST

Sense-a-Tag

In [44], a tag-like UHF RFID component is proposed, which is referred to as ST (Sense-a-Tag). The ST has dual functionality: it is capable of sensing the backscattering communication between standard RFID reader and nearby passive tags; it can also apply backscatter communication to talk back to RFID reader. ST is an EPCglobal Class1 Gen2 compliant component operating in the frequency band $902-928$ MHz.

Figure 2.16 depicts the block diagram of ST hardware. The antenna is followed by a backscatter modulator, a corresponding matching network and a conventional diode envelope detector circuit. The output of envelope detector is fed into the analog section, which has the ability to process both reader's PIE signal as well as the tag's backscattering signal. The analog processing of reader's PIE signal is exactly the same as the standard passive tag, which employs a hysteresis comparator to generate digital signal. The processing circuit of tag's backscattering signal is more complex, which consists of a band-pass filter for removing the DC offset, followed by a comparator acting as one-bit A/D converter. The output of analog section is the input of digital section, which runs FSM for Gen2-based ST locator protocol. As for rapid prototyping, the latest version of digital section is implemented on FPGA Xilinx Spartan 3AN chip.

ST locator protocol specifies two states of ST operations: *Listening* and *Responding*. In *Listening* state, ST does not respond to the RFID reader and instead listens to the backscatter signal of tags in its proximity. Once upon receiving any backscatter signal, ST decodes the signal, extracts the tags' IDs, and stores a hash value corresponding to the ID temporarily. In *Responding* state, ST itself functions as standard passive tag, and conveys the acquired ID information to RFID reader as part of its EPC payload. These operation states of ST are initiated by two distinct RFID reader queries (Q_T for *Listening*, Q_S for *Responding*). Q_T and Q_S queries are generated by manipulating the **SELECT** command in EPCglobal Class1 Gen2 protocol.

By augmenting ST to off-the-shelf UHF RFID system, it enables the fine-grained proximity-based indoor localization system, which deploys a grid of passive tags as landmarks and localizes the target with ST. In this way, both the landmarks and mobiles are simple and inexpensive compared with conventional proximity-based localization solutions.

2.4.2 Inference algorithm

Association

The association method estimates the target's location by assigning that of the detected reference landmark to it [3]. The association method is simple, fast and also adaptive to the dynamic change of indoor environment. However, the performance of the association method purely depends on the deployment of reference landmarks and the sensing range of mobile target. When detecting more than one reference landmark, the localization of mobile target often results in zigzagging.

Weighted Centroid Localization

The centroid localization (CL)-like method is proposed at first for wireless sensor network localization solutions, which is a typical range-free localization algorithm [48]. To localize the target of interest, CL performs only averaging the coordinates of landmarks in the range. Therefore, CL method inherently results in coarse localization.

To improve localization accuracy, a weighted centroid localization (WCL) method is proposed. Strictly speaking, WCL is not fully range-free localization method, since it depends on other information aside the simple connectivity. The key idea of WCL is to assign larger weight to closer landmarks and smaller weight to farther landmarks. The target is localized using the following weighted centroid formula:

$$L_{target} = \frac{\sum_{i=1}^{N}(w_i L_i)}{\sum_{i=1}^{N} w_i} \tag{2.6}$$

where w_i represents the weight assigned to landmark i. The weight should reflect the Euclidean distance from target to landmark [49].

Kalman Filter

The Kalman filter assumes that the state evolution and observation model are linear and the noises are Gaussian [50, 51]. The state evolution model is

$$x_t = \mathbf{A}x_{t-1} + \mathbf{B}u_t + w_{t-1} \tag{2.7}$$

with a observation that is

$$y_t = \mathbf{H}x_t + v_t \tag{2.8}$$

The random variables w_t and v_t represents the process and observation noise. They are assumed to be independent Gaussian distributions

$$p(w) \sim N(0, Q), \tag{2.9}$$

$$p(v) \sim N(0, R) \tag{2.10}$$

$\mathbf{A}$ relates the state of target at the previous time step $t-1$ to the current step t. $\mathbf{B}$ relates the control input. $\mathbf{H}$ relates the current state to the observation. Q and R are the covariance of Gaussian distribution.

The Kalman filter operates recursively in two logic steps: prediction and update [52]. In prediction step, the state estimation $\hat{x}_{t-1}$ and associated error covariance $\mathbf{P}_{t-1}$ are used to predict the priori state $\hat{x}_t^-$ and the associated error covariance $\mathbf{P}_t^-$ at time t. In update step, the priori $\hat{x}_t^-$ and $\mathbf{P}_t^-$ are refined by using the current observation y_t to provide a posterior estimate $\hat{x}_t$ and $\mathbf{P}_t$. The complete picture of the operations of Kalman filter is shown as following:

(i) Prediction step

$$\hat{x}_t^- = \mathbf{A}\hat{x}_{t-1} + \mathbf{B}u_t \qquad (\textit{a prior state estimation})$$

$$\mathbf{P}_t^- = \mathbf{A}\mathbf{P}_{t-1}\mathbf{A}^T + Q \qquad (\textit{a prior error covariance})$$

(ii) Update step

$$\hat{x}_t = \hat{x}_t^- + K_t(y_t - \mathbf{H}\hat{x}_t^-) \qquad (\textit{a posterior state estimation})$$

$$\mathbf{P}_t = \mathbf{P}_t^- - K_t\mathbf{H}\mathbf{P}_t^- \qquad (\textit{a posterior error covariance})$$

$$K_t = \mathbf{P}_t^-\mathbf{H}^T(\mathbf{H}\mathbf{P}_t^-\mathbf{H}^T + R)^{-1} \qquad (\textit{Kalman gain})$$

Particle Filter

Particle filtering belongs to the family of Monte Carlo method, where the distributions are approximated by discrete random measures defined by particles and associated weights [53]. For the distribution of interest $p(x)$, $\{x^{(m)}, m = 1, ..., M\}$ is a set of particles and $\{w^{(m)}, m = 1, ..., M\}$ is its weights. M is the number of particles in the approximation. The random measure, which characterizes $p(x)$ is $\chi = \{x^{(m)}, w^{(m)}\}_{m=1}^{M}$. Then, the posterior distribution at t can be approximated as

$$p(x) \approx \sum_{m=1}^{M} w^{(m)} \delta(x - x^{(m)}) \tag{2.11}$$

The weights can be chosen using the principle of importance sampling. Suppose that the distribution of interest $p(x)$ is difficult to draw samples, one can generate sample $x^{(m)}$ from a distribution $\pi(x)$, known as importance function. And the weight assigned to the particle is

$$w^{(m)} = \frac{p(x^{(m)})}{\pi(x^{(m)})} \tag{2.12}$$

In sequential signal processing, the systems are represented by state evolution and measurement equations, that is, in the form of

$$x_t = f_t(x_{t-1}, q_t) \tag{2.13}$$

$$y_t = g_t(x_t, n_t) \tag{2.14}$$

where y_t is a vector of measurements, x_t is a state vector, $g_t(\cdot)$ is measurement function, $f_t(\cdot)$ is a state evolution function, q_t and n_t are noise vectors. Let $\chi_{t-1} = \{x_{0:t-1}^{(m)}, w_{t-1}^{(m)}\}_{m=1}^{M}$ denote the random measure that characterizes the posterior distribution $p(x_{0:t-1}|y_{0:t-1})$. The importance function $\pi(x_{0:t}|y_{0:t})$ is chosen to factorize as

$$\pi(x_{0:t}|y_{0:t}) = \pi(x_t|x_{0:t-1}, y_{0:t})\pi(x_{0:t-1}|y_{0:t-1}) \tag{2.15}$$

Upon the measurement y_t updating at time t, PF algorithm run the following steps to approximate $p(x_{0:t}|y_{0:t})$.

- *Prediction.* The system state at time t is predicted by propagating all particles at time $t-1$ according to the distribution $\pi(x_t|x_{0:t-1}^{(m)}, y_{0:t})$, where $m = 1, ..., M$. In literature, there are two most frequently used importance functions, the prior function $p(x|x_{t-1}^m)$ and optimal function $p(x_t|x_{t-1}^m, y_{0:t})$.

- *Updating.* Particles are reweighed according to

$$w_t^{(m)} \propto \frac{p(y_t|x_t^{(m)})p(x_t^{(m)}|x_{t-1}^{(m)})}{\pi(x_t|x_{0:t-1}^{(m)}, y_{0:t})} w_{t-1}^{(m)} \tag{2.16}$$

  then the weights are normalized by $w_t^i = w_t^i / \sum w_t^i$.

- *Resampling.* Draw M particles, $x_t^{*(m)}$ from the discrete distribution χ_t. Then let $x_t^{(m)} = x_t^{*(m)}$, and assign equal weights $1/M$ to particles.

Auxiliary Particle Filter

The auxiliary particle filter builds on the conventional sequential importance sampling particle filter [54]. As aforementioned, if the particle measures is available at time $t-1$, the particle filter can predict the system state at time t according to the importance function $\pi(x_t|x_{0:t-1}^{(m)}, y_{0:t})$. Then the newly generated particles are reweighed. Last, the particle measure is resampled to construct a more evenly distributed particle set.

In the literature, the most frequently used importance function $\pi(x_t|x_{0:t-1}^{(m)}, y_{0:t})$ is the prior importance function $p(x_t|x_{0:t-1}^{(m)})$ [55], and thus the particle weight update in Equation (2.16) comes into

$$w_t^{(m)} \propto p(y_t|x_t^{(m)})w_{t-1}^{(m)} \quad (2.17)$$

However, the particle filter can perform poorly if the importance function π does not take into account the current measurement y_t [56]. The auxiliary particle filter introduces current measurement to the prediction step in an attempt to improve the performance [57]. The auxiliary particle filter includes two stages of weighting. In the first stage of weighting, the weight for each particle based on how well it explains the current measurement y_t. The likelihood is a good approximation to evaluate the weights.

$$p(y_t|x_{t-1}^{(m)}) = \int p(y_t|x_t)p(x_t|x_{t-1}^m)dx_t \quad (2.18)$$

Then the auxiliary particle filter resamples the particle according to the first-stage weights.

After obtaining the new particle measure of x_t, the particles is propagated according to the importance function $p(x_t|x_{t-1}^{(m)})$. And the following steps are the same with those of conventional sequential importance sampling particle filter.

Simultaneous localization and mapping

The simultaneous localization and mapping (SLAM) is a process by which the robot incrementally builds a map while simultaneously determining its location on the map [58]. Consider a robot moving in the environment at time instant t, the following quantities are defined in Table 2.1.

Table 2.1: Summary of terms and their definitions in SLAM

Term	Definition
x_t	the state vector describing the location of the vehicle at time t
u_t	the control vector applied at the time $t-1$
m_i	a vector describing the location of i_{th} landmark
z_t	the observations from the vehicle of landmarks at time t
$\mathbf{X}_{0:t}$	the history of vehicle locations
$\mathbf{U}_{0:t}$	the history of control inputs
$\mathbf{m}$	the set of all landmarks
$\mathbf{Z}_{0:t}$	the history of the set of observations

In probabilistic form, the SLAM process requires to compute

$$P(x_t, m|\mathbf{Z}_{0:t}, \mathbf{U}_{0:t}, x_0) \tag{2.19}$$

In general, a recursive solution to the SLAM is desirable. Given the distribution $P(x_{t-1}, m|\mathbf{Z}_{0:t-1}, \mathbf{U}_{0:t-1})$ at time $t-1$, the joint posterior distribution is computed by Bayes theorem with u_t and z_t. The observation model describes the probability of observation z_t with the vehicle location and landmark locations.

$$P(z_t|x_t, \mathbf{m}) \tag{2.20}$$

The motion model for the vehicle is in the form

$$P(x_t|x_{t-1}, u_t) \tag{2.21}$$

The SLAM is implemented in a recursive prediction and correction form. The prediction (time update) step is

$$P(x_t, m|\mathbf{Z}_{0:t-1}, \mathbf{U}_{0:t}, x_0) = \int P(x_t|x_{t-1}, u_k)P(x_{t-1}, m|\mathbf{Z}_{0:t-1}, \mathbf{U}_{0:t-1}, x_0)dx_{t-1} \tag{2.22}$$

The correction (measurement update) step is

$$P(x_t, m|\mathbf{Z}_{0:t}, \mathbf{U}_{0:t}, x_0) = \frac{P(z_t|x_t, m)P(x_t, m|\mathbf{Z}_{0:t-1}, \mathbf{U}_{0:t}, x_0)}{P(z_t|\mathbf{Z}_{0:t-1}, \mathbf{U}_{0:t})} \tag{2.23}$$

Equation 2.22 and 2.23 provide a recursive procedure to calculate the posterior distribution $P(x_t, m|\mathbf{Z}_{0:t}, \mathbf{U}_{0:t}, x_0)$.

2.4.3 Literature review on existing approaches

As stated in Section 2.4.1, the proximity-based UHF RFID indoor localization solutions can be categorized into reader-based, tag-based and ST-based methods. These methods are based on localizing objects using binary measurements. Binary measurements indicate whether the device is present or absent within the detection range of the landmarks. This section analyzes the literatures to gather knowledge on proximity-based UHF RFID indoor localization solutions in terms of the assumed model, localization algorithms and performance.

Reader-based method

a. An accurate and efficient object tracking system [7]

The author presents an object tracking system in indoor environment, which considers continuously locating RFID reader with passive RFID tags deployed as landmarks in the environment.

The assumed probabilistic sensing model of a specific tag by RFID reader is proposed as

$$p(r) = \begin{cases} \lambda e^{-\beta r^{\alpha}}, r \leq tr \\ 0, r > tr. \end{cases} \tag{2.24}$$

all tags that lie beyond the distance tr have the probability of 0 to be detected while tags lying within the range of tr have a detection probability that exponentially decreases as the distance r increases. λ, α and β are model parameters.

This work proposes a hybrid method which combines particle filter (PF) with weighted centroid localization (WCL). Based on the observation WCL has the same accuracy as PF with much lower cost if the object's velocity is low, which is due to the WCL algorithm itself and the measurement model of PF. The target keeps moving when the reader is gathering data. WCL method is extended in time domain. The current location is estimated by smoothing RFID readings of recent N observations. Historical RFID readings are assigned different weights, among which the latest RFID reading is given the largest weight based on the time elapsed and target velocity. Therefore, when the velocity of target is low the localization accuracy of WCL is higher compared with the target moving at high velocity.

In PF algorithm, two models are proposed: first, state evolution model, which uses the velocity estimation of target as control input; second, a measurement model, which is based on the Bernoulli distribution. The measurement model is given by

$$p(z_k|l_k) = \prod_{i=1}^{M} p(r_k^i|l_k) \tag{2.25}$$

$$p(r_k^i|l_k) = r_k^i p(d_i) + (1 - r_k^i)(1 - p(d_i)) \tag{2.26}$$

where d_i is the distance of landmark i from target and $p(d_i)$ is the RFID sensor model in Equation 2.28. $z_k = \{r_k^i\}_{i=1}^{M}$ are the RFID readings from M landmarks.

When the velocity of target is low, the measurement model does not benefit from more measurements for certain target locations, which is in the form of Bernoulli distribution. We could anticipate that the localization performance of PF would be improved by modifying the measurement model to Binomial distribution based on aggregated binary measurements.

The key ingredient of the algorithm is the estimation of target velocity. This work roughly estimates the average speed as

$$v = \frac{2tr \cdot c}{d_{max}(N)} \tag{2.27}$$

$d_{max}(N) = max\ d_i$. The time duration $d_i(N)$ in which the tag i stays in the reader's reading range in the last N time slots. c is scaling constant depending on the landmark tag density.

The simulation is conducted in the scenario, where the tags are densely deployed onto the plane. The spacing size of tags was 0.27 m. The reading range of the reader is 0.3 m. The average of localization error achieves 0.062 m.

***b*. Indoor navigation system for visually impaired people** [45]

The indoor navigation system allows the user to move autonomously resorting to a grid of UHF RFID tags for localization and simple procedures to plan the route. Since UHF RFID tags have longer detection range and less constraints in placing the tags in the environment compared to HF and LF tags, UHF RFID tags can be placed far from the path of the user, like the ceiling, allowing more degrees of freedom for localization infrastructure.

In the proposed localization infrastructure, a grid of UHF RFID tags is deployed on the ceiling of the whole building. The tag on the ceiling is detected when it enters the read region of RFID reader, which is a space that the power collected by the tag exceeds the tag sensitivity. The read region of each tag is shown as an ellipse tangent to the ceiling in Figure 2.17. Therefore, the cross section of read regions at 1 m from the floor are the circles with center at the position of each tag.

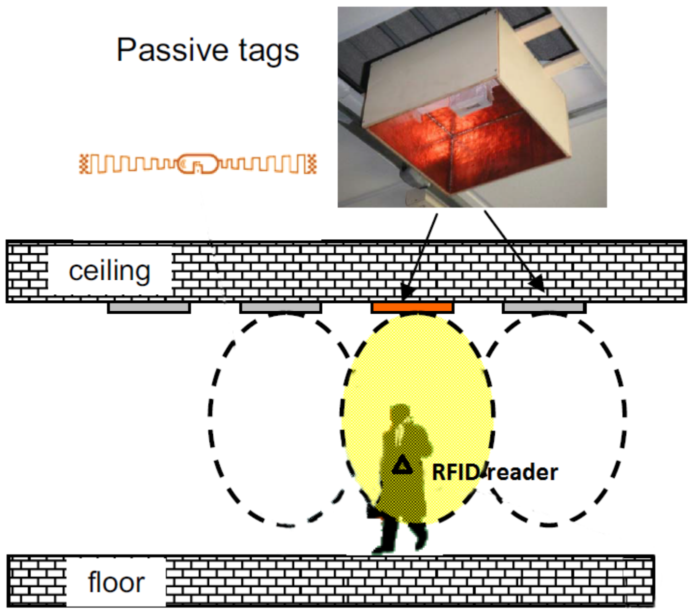

Figure 2.17: Localization infrastructure

The assumed sensing model of a specific tag by RFID reader is

$$p(r) = \begin{cases} 1, r \leq tr \\ 0, r > tr. \end{cases} \tag{2.28}$$

r is the distance between reader to tag's projection on the cross section of read region of the tag at the horizontal plane of reader.

The localization algorithm is simple, which is based on the centroid localization. The experiment is conducted in lab environment. The UHF RFID tags are deployed on the ceiling with 3 m height to form a square mesh having 1.2 m space. The localization error is lower than 0.5 m.

In [46], the same author proposes to localize indoor autonomous vehicle in the infrastructure as shown in Figure 2.17. The author designs a Kalman filtering-based method to fuse RFID readings with the vehicle odometry data. The localization error of the proposed system achieves 0.135 m.

Tag-based method

a. Indoor tracking system with a network of RFID readers [12]

The author proposes a method for accurate real time tracking of objects tagged by UHF RFID tags with a network of RFID readers. The method is based on the aggregated binary measurements in the number of times that a tag is detected while it is in the read range of RFID reader. The tracking of tagged objects are performed by particle filter.

The probability of the tag being detected by a reader is a random variable $p(d)$, where d is the distance between the tag and the reader. The distribution $p(d)$ is modelled by Beta distribution.

$$\pi(p(d)) \quad \propto \quad p(d)^{\alpha(d)-1}(1-p(d))^{\beta(d)-1} \tag{2.29}$$

where $\alpha(d)$ and $\beta(d)$ are the parameters. The mean of $p(d)$ is assumed to have the form

$$E(p(d)) \quad = \quad \frac{1}{1+e^{a(d-d_0)}} \tag{2.30}$$

where $a > 0$, and $d_0 > 0$ is the distance from reader where the detection probability is 1/2. The mean of Beta random variable is $\alpha(d)/(\alpha(d)+\beta(d))$. Therefore, we have

$$\frac{\alpha(d)}{\alpha(d)+\beta(d)} = \frac{1}{1+e^{a(d-d_0)}} \tag{2.31}$$

The variance of $p(d)$ is assumed to have the form

$$\sigma^2(d) = \sum_{i=0}^{6} c_i d^i \tag{2.32}$$

where $\{c_i, i = 0, \cdots, 6\}$ are parameters. Modelling the variance of $p(d)$ as polynomial regression comes as a result of Taylor expansion of the variance as a function of d. With the known variance of Beta random variable, we have

$$\frac{\alpha(d)\beta(d)}{(\alpha(d)+\beta(d))^2(\alpha(a)+\beta(d)+1)} = \sum_{i=0}^{6} c_i d^i \tag{2.33}$$

With the mean $E(p(d))$ and variance $\sigma^2(d)$, we can uniquely obtain the $\alpha(d)$ and $\beta(d)$. Then we could determine the distribution $\pi(p(d))$ of $p(d)$.

Each reader sends a fixed number N of queries in a fixed time interval, the number of reads is n is given by binomial distribution

$$p(n|p(d), d) = \binom{N}{n} p(d)^n (1-p(d))^{N-n} \tag{2.34}$$

Since $p(d)$ is random variable, $p(n|d)$ is

$$p(n|d) = \int_0^1 p(n|p, d)\pi(p)dp \tag{2.35}$$

$$= \binom{N}{n} \frac{B(n+\alpha(d), N-n+\beta(d))}{B(\alpha(d), \beta(d))} \tag{2.36}$$

where $B(\cdot, \cdot)$ is the Beta function.

With the obtained model the author designs a particle filtering scheme to track tagged objects based on the readings. The simulation is conducted in the scenario, in which a network of RFID readers are deployed to form a square mesh having 10 m between neighboring readers. For both of these two papers, the velocity of target attached with RFID reader is 1 m/s, and variance of the zero mean Gaussian noise is 0.01. Therefore, the dynamic pattern of target is comparatively linear with constant speed. The average of localization error is around 1 m.

***b*. Indoor tracking with RFID systems [8]**

In this paper, the same author addresses the indoor tracking of tagged objects with a network of RFID readers. A new and more realistic detection probability model is proposed. The detection probability is described by Beta distribution. The probability of detection is modelled as a function of distance and angle between the tag and the reader. In addition, the model also accounts for the possibility that the tag is placed in the dead-zone.

Besides the proposed detection probability model, the novelty of the paper is that an asynchronism of RFID readings is described, and a particle filtering-based method is proposed to resolve this problem. Each reader sends a fixed number N of queries in a fixed time interval between $(k-1)T_s$ and kT_s. In an ideal synchronous system, all the measurements are obtained by the readers at the sampling instance kT_s as in Figure 2.18(a). However, in the real system the measurements are obtained asynchronously, but mistakenly considered as synchronous measurements as in Figure 2.18(b).

Figure 2.18(c) depicts the true asynchronous measurements. Let the random measure at the time instance $(k-1)T_s$ be $\chi_{(k-1)T_s} = \{x^{(m)}_{(k-1)T_s}, w^{(m)}_{(k-1)T_s}\}_{m=1}^{M}$, where $x_{(k-1)T_s}$ are the particles of the measure, and $w^{(m)}_{(k-1)T_s}$ denotes the corresponding weights. Suppose the first available reading in the k_{th} round is at the time instance $\tau_{1,k}$ and the measurement is $y_{1,k}$. First, the particles are propagated according to

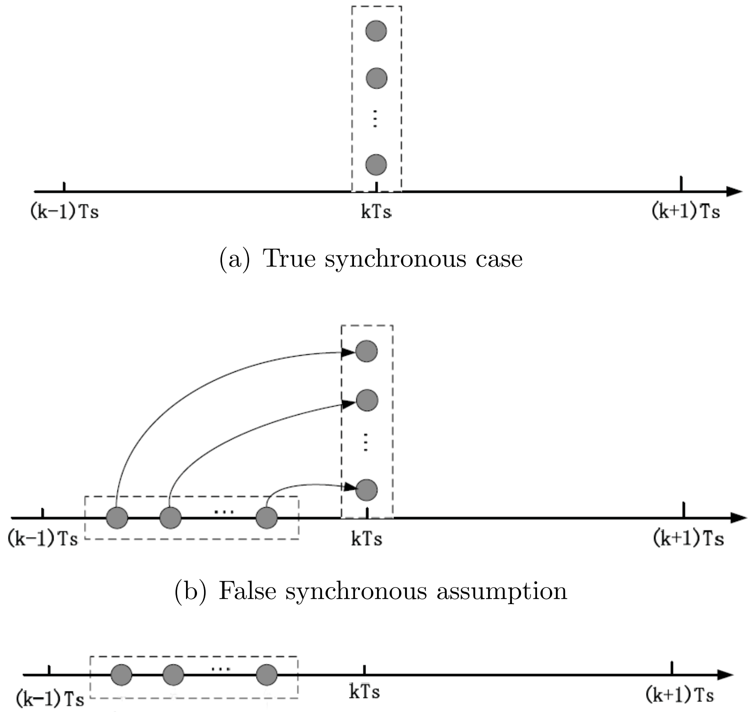

(a) True synchronous case

(b) False synchronous assumption

(c) True asynchronous case

Figure 2.18: Synchronous and asynchronous measurements.

state evolution model

$$x_{\tau_{1,k}}^{(m)} \sim p(x_{\tau_{1,k}} | x_{(k-1)T_s}^{(m)}) \tag{2.37}$$

Next, the weights are updated according to the measurement model given the measurements $y_{1,k}$.

$$w_{\tau_{1,k}}^{(m)} \propto w_{(k-1)T_s}^{(m)} p(y_{1,k} | x_{\tau_{1,k}}^{(m)}) \tag{2.38}$$

The Equation 2.38 is an approximation to capture the measurement information from one round of N queries. The location of the tag changes during the N queries.

Through the proposed particle filter the asynchronous measurements during the N queries are addressed. The simulation is conducted in the scenario, which is the same with the previous analyzed paper. The localization error is around 1 m with the proposed PF, while the localization error is around 1.5 m with the PF with false synchronous assumption.

ST-based method

a. A semi-passive RFID system for indoor localization [5]

This paper is the seminal work on ST, which describes the design of ST and explores several applications for ST. One of the major applications is to investigate the ST-based indoor localization. The goal is to achieve satisfactory localization accuracy without any calibration after the landmark tags are placed in the environment.

There are M landmark tags placed at known locations $x_i, i = 1, \cdots, M$ and one ST at unknown location l. A landmark tag can be detected by ST with the probability p_i, which is estimated by counting the number of detection out of a fixed number of reader queries. With the obtained detections the author proposes three location inference algorithms as association, centroid localization and weighted centroid localization.

First, the location of ST is associated with the nearest landmark tag. The proximity is measured by comparing the p_i of landmark tags.

Second, the location of ST is estimated by the centroid of the locations of detected landmark tags.

$$\hat{l} = \frac{\sum_i x_i}{n} \tag{2.39}$$

where n is the total number of landmark tags detected by ST.

Third, the location of ST is estimated by the weighted average of the locations of the detected landmark tags.

$$\hat{l} \;=\; \sum_i \hat{p}_i x_i = \sum_i \frac{n_d^i}{n_q} x_i \tag{2.40}$$

where n_q is the number of queries, n_d^i is the number of detections of i_{th} landmark tag by ST.

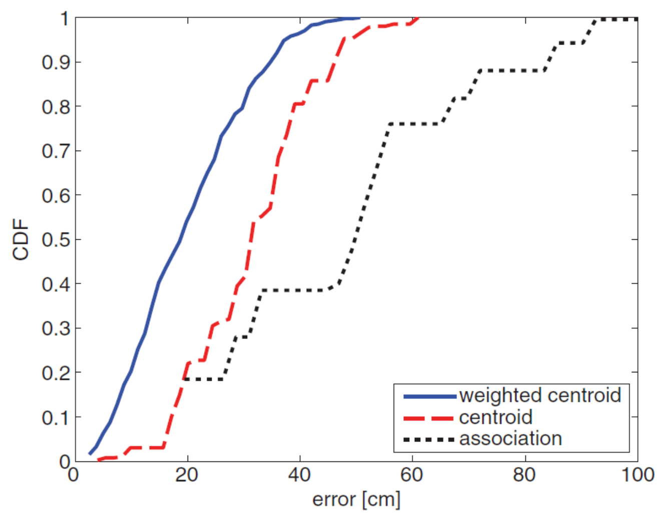

Figure 2.19: CDF of location errors for three inference algorithms.

To evaluate these three inference algorithms the author deployed 12 landmark tags at 6 reference points, where two tags per point. The area is 1.6 $m \times 1.2$ m. The reader is located 1.8 m above the center of the plane of ST and landmark tags. The author provides the CDF of the location error of the three algorithms in Figure 2.19. The probability of location error being less than 40 cm is about 40% for association algorithm, 82% for centroid algorithm and 95% for WCL. We can see that WCL performs better than the other two algorithms. However, one problem in the experiment is that the author does not provide the number of query rounds.

***b*. Indoor ST tracking with PF** [11]

The author proposes to track ST-tagged objects with RFID system based on aggregated binary measurements. First, the probability of detection of a tag by a ST is modelled as

$$p(d) = \frac{1}{1+e^{a(d-d_0)}} \tag{2.41}$$

where d is the distance between ST and the tag, $a > 0$, $d_0 > 0$ are model parameters. d_0 is the distance where the probability of detection being $1/2$, and a is the parameter which determines the steepness of function curve.

To design the particle filtering-based inference algorithm this work uses the following state evolution model.

$$x_{t+1} = Ax_t + Bu_t \tag{2.42}$$

and

$$A = \begin{pmatrix} 1 & 0 & T_S & 0 \\ 0 & 1 & 0 & T_S \\ 0 & 0 & 1 & 0 \\ 0 & 0 & 0 & 1 \end{pmatrix} \qquad B = \begin{pmatrix} T_S & 0 \\ 0 & T_S \\ 1 & 0 \\ 0 & 1 \end{pmatrix}$$

where $x_t = [x_{1,t}, x_{2,t}, \dot{x}_{1,t}, \dot{x}_{2,t}]^T$ is the state vector at time t. The first two elements of the state vector denote the location of target in the two-dimension Cartesian coordinate system, and the other two elements are the velocity of the target. $u_t = [u_{1,t}, u_{2,t}]^T$ is the process noise with known distribution which accounts for the variation of target speed.

The measurements are the detections of a tag by ST in N query rounds. Therefore, the probability of n_k times of detections is modelled by binomial distribution.

$$P(n_k) \quad = \quad \binom{N}{n_k} p_k^{n_k}(1-p_k)^{N-n_k} \tag{2.43}$$

where p_k is according to Equation 2.41 for the k_{th} landmark tag. Let's consider that there are K landmark tags, the number of detections for them is $\{n_k|0 \leq n_k \leq N\}_{k=1}^{K}$.

With the state evolution model and measurement model, the author proposes particle filtering-based algorithm. To evaluate the proposed algorithm this work conduct extensive computer simulation. 16 landmark tags are deployed in 4 m × 4 m. The mean RMSE of location error is around 0.25 m.

Summary

Through the study of state-of-art works related to proximity-based UHF RFID indoor localization, this section clarifies the assumed model, inference algorithm and localization performance of existing approaches. There are also other studies [6, 47, 59, 60] covering the similar topics. A comparison table with 7 analyzed works is presented in Table 2.2.

In general, the reader-based approach is capable to provide highly accurate localization for indoor environment. But the cumbersome, complex and energy-demanding RFID reader confines the application to localize certain sizable and expensive objects, such as autonomous household robot. The tag-based approach is less popular than the reader-based approach. The read range of RFID readers is comparatively large, thus the proximity information could not represent the tag's location accurately. On the other hand, it is not cost-efficient to densely deploy readers merely exploiting proximity information. While for ST-based methods the problems could be found in Section 1.1, which are listed as our primary research challenges. The existing approaches for ST-based solutions do not tackle the phase cancellation effect. The particle filtering-based algorithm should address the asynchronism of detections of ST-to-tag and constraint state evolution model. Furthermore, the localization capability of ST-based AURIS could expand to passive tags with unknown locations, which in turn benefits the localization of ST.

2.4.4 PASS simulation framework

Proximity-detection-based **A**ugmented UHF RFID **S**ystem **S**imulator (PASS) is a time-domain system-level MATLAB-based simulator, which is based on position aware RFID system (PARIS) simulator [61, 62]. From PARIS simulation framework, PASS inherits the behavioral model of a NXP UCODE G2XM-based passive UHF RFID tags and wireless propagation channel, as well as a core framework to perform simple control and logging. While PARIS mainly focuses on channel modeling and ranging with UWB signal rather than system behavior, PASS completes the functionality of generic reader and tag, by which the simulator behaves according to ISO 18000-6C protocol. Further, the behavioral model of ST is developed, and is integrated into the simulation framework. PASS provides accurate physical models and lots of powerful functions. Various characteristics of implemented RFID models can be configured, such as scenario deployment, parameters of wireless channel and so on. With the simulator-provided functions and basic functions, behaviors of implemented components in simulator can be measured, such as wireless signal delay and attenuation.

The PASS simulation framework is organized in a hierarchical fashion, shown in Figure 2.20. Following the modular and hierarchical design pattern, the levels of PASS hierarchy are separated, and different models for reader, tag, ST and channel are also strictly separated.

The user description script *st_room.m* defines the simulation setup, which is scenario-dependent. The setup is transferred to the simulator via *setting* data structure. The behavior description script *sim_st_room.m* describes the type of simulation, the signal model, as well as the signal and control flow. The behavior description script configures the behavior of components through maintaining the *setting* struct. Reader, tag, ST and channel are controlled by the basic main function based on the common interface for the underlying model, calculation and characteristic lookup table.

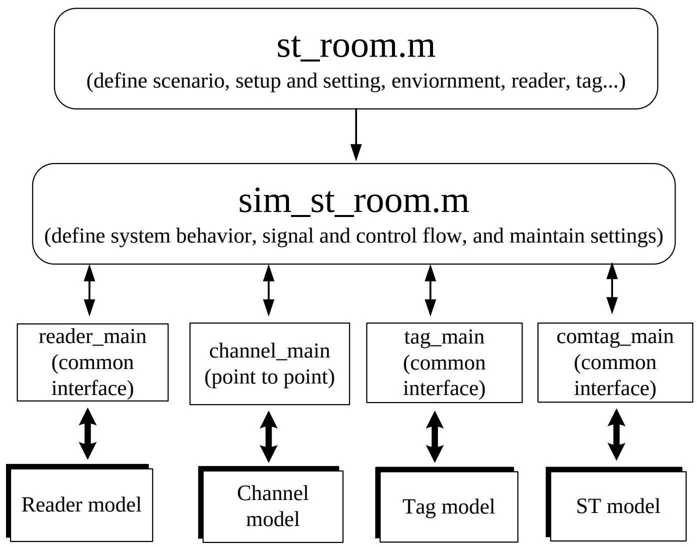

Figure 2.20: The hierarchical structure of PASS

In this section we briefly introduce the large-scale model and statistical small-scale model under the channel model, which are inherited from PARIS. Besides that, the channel model also includes virtual transmitter model, which accounts for surface reflection. The detailed structure and component description are presented in Appendix A. The software and tutorial are available on Github repository `https://github.com/wacoder/PASS.git`.

Large-scale model

In the simulator the large-scale power gain is obtained according to Friis equation

$$\Theta_{LS} \propto (\frac{c}{4\pi f_c d})^{\xi} \tag{2.44}$$

and the propagation delay is

$$\tau_{LS} = round(\frac{f_s d}{c}) \tag{2.45}$$

where c is the speed of light, f_c is the carrier frequency, d is the path length, f_s is the sampling frequency of the simulator, and ξ is the path loss factor.

Directivity patterns of antenna are implemented using lookup tables. These characteristics are loaded from files, which are either 2×2 dimensions or full 3 dimensions gain patterns.

Statistical small-scale model

Statistical small-scale model is implemented according to an exponentially decaying continuous average power-delay profile (APDP), which is defined as

$$\bar{\psi}(\tau) = \begin{cases} 0 & , \tau < 0 \\ \rho^2 \delta(\tau) & , \tau = 0 \\ \Pi e^{-\gamma\tau} & , \tau > 0 \end{cases} \tag{2.46}$$

where τ is the delay, ρ^2 is the power of LoS, $\delta(\tau)$ is the Dirac function, and Π is the NLoS power density. The K-factor and RMS delay spread of this APDP are

$$K_{LoS} = \frac{P_{LoS}}{P_{NLoS}} = \frac{\rho^2 \gamma}{\Pi} \tag{2.47}$$

and

$$\tau_{RMS} = \frac{1}{\gamma} \cdot \frac{\sqrt{2K_{LoS} + 1}}{K_{LoS} + 1} \qquad (2.48)$$

Table 2.2: Comparison table of the analyzed solutions

Solution	Category	Algorithm	Accuracy	Pros	Cons
[7]	Reader-based	WCL + PF	$\sim 0.062\ m$	• High accuracy • Comparatively low computation cost	• RFID reader as mobile target • PF's localization accuracy is not satisfactory compared with WCL • Rough velocity estimation
[45]	Reader-based	Centroid	$\sim 0.5\ m$	• Low computation cost • Simple localization infrastructure	• RFID reader as mobile target • Low accuracy for expensive RFID reader as mobile target
[46]	Reader-based	Kalman filter	$\sim 0.135\ m$	• High accuracy • Simple localization infrastructure	• RFID reader as mobile target • Extra motion sensor data
[12]	Tag-based	PF	$\sim 1\ m$	• More realistic detection probability model • Satisfactory accuracy with the landmark density	• Low accuracy for small items to which passive tags are attached • It is waste for RFID readers to merely exploiting proximity information

Solution	Category	Algorithm	Accuracy	Pros	Cons
[8]	Tag-based	PF	$\sim 1\ m$	• More realistic detection probability model • PF resolving the asynchronous case of RFID readings • Satisfactory accuracy with the deployment density of the readers	• Low accuracy for small items to which passive tags are attached • It is waste for RFID readers to merely exploiting proximity information • The state evolution model of PF could not handle sharp maneuver and speed change
[5]	ST-based	Association Centroid WCL	Figure 2.19	• Both landmarks and mobile targets are simple and inexpensive • Low computation cost • Simple localization infrastructure	• Location accuracy can be improved with more complex algorithms • It is difficult to compare with other algorithms since it does not provide the number of query rounds

Solution	Category	Algorithm	Accuracy	Pros	Cons
[11]	ST-based	PF	$\sim 0.25\ m$	• Both landmarks and mobile targets are simple and inexpensive • Satisfactory accuracy • Simple localization infrastructure	• The model of detection probability is too ideal and simplistic • The state evolution model of PF could not handle sharp maneuver and speed change • The asynchronism of ST-to-tag detections is not addressed

Chapter 3

Phase cancellation in AURIS

Backscatter radio - the broad system that communicates using scattered electromagnetic waves - is the driving technology behind RFID [63]. The research on backscatter radio has grown drastically in recent year, and it even extends to other technologies including Bluetooth and WiFi [30, 31]. UHF RFID provides superior performance among passive RFID systems, ensuring a larger operating distance (up to several meters), a high data rate (up to hundreds of kb/s), and smaller antenna size [2]. The conventional UHF RFID system is characterized as asymmetric communication where the majority of communication burden is shifted to the carrier-modulated transceiver RFID reader. Both reader-to-tag and tag-to-reader communication link have been thoroughly studied [63–65].

Unlike the conventional UHF RFID reader, tag-to-tag communication relies on neither an active radio for transmitting query signal nor a full-scale IQ demodulator to receive the response. It relies purely on backscatter modulator to convey data to other tags and passive envelope detector for receiving the response. In AURIS, during the communication between ST and passive tag, the RFID reader must transmit CW for tag to backscatter. Consequently, the signal at the ST's antenna is the superposition of reader's CW and the passive tag's backscattering signal. Unfortunately, due to the random phase difference between these two signals, the modulation depth of

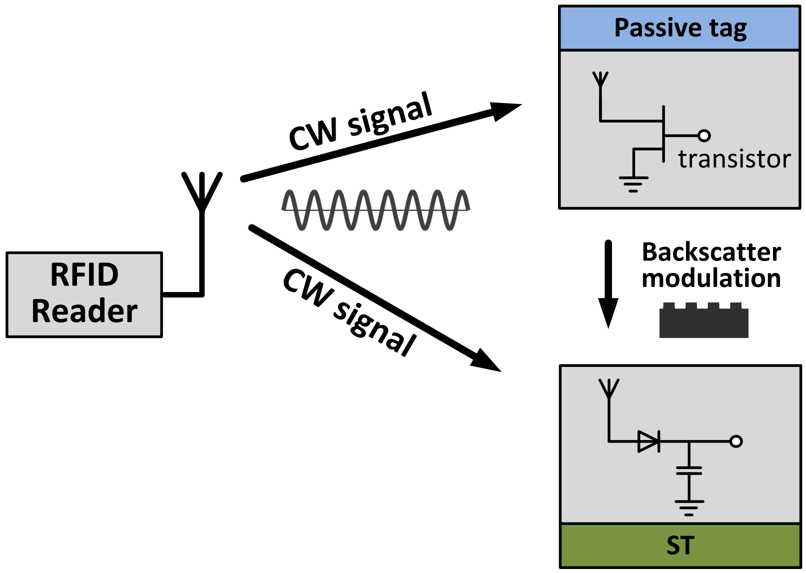

Figure 3.1: Schematic depiction of ST-to-tag backscatter link

tag's backscattering signal at ST's envelope detector could be significantly attenuated or even cancelled out. We refer such effect as phase cancellation effect. The phase cancellation effect originates from the very nature of tag-to-tag backscatter communication. Since the proximity-based localization method purely depends on successive detection of proximal tags by ST, handling the challenge of phase cancellation effect is the critical step to achieve robust localization.

3.1 Problem formulation

Figure 3.1 depicts the scheme of ST-to-tag backscattering communication link wherein the CW signal is provided by RFID reader. In this section, we will analyze the phase cancellation in detail while passive tag employs ASK and PSK modulation respectively.

3.1.1 ASK modulated tag's backscattering signal

Let's assume that A_R is the amplitude of the reader CW at the ST antenna. The passive tags apply ohmic load modulation, thus the backscattering is ASK modulated signal. Let A_{T1} and A_{T2} be the amplitudes of the tag backscattering in the two different RCS states. Let θ be the relative phase between the reader signal and the tag signal. Then the resultant signals at the ST antenna for the two RCS states are given as following:

$$\begin{cases} S_1 &= A_R e^{j\omega t} + A_{T1} e^{j(\omega t+\theta)} \\ S_2 &= A_R e^{j\omega t} + A_{T2} e^{j(\omega t+\theta)} \end{cases} \tag{3.1}$$

The sinusoidal form of the signal is the real part of the phasor expression. Let's denote the sinusoidal functions by C_1, C_2 respectively.

$$\begin{cases} C_1(t) &= A_R cos(\omega t) + A_{T1} cos(\omega t + \theta) \\ &= A_R cos(\omega t) + A_{T1} cos(\omega t) cos(\theta) - A_{T1} sin(\omega t) sin(\theta) \\ C_2(t) &= A_R cos(\omega t) + A_{T2} cos(\omega t + \theta) \\ &= A_R cos(\omega t) + A_{T2} cos(\omega t) cos(\theta) - A_{T2} sin(\omega t) sin(\theta) \end{cases} \tag{3.2}$$

The amplitude of the signals as detected by the envelope detector in two RCS states could be written as

$$\begin{cases} A_1 &= \sqrt{(A_R + A_{T1} cos(\theta))^2 + (A_{T1} sin(\theta))^2} \\ &= \sqrt{{A_R}^2 + 2 A_R A_{T1} cos(\theta) + {A_{T1}}^2} \\ A_2 &= \sqrt{(A_R + A_{T2} cos(\theta))^2 + (A_{T2} sin(\theta))^2} \\ &= \sqrt{{A_R}^2 + 2 A_R A_{T2} cos(\theta) + {A_{T2}}^2} \end{cases} \tag{3.3}$$

The ability of ST to detect backscatter from tags depends on the small change of the superimposed signal's amplitude. The larger this change is, the higher is the likelihood that the ST will detect tags' backscatter. The value of amplitude change $|A_1 - A_2|$ is

$$\begin{aligned} |A_1 - A_2| &= \left| \sqrt{A_R^2 + 2A_R A_{T1} cos(\theta) + A_{T1}^2} - \sqrt{A_R^2 + 2A_R A_{T2} cos(\theta) + A_{T2}^2} \right| \\ &= \frac{|A_{T1} - A_{T2}||A_{T1} + A_{T2} + 2A_R cos(\theta)|}{\sqrt{A_R^2 + 2A_R A_{T1} cos(\theta) + A_{T1}^2} + \sqrt{A_R^2 + 2A_R A_{T2} cos(\theta) + A_{T2}^2}} \end{aligned} \tag{3.4}$$

The complete phase cancellation effect occurs when $A_1 = A_2$. From the equation sets above, we could know that the phase cancellation will occur when

$$\theta_{cancel} = \arccos\Big(- \frac{A_{T1} + A_{T2}}{2A_R} \Big) \tag{3.5}$$

The condition of phase cancellation effect is satisfied by certain combination of θ, A_R, A_{T1} and A_{T2}, which are dependent on the distance, tag's RCS and the wireless channel. Besides that, any amplitude difference $|A_1 - A_2|$ that is lower than ST's sensitivity, would be missed by the ST. Theoretically, for some locations ST would completely miss the tag due to such destructive superposition. The localization accuracy would be deteriorated significantly, since the localization algorithm mainly depends on the read rate of tags on the ST side. The destructive superposition takes effect at the ST antenna. Thus it is difficult to address this problem through modifying the demodulation or signal processing method of the ST receiving path.

Figure 3.2 shows the phasor diagram of the superimposed signal at ST antenna according to Equation 3.1 and 3.2. The dotted circles represent the locus of A_{T1} and A_{T2} with varying θ. Since the tag's backscattering modulation applies ASK, A_{T1} and A_{T2} have the same θ. Figure 3.2(a) depicts an example with no phase cancellation.

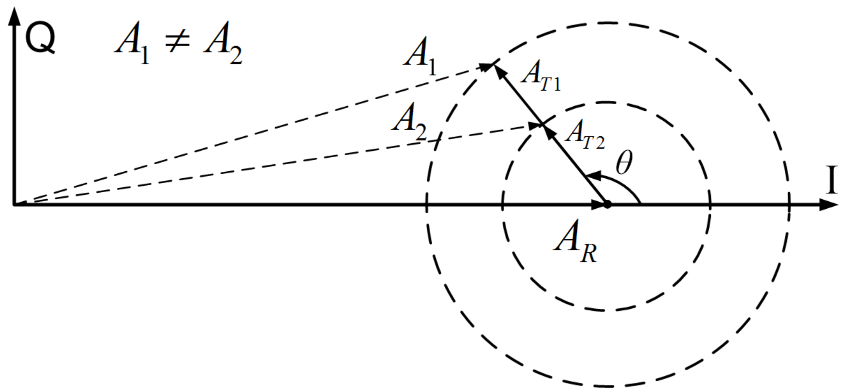

(a) Without phase cancellation

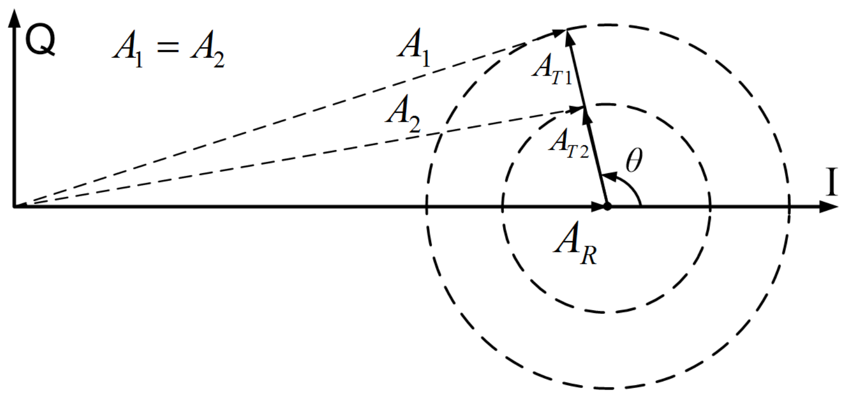

(b) With phase cancellation

Figure 3.2: Phasor diagram that shows superimposed signal at the ST antenna when the tag transmits logic zero and logic one with ASK modulation.

The envelope amplitude A_1 and A_2 are not equal, thus the ST could capture tag's backscattering information. Figure 3.2(b) depicts an example with phase cancellation. In this case, the amplitude difference $|A_1 - A_2|$ is negligible and $\theta \approx \theta_{cancel}$.

The amplitude difference $|A_1 - A_2|$ of the superimposed signals at the ST antenna with varying θ from $-\pi$ to π is shown in Figure 3.3. According to the backscattering principle A_{T1} and A_{T2} are expressed as fraction of A_R. A_R can be normalized to 1. A_{T1} and A_{T2} are varied, but they are kept smaller than A_R. The amplitude of $|A_1 - A_2|$ is calculated in MATLAB according to Equation 3.4. As from the figure, we could see that the maxima of $|A_1 - A_2|$ occurs at $\theta = 0$ and $\theta = \pm\pi$. As the value of

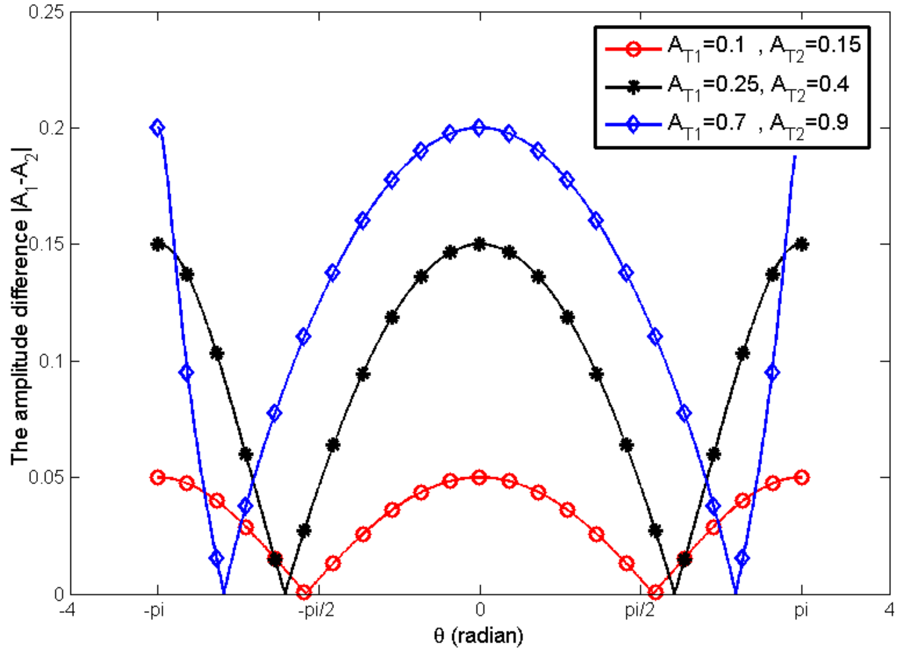

Figure 3.3: Variations of amplitude difference $|A_1 - A_2|$ with varying θ ($A_R = 1$)

summation of A_{T1} and A_{T2} decreases, θ_{cancel} approaches $\pm\pi/2$ from $\pm\pi$ respectively.

3.1.2 PSK modulated tag's backscattering signal

Let's assume that A_R is the amplitude of the reader CW at the ST antenna. Applying capacitive load modulation, tag's backscattering signal is PSK modulated. The amplitude of tag's backscatter signal remains constant for two RCS states, while the phase of RCS states varies. Let A_T be the amplitude of the tag backscattering signal, and ψ be the phase difference of two RCS states. Let θ be the relative phase difference between the reader CW and the tag's backscattering signal. Then the resultant signals at the ST antenna for the two RCS states are given as following:

$$\begin{cases} S_1 = A_R e^{j\omega t} + A_T e^{j(\omega t+\theta)} \\ S_2 = A_R e^{j\omega t} + A_T e^{j(\omega t+\theta+\psi)} \end{cases} \tag{3.6}$$

The sinusoidal form of the signal is the real part of the phasor expression. Let's denote the sinusoidal functions by C_1, C_2 respectively.

$$\begin{cases} C_1(t) &= A_R cos(\omega t) + A_T cos(\omega t + \theta) \\ &= A_R cos(\omega t) + A_T cos(\omega t) cos(\theta) - A_T sin(\omega t) sin(\theta) \\ C_2(t) &= A_R cos(\omega t) + A_T cos(\omega t + \theta + \psi) \\ &= A_R cos(\omega t) + A_T cos(\omega t) cos(\theta+\psi) - A_T sin(\omega t) sin(\theta+\psi) \end{cases} \tag{3.7}$$

The amplitude of the signals as detected by the envelope detector in two RCS states could be written as

$$\begin{cases} A_1 &= \sqrt{(A_R + A_T cos(\theta))^2 + (A_T sin(\theta))^2} \\ &= \sqrt{{A_R}^2 + 2A_R A_T cos(\theta) + {A_T}^2} \\ A_2 &= \sqrt{(A_R + A_T cos(\theta+\psi))^2 + (A_T sin(\theta+\psi))^2} \\ &= \sqrt{{A_R}^2 + 2A_R A_{T2} cos(\theta+\psi) + {A_T}^2} \end{cases} \tag{3.8}$$

The value of amplitude difference $|A_1 - A_2|$ is

$$\begin{aligned} |A_1 - A_2| &= \left| \sqrt{A_R^2 + 2A_R A_T cos(\theta) + A_T^2} - \sqrt{A_R^2 + 2A_R A_T cos(\theta + \psi) + A_T^2} \right| \\ &= \frac{2A_R A_T |cos(\theta) - cos(\theta + \psi)|}{\sqrt{A_R^2 + 2A_R A_T cos(\theta) + A_T^2} + \sqrt{A_R^2 + 2A_R A_T cos(\theta + \psi) + A_T^2}} \end{aligned} \tag{3.9}$$

As the case in ASK, the complete phase cancellation effect occurs when $A_1 = A_2$. This will occur when

$$cos(\theta) = cos(\theta + \psi) \tag{3.10}$$

Thus the null phase θ_{cancel} is

$$\theta_{cancel} = -\frac{\psi}{2} + k\pi, \quad \textit{where } k \textit{ is integer} \tag{3.11}$$

Figure 3.4 depicts the phasor diagram of the superimposed signal at the ST antenna according to Equation 3.6 and 3.7. The dotted circles represent the locus of A_{T1} and A_{T2} with varying θ. Since the tags' backscattering applies PSK modulation, A_{T1} and A_{T2} have the same amplitude A_T, the phase difference is ψ. Figure 3.4(a) shows an example when phase cancellation does not occur, $\theta \neq \theta_{cancel}$. In this case, ST could detect tag's backscattering information. Figure 3.4(b) shows an example which satisfies Equation 3.11 $\theta = \theta_{cancel}$. In this case, the amplitude A_1 and A_2 are the same when A_{T1} and A_{T2} are separated by the phase difference ψ.

The amplitude difference $|A_1 - A_2|$ of the superimposed signals at the ST antenna with varying θ from $-\pi$ to π is shown in Figure 3.5. As in ASK case, A_R is normalized

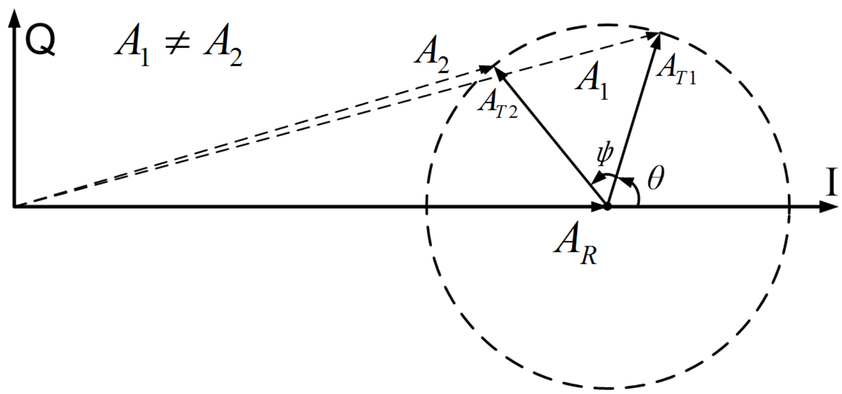

(a) Without phase cancellation

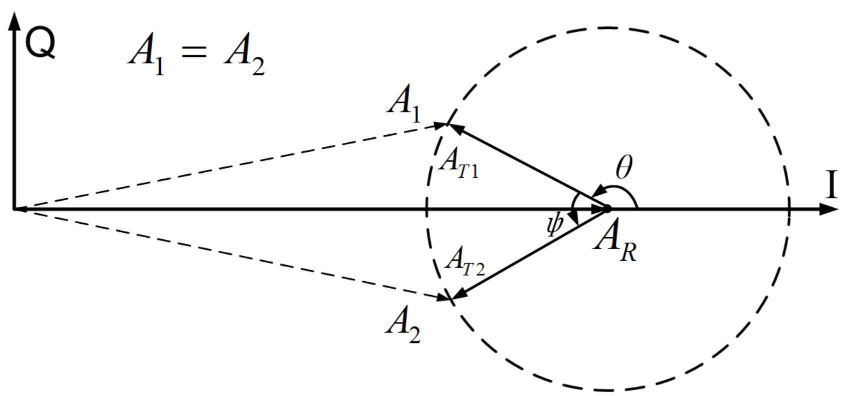

(b) With phase cancellation

Figure 3.4: Phasor diagram that shows superimposed signal at the ST antenna when the tag transmits logic zero and logic one with PSK modulation.

to 1, and A_T is set as 0.4. The calculation is conducted for four values of ψ as π, $\pi/2$, $\pi/4$ and $\pi/8$. The figure can verify that the phase cancellation occurs according to Equation 3.11. The maxima of the amplitude difference curve depends on the phase difference ψ. As phase difference ψ decreases from π to $\pi/8$, the level of amplitude difference $|A_1 - A_2|$ decreases as well. This situation is due to the decreasing Hamming distance for two RCS states with the same amplitude A_T.

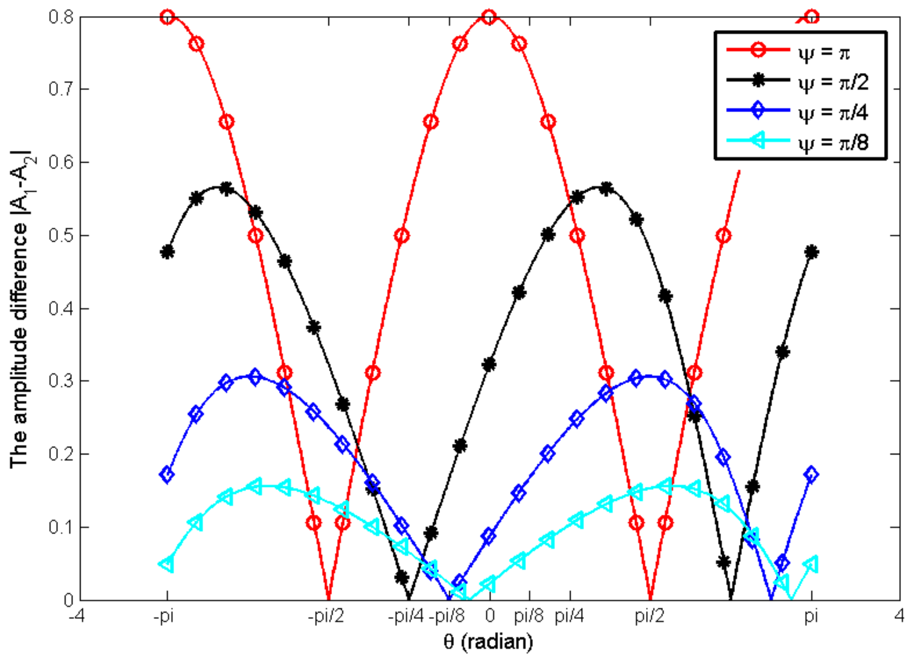

Figure 3.5: Variations of amplitude difference $|A_1 - A_2|$ with varying θ ($A_R = 1, A_T = 0.4$)

3.2 Dual-antenna technique

Phase cancellation effect originates from the nature of backscatter modulation and the unique design of ST. Destructive superposition takes effect at the ST's antenna, which excludes the possibility of system's awareness of the occurrence of phase cancellation. Thus it is difficult to counter the phase cancellation effect through altering parameters of wireless signals, such as the power and phase of transmitting signal, or the modulation scheme. The very nature of phase cancellation effect motivates the usage of dual antenna technique. Two ST antennas offer two reference points for the reception of the superimposed signal. With the introduction of spatial diversity, it is reasonable to expect that the likelihood of phase cancellation would be reduced. Signals from two antennas could be combined using several technique such as simple combination or the selection scheme [66]. The phase cancellation effect merely deteriorates the information-conveyed small amplitude difference in the superimposed signal, which is different from the destructive wireless multipath superimposition. Thus the combination method based on the signal noise ratio (SNR) of multiple receiving paths is not feasible [67]. The simple combination technique adds the receiving signals from the two ST antennas together. On the contrary, the receiving path selection technique depends on two parallel co-operating receiving path in ST. The specific description of these two techniques are presented in the following section.

3.2.1 Simple combination technique

The model for the simple combination of dual antenna is as following. Let us assume that A_R and $A_R{}'$ are the amplitude of the reader CW at the ST's antenna SA_1 and SA_2. Let $\{A_{T1}, A_{T2}\}$ and $\{A'_{T1}, A'_{T2}\}$ be the amplitude of the tag backscatter signal in two RCS states measured at the ST's antennas SA_1 and SA_2 respectively. Let θ and θ' be the relative phase difference between the reader CW and the tag's backscatter signal at the ST antennas. Such relative phase difference is the same for the tag's two RCS states because of the applied ASK modulation scheme. Let θ_1 be the relative phase difference between the reader's CW at the ST's two antennas. In addition, the radiation pattern of ST antennas are modelled as omnidirectional. The resultant signals at the ST antennas for the two RCS states are given as

$$\begin{cases} S_1(t) &= A_R e^{j\omega t} + A_{T1} e^{j(\omega t+\theta)} \\ S_2(t) &= A_R e^{j\omega t} + A_{T2} e^{j(\omega t+\theta)} \end{cases} \tag{3.12}$$

$$\begin{cases} S'_1(t) &= A'_R e^{j(\omega t+\theta_1)} + A'_{T1} e^{j(\omega t+\theta_1+\theta')} \\ S'_2(t) &= A'_R e^{j(\omega t+\theta_1)} + A'_{T2} e^{j(\omega t+\theta_1+\theta')} \end{cases} \tag{3.13}$$

Then the signals after the simple combination for the tag's two RCS states are

$$\begin{cases} \widehat{S_1} &= (A_R + A_R^{'} e^{j\theta_1}) e^{j\omega t} + (A_{T1} + A_{T1}^{'} e^{j(\theta_1 + \theta^{'} - \theta)}) e^{j(\omega t + \theta)} \\ \widehat{S_2} &= (A_R + A_R^{'} e^{j\theta_1}) e^{j\omega t} + (A_{T2} + A_{T2}^{'} e^{j(\theta_1 + \theta^{'} - \theta)}) e^{j(\omega t + \theta)} \end{cases} \tag{3.14}$$

Let

$$\begin{cases} \hat{A}_R e^{j\alpha} &= A_R + A'_R e^{j\theta_1} \\ \hat{A}_{T1} e^{j\beta_1} &= A_{T1} + A'_{T1} e^{j(\theta_1 + \theta' - \theta)} \\ \hat{A}_{T2} e^{j\beta_2} &= A_{T2} + A'_{T2} e^{j(\theta_1 + \theta' - \theta)} \end{cases} \tag{3.15}$$

According to Friis transmission equation [68], the power density PD at the ST's antenna from tag:

$$PD_{tag \to ST} = \frac{P_R G_R G_T \sigma}{(4\pi)^2 R^2 r^2} \tag{3.16}$$

In this simple form, P_R is the output power of the transmitting antenna of the reader, G_R is the reader antenna gain (with respect to an isotropic radiator), G_R is the tag antenna gain, σ is the RCS of the tag antenna, R is the distance between reader and tag's antennas, and r is distance between tag and ST's antenna.

On the tag side, the value of RCS for two backscatter states are σ_1 and σ_2 respectively. The distance from the tag's antenna to ST's antennas are r_1 and r_2. Moreover, the power of imping wireless signal is proportional to the square of the amplitude of the signal. Therefore,

$$\begin{array}{cc} \frac{\sigma_1}{r_1^2} \propto A_{T1}^2 & \frac{\sigma_2}{r_1^2} \propto A_{T2}^2 \\ \frac{\sigma_1}{r_2^2} \propto A_{T1}'^2 & \frac{\sigma_2}{r_2^2} \propto A_{T2}'^2 \end{array}$$

$$\Downarrow$$

$$\frac{A_{T1}}{A'_{T1}} = \frac{A_{T2}}{A'_{T2}} \tag{3.17}$$
$$\Downarrow$$
$$\beta_1 = \beta_2 = \beta$$

The resultant signal in Equation 3.14 could be written as following

$$\begin{cases} \widehat{S_1}(t) = \hat{A}_R e^{j\alpha} e^{j\omega t} + \hat{A}_{T1} e^{j(\beta+\theta)} e^{j\omega t} \\ \widehat{S_2}(t) = \hat{A}_R e^{j\alpha} e^{j\omega t} + \hat{A}_{T2} e^{j(\beta+\theta)} e^{j\omega t} \end{cases} \tag{3.18}$$

The sinusoidal form of the signals is the real part of the phasor expression. Let's denote the sinusoidal functions by C_1, C_2 respectively.

$$\begin{cases} C_1(t) = \hat{A}_R cos(\omega t + \alpha) + \hat{A}_{T1} cos(\omega t + \beta + \theta) \\ \quad = \hat{A}_R cos(\omega t) cos(\alpha) - \hat{A}_R sin(\omega t) sin(\alpha) + \\ \quad \hat{A}_{T1} cos(\omega t) cos(\beta + \theta) - \hat{A}_{T1} sin(\omega t) sin(\beta + \theta) \\ \\ C_2(t) = \hat{A}_R cos(\omega t + \alpha) + \hat{A}_{T2} cos(\omega t + \beta + \theta) \\ \quad = \hat{A}_R cos(\omega t) cos(\alpha) - \hat{A}_R sin(\omega t) sin(\alpha) + \\ \quad \hat{A}_{T2} cos(\omega t) cos(\beta + \theta) - \hat{A}_{T2} sin(\omega t) sin(\beta + \theta) \end{cases} \tag{3.19}$$

The amplitudes of the signals detected by the envelope detector for two RCS states are

$$\begin{cases} A_1 &= \sqrt{(\hat{A}_R cos(\alpha) + \hat{A}_{T1} cos(\beta+\theta))^2 + (\hat{A}_R sin(\alpha) + \hat{A}_{T1} sin(\beta+\theta))^2} \\ &= \sqrt{\hat{A}_R^2 + \hat{A}_{T1}^2 + 2\hat{A}_R \hat{A}_{T1} cos(\beta+\theta-\alpha)} \\ \\ A_2 &= \sqrt{(\hat{A}_R cos(\alpha) + \hat{A}_{T2} cos(\beta+\theta))^2 + (\hat{A}_R sin(\alpha) + \hat{A}_{T2} sin(\beta+\theta))^2} \\ &= \sqrt{\hat{A}_R^2 + \hat{A}_{T2}^2 + 2\hat{A}_R \hat{A}_{T2} cos(\beta+\theta-\alpha)} \end{cases} \tag{3.20}$$

The value of amplitude change is

$$|A_1 - A_2| = \frac{|\hat{A}_{T1} - \hat{A}_{T2}||\hat{A}_{T1} + \hat{A}_{T2} + 2\hat{A}_R cos(\beta+\theta-\alpha)|}{\sqrt{\hat{A}_R^2 + \hat{A}_{T1}^2 + 2\hat{A}_R \hat{A}_{T1} cos(\beta+\theta-\alpha)} + \sqrt{\hat{A}_R^2 + \hat{A}_{T2}^2 + 2\hat{A}_R \hat{A}_{T2} cos(\beta+\theta-\alpha)}} \tag{3.21}$$

The phase cancellation occurs when $A_1 = A_2$

$$\beta + \theta - \alpha = arcos(-\frac{\hat{A}_{T1} + \hat{A}_{T2}}{2\hat{A}_R}) \tag{3.22}$$

Figure 3.6 shows that the phasor diagram of the simple combination of two antenna inputs. $\hat{A}_R$ and α correspond to the phasor representation for the combination of reader's CWs at the ST's antennas. The two dotted circles represent the locus of $\hat{A}_{T1}$ and $\hat{A}_{T2}$ with varying phase $\beta+\theta$. 3.6(a) shows one example where phase cancellation does not occur, while 3.6(b) shows one example where phase cancellation does occur.

According to the phasor diagrams and Equation 3.21, the amplitude difference $|A_1 - A_2|$ depends on $\hat{A}_R$, $\hat{A}_{T1}$, $\hat{A}_{T2}$, α, β and θ. Nota that, for the single antenna

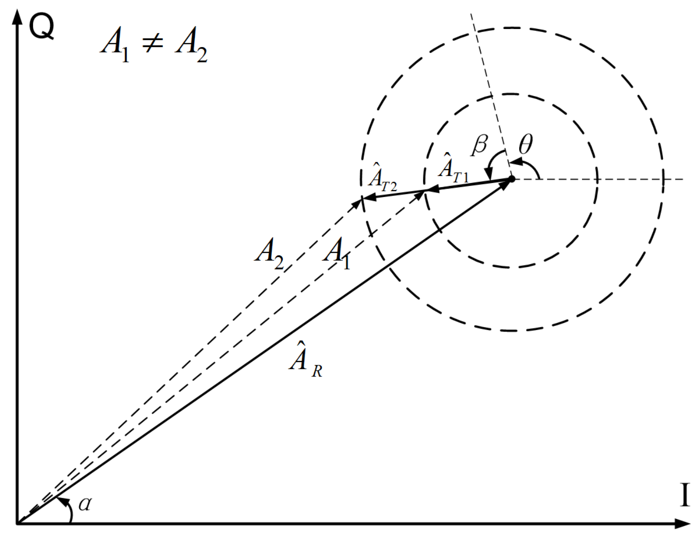

(a) Without phase cancellation

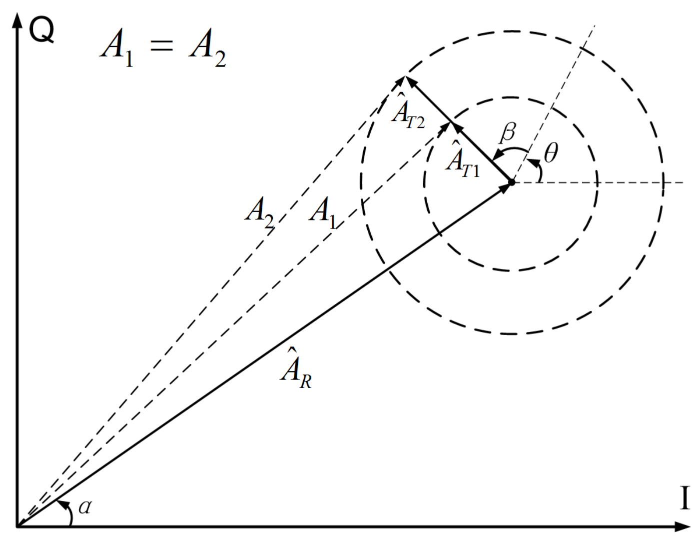

(b) With phase cancellation

Figure 3.6: Phasor diagram that shows superimposed signal at the ST antenna when the tag transmits logic zero and logic one.

implementation of ST the amplitude difference merely depends on A_R, A_{T1}, A_{T2} and θ. Consequently, the dual-antenna based simple combination technique possesses higher degree of freedom than that of the single antenna case. Intuitively, we could assume that there is less likelihood of phase cancellation occurrence for the simple

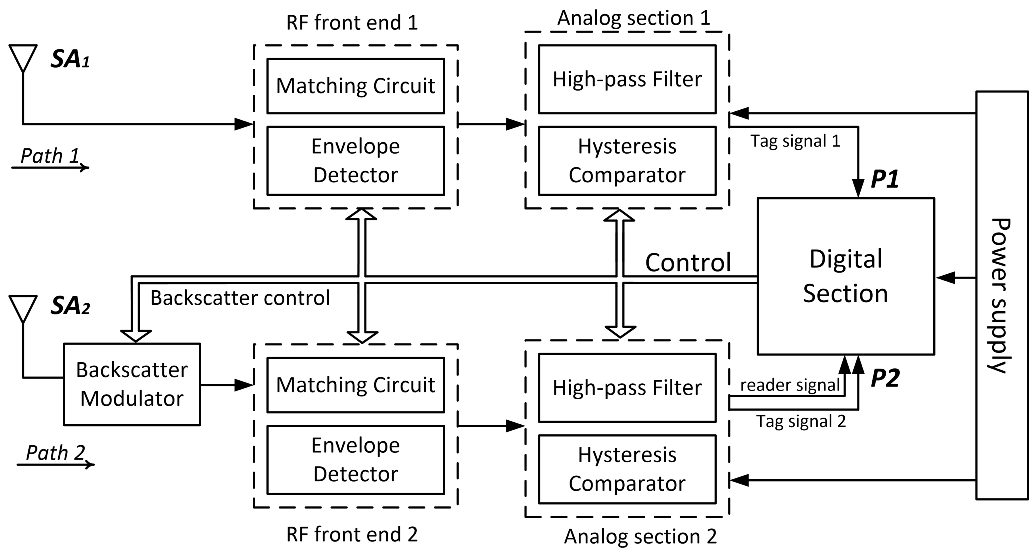

Figure 3.7: Block diagram of the ST model with receiving path selection technique

combination technique on account of diversity gain. In next section, we verify this assumption through simulation.

3.2.2 Receiving path selection technique

The diversity selection scheme with multiple antenna inputs has long been used in wireless communication system as a tool to mitigate multipath fading effect. Such scheme selects, among multiple diversity branches, the branch providing the largest SNR [67]. The receiving path selection scheme requires a novel ST design with the chance of resolving the phase cancellation in AURIS. The proposed approach is to implement two separate receiving paths for tag's backscattering in the ST. The block diagram of the new ST model is shown in Figure 3.7.

Figure 3.7 shows that the proposed structure of ST model has two major branches labelled as *Path1* and *Path2*. In *Path2* the full functionality of ST is implemented, and ST retains the capability to sense the backscattering communication between the reader and tags in its proximity, as well as backscatter the sensed information to the reader. In addition, *Path1* is an extra parallel co-operating receiving path based on the envelope detection technique. The embedded algorithm of ST inherits the EPCglobal Class1 Gen2 protocol-based ST locator protocol.

Following the ST locator protocol the ST does not respond, instead it just listens for the backscatter signal from tags. The main modification of the ST is that it is equipped with two co-operating receiving paths for the tags's backscatter signal. In *Path1*, the antenna is followed by a passive envelope detector with corresponding matching circuits. The output of the envelope detector is fed into the analog section, which employs a band-pass filter and a comparator. The output of analog section is the input the digital section. Comparing with *Path2*, there is no backscatter modulator. Therefore, *Path1* acts as a pure receiver rather than a fully functional passive transceiver. After extracting two sets of tag's IDs *ID1* and *ID2* from the backscattering signal, the receiving path selection technique applies a simple selection algorithm Algorithm. 1 to discriminate the cases whether the phase cancellation occurs.

ALGORITHM 1: The selection algorithm

```
Initialization: ID1 = Decode(P1); ID2 = Decode(P2);
Procedure SELECTION(ID1, ID2):
    if ID2 != NULL then
        return (ID2)
    else
        return (ID1)
    end
end Procedure
```

The prior consideration of ST is to avoid the occurrence of phase cancellation effect at the two antennas concurrently. For a given time the parameters of reader's CW at reader antenna and tag's backscatter signal at tag antenna could be considered as stable. According to Equation 3.4, we could obtain the amplitude difference $|A_1 - A_2|$ for various situation and locations of reader, tag and ST. According to Equation

(3.16 ∼3.17) and the propagation parameters of wireless signal, we could obtain the following equations.

$$\begin{cases} A_{T1} & = \frac{A_{T1\_bsk}}{r} \\ A_{T2} & = \frac{A_{T2\_bsk}}{r} \\ A_{R} & = \frac{A_{R\_trans}}{\tilde{R}} \\ \theta & = 2\pi\frac{\tilde{R}-r}{\lambda} + \theta_C \end{cases} \tag{3.23}$$

A_{T1}, A_{T2}, A_R and θ are in agreement with Equation 3.4. A_{T1_bsk} and A_{T2_bsk} are the amplitudes of tag's backscatter signal at tag's antenna for two different RCS states. A_{R_trans} is the amplitude of reader's transmitting signal at the reader's antenna. $\tilde{R}$ is the distance between the antennas of reader and ST, while r is the distance between the antennas of tag and ST. λ is the wavelength of the signal at 915 MHz. θ is the phase difference between reader's transmitting signal and tag's backscattering signal at ST's antenna. θ_C is the phase difference between reader's transmitting signal at reader's antenna and tag's backscattering signal at tag's antenna. For the locations within the proximity of tags, θ_C could be considered as stable at a particular time instance. ST's two antennas could be placed at any pair of positions in the field.

We obtain the measurements of A_{T1_bsk}, A_{T2_bsk}, A_{R_trans} and θ_C from PASS simulator as, $A_{T1\_bsk} = 0.0526$, $A_{T2\_bsk} = 0.0485$, $A_{R\_trans} = 2.5612$ and $\theta_C = \pi/8$ for the case the distance between tag's and reader's antenna $R = 2\ m$. The reader is placed at $(0, 0)$, while the tag is at $(0, 2)$. Based on the measurements and equations, we model Equation 3.4 in MATLAB. The result is shown in Figure 3.8.

Figure 3.8 shows the pattern of phase cancellation effect at the proximity of passive tag. The colorbar shows that the darker color stands for lower amplitude difference $|A_1 - A_2|$. From $(0, 2)$ to $(0, 0)$ the distance between nearby phase cancellation curves

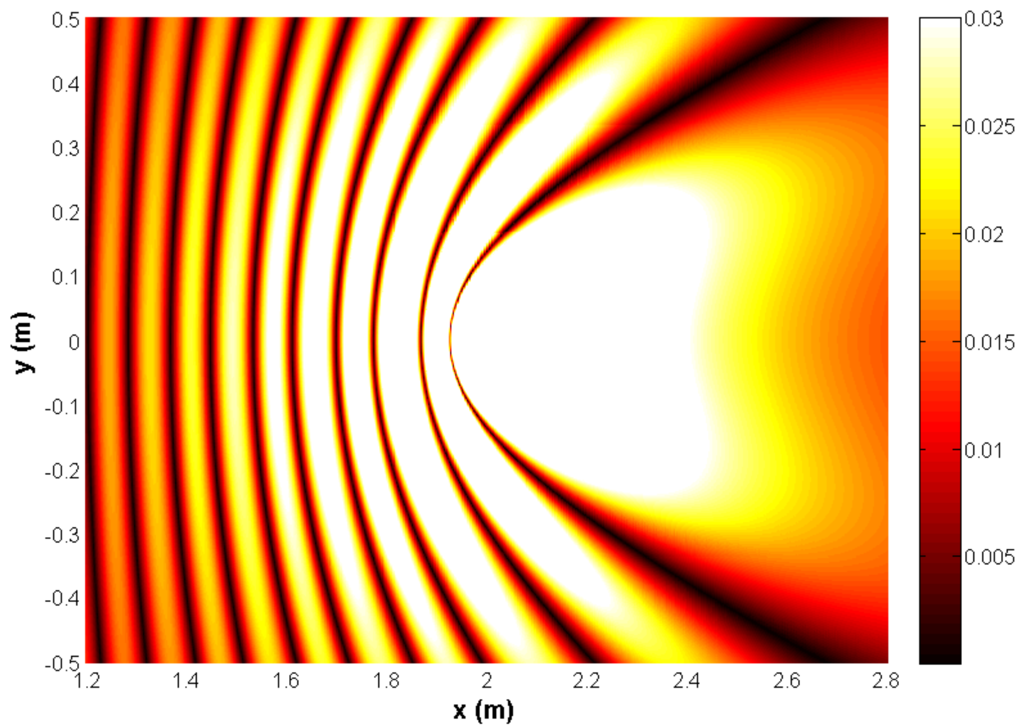

Figure 3.8: The pattern of amplitude difference $|A_1 - A_2|$ at ST's antenna for the case when reader is at $(0, 0)$ and the tag is at $(2, 0)$.

is around $\lambda/4 = 0.082\ m$. Such periodic pattern verifies the variation of amplitude difference in Figure 3.3. As the ratio of A_R to A_{T1}, A_{T2} increases, the null phase θ_cancel approaches $\pm\pi/2$. In addition, the phase difference θ alters by π for any two locations on x-axis, whose distance is $\lambda/4$.

From the figure, we could see that the possibility of concurrent occurrence of phase cancellation effect at two antennas cannot be eliminated, because it is possible to place these two antennas at the phase cancellation spots at the same time. However, the phase cancellation effect is mitigated significantly using the receiving path selection technique when compared with single antenna and simple combination technique.

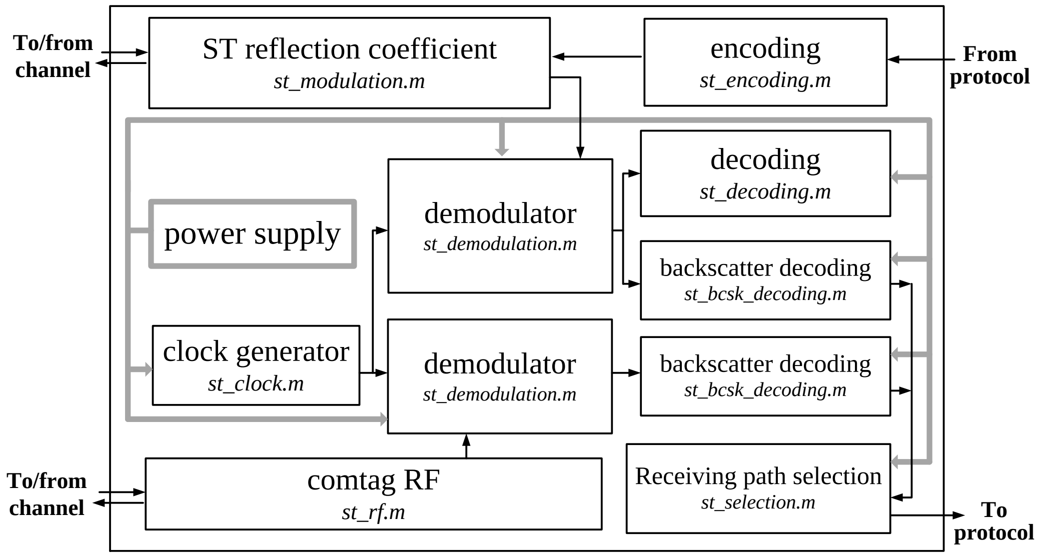

Figure 3.9: The structure and functions of ST

3.2.3 Simulation results

Simulation setup

The AURIS is modelled in PASS simulation framework as described in Appendix A. The development environment framework is MATLAB 2012a on Windows 8.1 (64 bits). Furthermore, the behavioral model of ST with receiving path selection technique is developed, and integrated into the simulation framework. The structure and functions of new ST model is presented in Figure 3.9.

The major modification of the ST in comparison with ST model is one extra receiving branch, which consists of the RF front end *st_rf.m*, demodulator *st_demodulation.m* and backscattering decoding section *st_bsck_decoding.m*. The receiving path section algorithm is implemented in *st_selection.m*.

Figure 3.10 shows the experiment setup, which is used to evaluate the effectiveness of the proposed techniques. The reader is placed at the origin $(0, 0)$ of the area. The trajectory of the tag is along the x-axis from $(1, 0)$ to $(7, 0)$ in the increment of 0.5

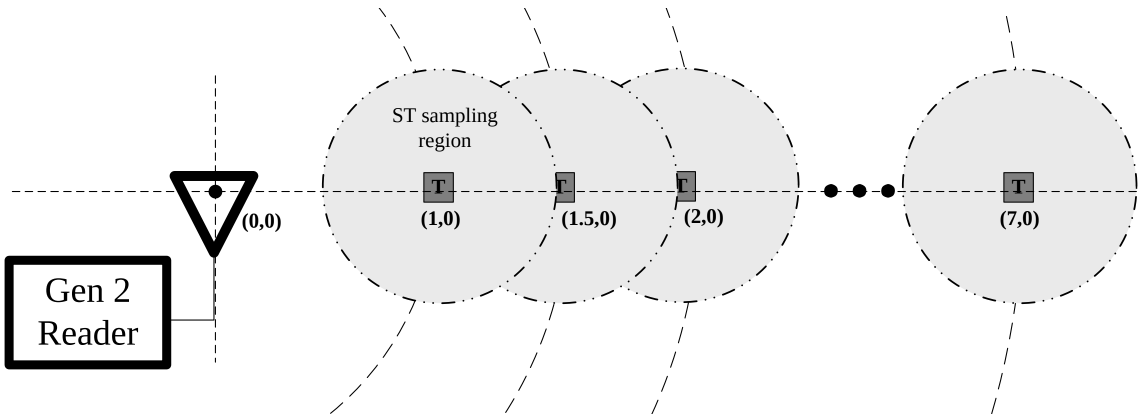

Figure 3.10: Experiment setup.

m. The position of ST is uniformly distributed over the circle plane centering at the tag and with the radius of 0.5 m. An instance of the experiment of one tag position and its associated ST's sampling positions is referred as a cell. In a cell there are 300 possible positions for ST based on uniform distribution which are obtained by Monte Carlo sampling [69]. We establish this experimental scenario in PASS simulation framework. Figure 3.11 shows the simulation setup by side-way view and nadir view. The transmitter is represented by the colored radiation pattern. A darker color signifies higher gain.

Experimental result

The first set of experiments is to observe the reader's transmitting signal and passive tag's backscattering signal at ST antenna for the two cases when phase cancellation happens. The output of the envelope detector serves as the indicator of phase cancellation effect. We conducted the simulation trial in the first cell, and captured a phase cancellation point for ST. As we can see in the Figure 3.12(a), tag's backscattering ASK signal arrived at ST's antenna with the amplitude difference 0.0017 V. However, the envelope amplitude difference of the superimposed signal from envelope

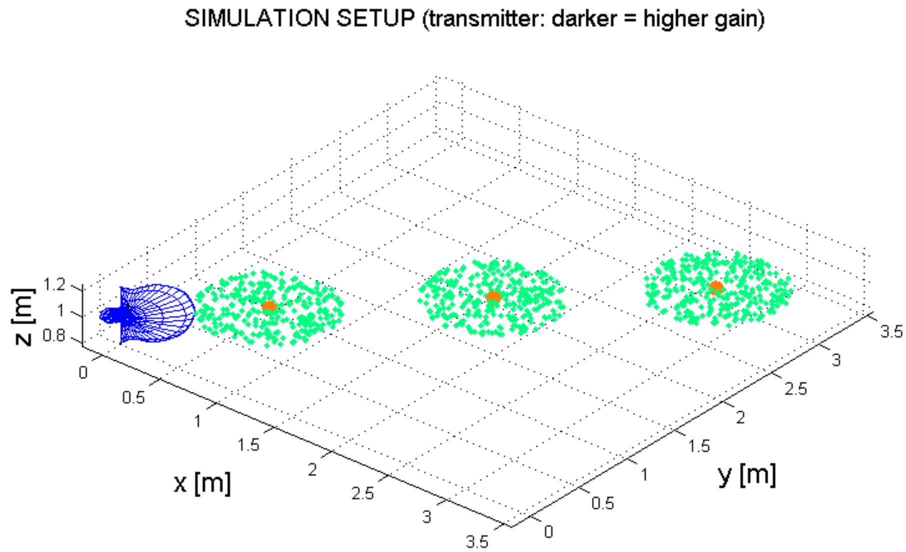

(a) Side-way view

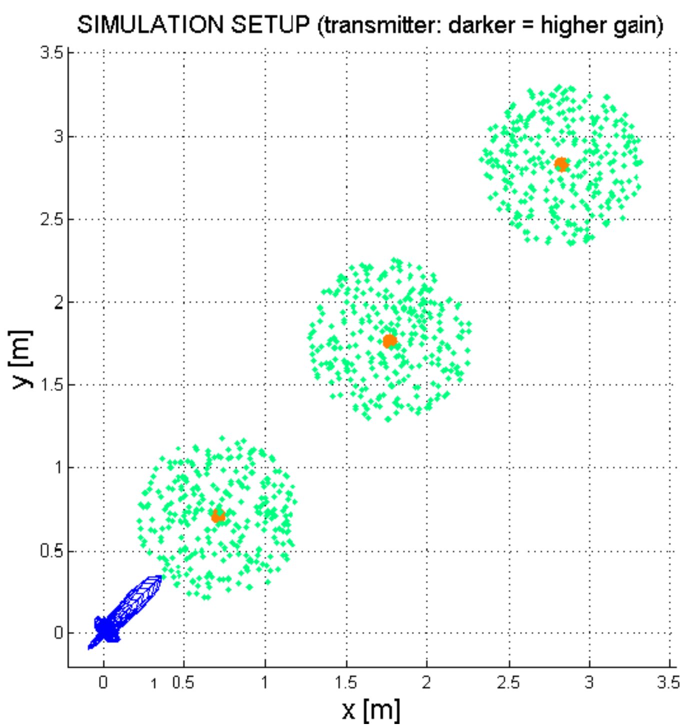

(b) Nadir view

Figure 3.11: Simulation setup in PASS (1, 3, 5 cells).

detector for two RCS states is negligible as shown in Figure 3.12(b). On the contrary, the case without phase cancellation is shown in Figure 3.13. In Figure 3.13(a) the amplitude difference of tag backscattering ASK signal is also 0.0017 V, but the amplitude difference of the envelope for two RCS states is 0.01 V, which could be easily detected by the analog section of ST. We present the relative physical quantities in Table 3.1. Based on these measurements of signals, we could calculate $|A_1 - A_2|$ and θ_{cancel} according to Equation 3.4.

Table 3.1: The values of physical quantities and phase cancellation condition calculation

Case index	A_R (V)	A_{T1} (V)	A_{T2} (V)	θ (rad)	$\|A_1 - A_2\|$ (V)	θ_{cancel} (V)
Phase cancellation	0.0802	0.0576	0.0560	2.2710	0.000133	2.3578
No phase cancellation	0.1087	0.0585	0.0568	0.7570	0.0015	2.1298

The designation of physical quantities and calculation results as in Equation 3.4.

In the second set of experiments, our goal is to observe the pattern of phase cancellation curve as shown in Figure 3.8. We conducted the simulation with 4 line trajectories of ST in the third cell. The simulation setup is shown in Figure 3.14. The angle between four ST tracks with tag to reader vector are 0, $\pi/4$, $\pi/2$ and π respectively. For each track ST is moving away from the tag with the distance from 0.04 m to 1 m in intervals of 0.02 m. The amplitude difference of the superimposed signal is measured for each steps as shown in Figure 3.15. In Figure 3.15(a) the distances between the positions of minima that are spaced around 0.08 m on average. Correspondingly, the distance between the dark colored phase cancellation curves in Figure 3.8 on x-axis is around $\lambda/4 = 0.082\ m$. In addition, for other three tracks of ST, amplitude difference pattern from PASS simulator also matches with that from

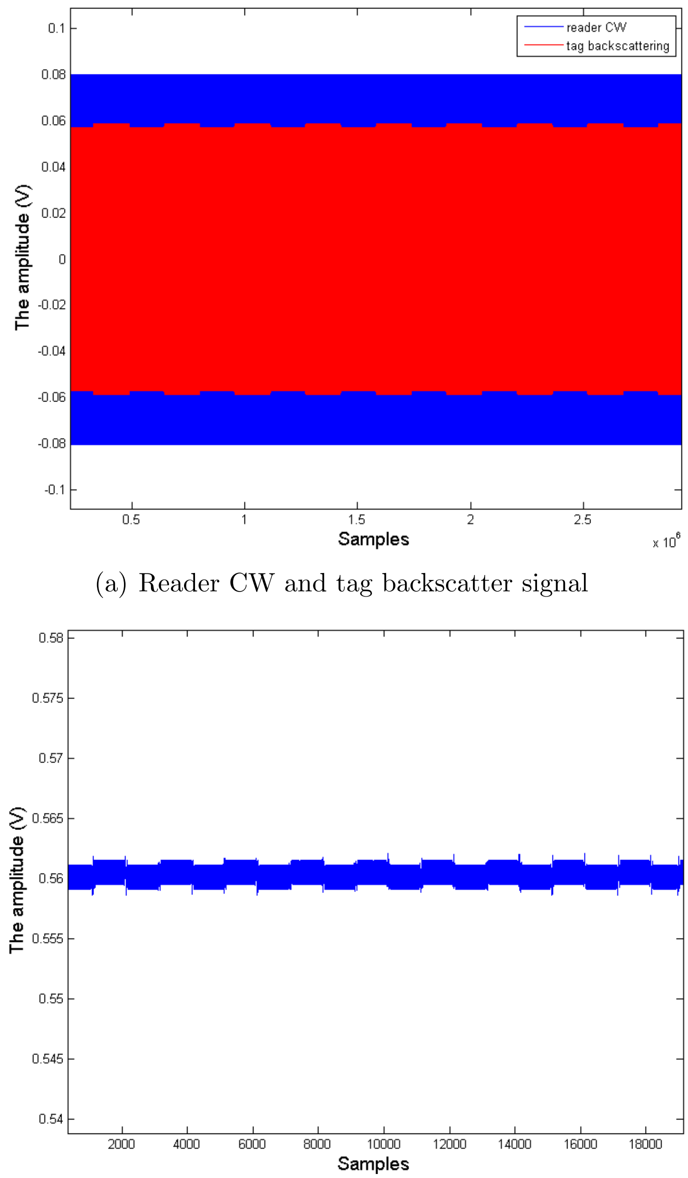

(a) Reader CW and tag backscatter signal

(b) The output of envelope detector

Figure 3.12: With phase cancellation.

mathematical model.

In the third set of experiments, we measured relative physical quantities of tag backscattering and reader CW at both antennas of ST. Two antennas are randomly placed with the constraint as that the distance between these two antenna is

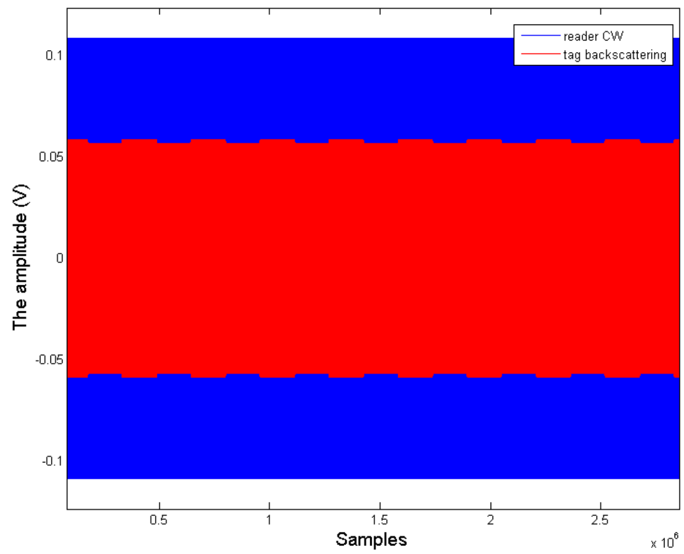

(a) Reader CW and tag backscatter signal

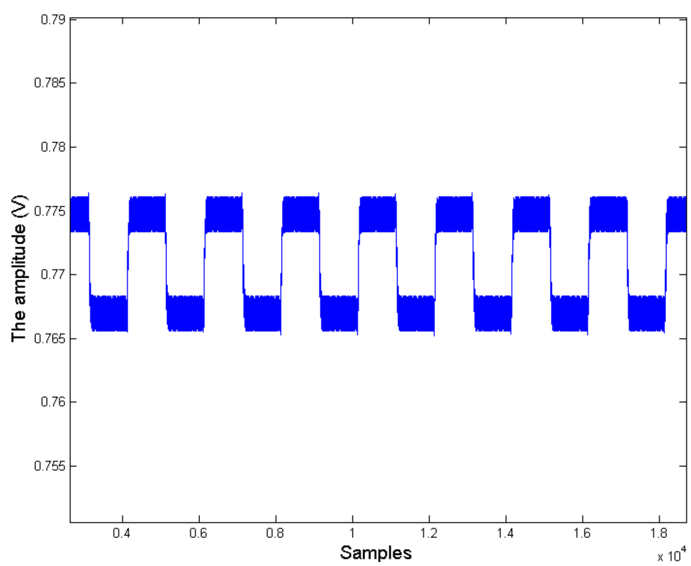

(b) The output of envelope detector

Figure 3.13: Without phase cancellation.

$\lambda/4 = 0.082\ m$ [70]. We carried out the experiment in first cell, and located a phase cancellation point for the dual-antenna based simple combination implementation. The output of envelope detector serves as the indicator for phase cancellation. The values of these physical quantities are presented in Table 3.2. Based on the Equation

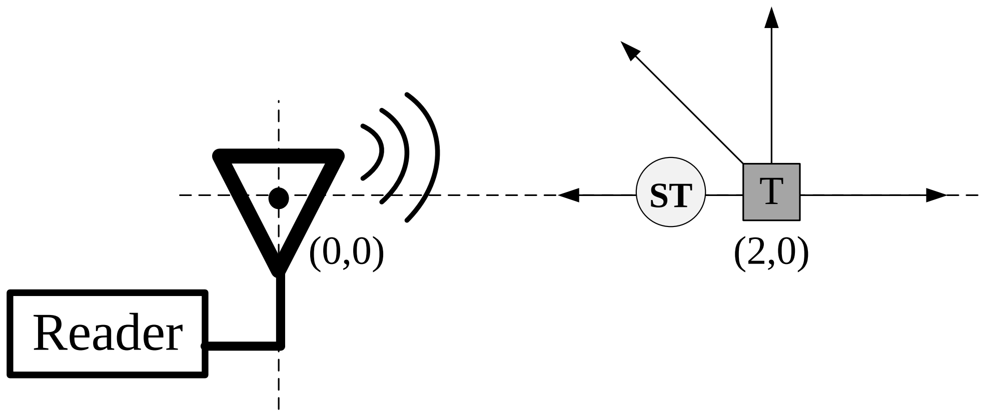

Figure 3.14: Experiment setup for the second experiment.

3.14-3.21, we could calculate relative physical quantities $\hat{A}_R$, $\hat{A}_{T1}$, $\hat{A}_{T2}$, α, β, and θ of simple combined signal as shown in Table 3.3. Then the amplitude difference of the combined signal $|A_1 - A_2|$ equals to 0.0009 V according to Equation 3.21, which could not be detected by the comparator in the analog section of ST. Meanwhile, for receiving path selection technique the amplitude difference of the receiving signal at antenna SA_1 is 0.0019 V according to Equation 3.21, and the amplitude difference of envelope detector's output is 0.012 V, which is larger than the phase cancellation threshold 0.005 V.

Table 3.2: The values of physical quantities at dual antennas of ST

Antenna SA_1	A_R (V)	A_{T1} (V)	A_{T2} (V)	θ (rad)	
	0.0976	0.066	0.064	3.2536	
Antenna SA_2	A'_R (V)	A'_{T1} (V)	A'_{T2} (V)	θ' (rad)	θ_1 (rad)
	0.1247	0.1233	0.1196	1.3365	0.1916

The designation of physical quantities and calculation results as in Equation 3.14-3.15.

Finally, we studied the anti-phase cancellation performance of two dual-antenna

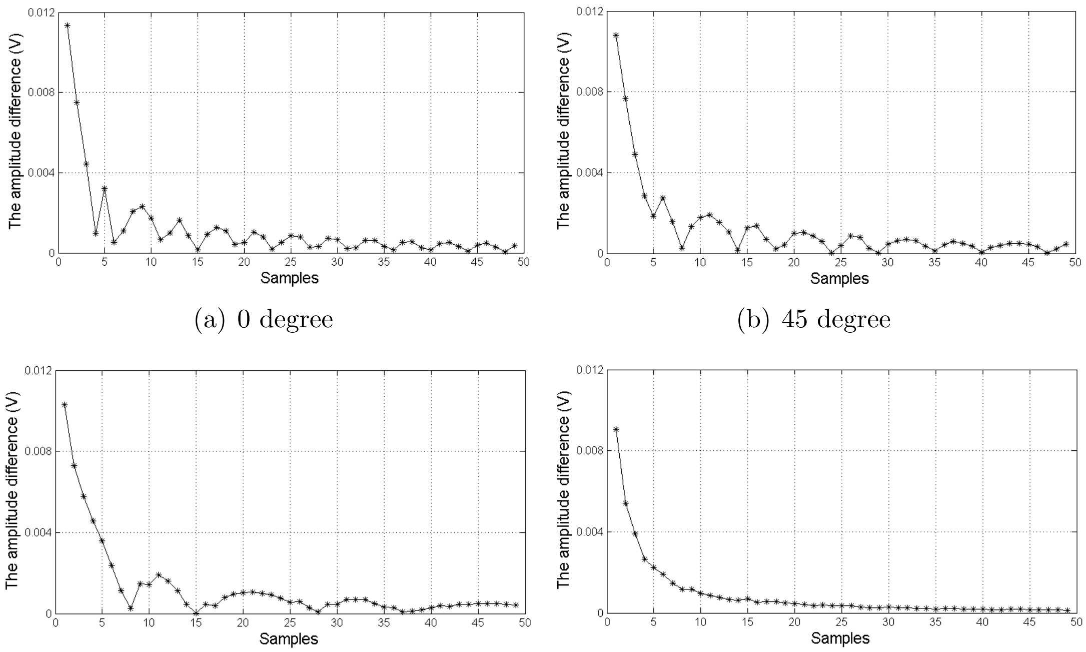

(a) 0 degree

(b) 45 degree

(c) 90 degree

(d) 180 degree

Figure 3.15: Measurements of amplitude difference.

Table 3.3: The physical quantities of simple combined signal

Simple combination	$\hat{A}_R$ (V)	$\hat{A}_{T1}$ (V)	$\hat{A}_{T2}$ (V)	θ (rad)	β (rad)	α (rad)
	0.2213	0.1306	0.1267	3.2536	-1.2026	0.1075

The designation of physical quantities and calculation results as in Equation 3.14-3.15.

based technique and compared with the single antenna implementation. As in the simulation setup in Figure 3.10, we conducted experiment through 3900 sampling points in 13 cells. In addition we repeated the trial three times with different Monte Carlo sampling positions of ST. In Figure 3.16, the probabilities of phase cancellation for three implementations are shown over 13 cells. The dual-antenna based implementation performs better than the simple antenna implementation. Especially, the overall probability of phase cancellation for receiving path selection technique is below 1%. Nota that, the decline phenomenon of phase cancellation probability with

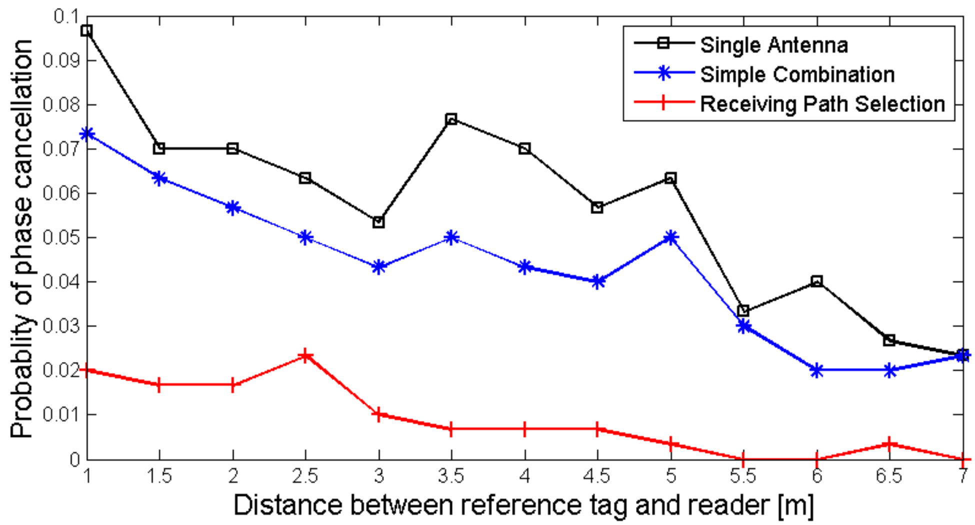

Figure 3.16: Probability of phase cancellation.

increasing distance is due to the condition of phase cancellation that the envelope detector output of the superimposed signal of tag's backscattering signal and synchronized Reader's CW (with no phase difference) should be larger than the phase cancellation threshold 0.005 V.

3.3 Summary

In this chapter, we analyze the phase cancellation effect in AURIS and provide solutions to counter such effect. In AURIS, the signal at ST's antenna is the superposition of RFID reader's CW and passive tag's backscattering signal. The combination of such two signals with different phase may cause the ST could not capture the modulated information in tag's backscattering signal. We model the phase cancellation effect mathematically, and then demonstrate the model with extensive computer simulation. To resolve the phase cancellation effect we propose techniques by exploiting the spatial diversity of dual antennas.

Chapter 4

Indoor localization with AURIS

We address the problem of indoor localization with AURIS. The probabilistic model of detecting a tag by ST is proposed. This new and more realistic detection model is formulated by integrating the distance and relative angle between the tag and the reader's antenna, as well as considering the interference of reader's CW on ST. For indoor localization, we propose a novel particle filter method (PF-AA) as inference algorithm for AURIS. To this end, we identify two technical roadblocks of AURIS as false synchronous detection assumption and state evolution constraints. It is demonstrated that the proposed PF-AA algorithm overcomes such roadblocks. Furthermore, we propose a landmark-based sequential localization and mapping framework (SQLAM) for AURIS, which enables the accurate mapping of passive tags with unknown locations in the environment, but also improves the accuracy and robustness of ST localization.

4.1 The detection probability model

The location inference algorithm of AURIS relies on the detection probability model of ST-to-tag, which describes the relationship between detection and the true state of reader, tag and ST. The traditional detection probability model used in RFID, which is simply modeled as the function of the distance between two communication participants [8,11,71]. However, according to the research on tag-to-tag backscattering communication link, the detection probability of ST-to-tag depends on various factors.

Tag-to-tag backscattering communication link has been explored in literature, but mainly as a feasibility study [44,72]. While the general feasibility has been established, virtually no much attention has been paid to characterize the tag-to-tag communication link. One of the pioneering works in the field characterizes the inter-tags communication link by the near-field mutual coupling model [73]. However, it is not applicable for the ever increasing tag-to-tag range. The rest of this section aims to present the propagation mechanism governing tag-to-tag backscattering communication theoretically, and then set up some design guidelines for modeling ST-to-tag detection probability.

4.1.1 ST-to-tag link budget

Figure 3.1 depicts the scheme of ST-to-tag backscattering communication link wherein the CW signal is provided by RFID reader. The first radio link budget is the linear scale, power-up link budget that describes the amount of power arriving at the passive tag's antenna from RFID reader [63].

$$P_T = \frac{P_R G_R G_T \lambda^2 X_{RT}}{(4\pi D)^2 \Theta_T B_{RT}} \tag{4.1}$$

- P_T power received by the passive tag antenna (W)
- P_R power transmitted by RFID reader antenna (W)
- G_R load-matched, free-space gain of RFID reader antenna
- G_T load-matched, free-space gain of passive tag antenna

- Θ_T passive tag antenna on-object gain penalty
- X_{RT} reader to tag link polarization mismatch
- B_{RT} reader to tag link blockage loss
- λ carrier frequency wavelength (m)
- D reader to tag separation distance (m)

Equation 4.1 is similar to the form of *Friis Equation* [22], but accounts for losses Θ, B, which are commonly encountered in indoor environment.

The second link budget is the ST-to-tag backscatter link budget that governs the amount of modulated backscatter power from passive tag received by ST.

$$P_S = \frac{P_R G_R G_T^2 G_S \lambda^4 X_{RT} X_{TS} \sigma}{(4\pi)^4 D^2 d^2 \Theta_T \Theta_S B_{RT} B_{TS}} \tag{4.2}$$

- P_S power received by ST antenna from the tag (W)
- G_S load-matched, free-space gain of ST antenna
- X_{TS} tag to ST link polarization mismatch
- Θ_S ST antenna on-object gain penalty
- B_{TS} tag to ST link blockage loss
- d tag to ST separation distance (m)
- σ radar cross section (RCS) of passive tag antenna

Radar cross section σ is a measure of the amount of power backscattered by an antenna [22]. Traditionally, the RCS of UHF RFID tag is measured considering the reflection direction is the same as the incident direction [74]. However, the RCS in

ST-to-tag link is not the case. In general, the RCS in ST-to-tag link can be written as

$$\sigma \propto |A_s - \Gamma|^2 \tag{4.3}$$

where A_s is the load-independent structural component, and Γ is reflection coefficient, which is the load-dependent antenna component. A backscatter modulator manipulates the signal backscattered from its antenna by switching the load impedance between two states. The load-dependent reflection coefficient Γ is defined as [75]

$$\Gamma = \frac{Z_{load} - Z_{ant}^*}{Z_{load} + Z_{ant}} \tag{4.4}$$

where Z_{load} is the load impedance, and Z_{ant} is the input impedance of tag antenna as shown in Figure 4.1. When an open circuit is presented to the antenna, the path to ground is blocked. There is no current flow in the antenna, thus there is no power backscattered. When a short circuit is presented to the antenna, the current flows directly to the ground without any resistance. In this state, a large amount of power is backscattered, but there is no power dissipated in the load. The optimum power transfer occurs in the matched state. The power dissipated in the load is equal to the power backscattered in the space.

According to [76], the differential RCS is only dependent on the antenna component, while the structure component is cancelled out. The differential RCS $\Delta\sigma$ is

$$\Delta\sigma \propto |\Gamma_A - \Gamma_B|^2, \tag{4.5}$$

where Γ_A and Γ_B are the reflection coefficients for load impedance Z_A and Z_B respectively.

In Equation 4.2, the power received at the receiving tag goes as the inverse square of the separation distance between reader and the transmitting tag, as well as the

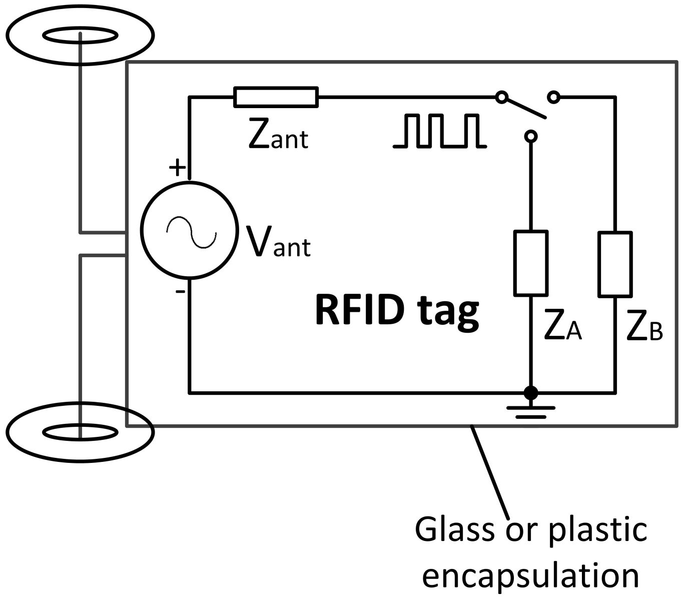

Figure 4.1: Block diagram of passive tag

inverse square of the separation distance between the transmitting tag and the receiving tag. It is also proportional to the antenna gains. Additionally, it shows that the modulated-backscattered power is dependent on the difference between reflection coefficient of each antenna load in Equation 4.5. Since the detection of ST-to-tag depends on hamming distance between received signals for two difference RCS states, it is evident that detection model should integrate these two separation distances and antenna gains.

4.1.2 Model description

According to the study on ST-to-tag backscattering communication link, the detection probability of ST-to-tag depends on numerous factors, including the distance from reader antenna, the orientation of antenna and phase cancelation et al. In this section, we therefore develop a more realistic detection probability model that is better suited for ST-to-tag communication link.

First, the detection probability model is modelled as the function of the distance

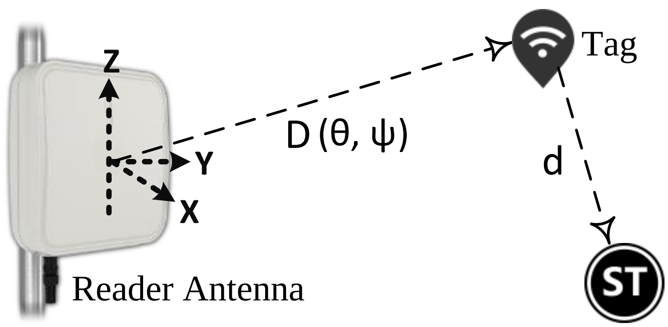

Figure 4.2: Representation of detection probability model parameters.

and (elevation, azimuth) angle pair from reader antenna to tag, as well as the distance between tag to ST. Second, augmented by phase cancellation-reducing technique, phase cancellation has an insignificant effect on detection probability as mentioned in Section 3.2.2. Therefore, the detection probability does not take into account the superposition of reader CW and tag's backscattering. Noteworthily, due to the very nature of phase cancellation, it is highly possible that the detection probability model will suffer from overfitting issue by integrating phase cancellation effect without the effect-reducing techniques [66].

Figure 4.2 depicts the distance D, azimuth θ and elevation ϕ from reader antenna to tag, as well as the distance d from tag to ST. The azimuth θ represents the relative orientation angle between antenna (X, Z) plane and antenna-to-tag direction. The elevation ϕ represents the relative orientation angle between antenna (X, Y) plane and antenna-to-tag direction. Both of these angles have the range of $[-\pi/2, \pi/2]$. The detection probability of ST-to-tag $p(D, d, \theta, \phi)$ is formulated as logistic regression model.

$$p(D, d, \theta, \phi) = \frac{1}{1 + e^{a_0 + a_1 D + a_2 d + a_3 |\theta| + a_4 |\phi|}} \tag{4.6}$$

where $\{a_k, k = 0, 1, 2, 3, 4\}$ are the model coefficients. The logistic regression model is used to estimate the probability of a binary response based on one or more variables, therefore restricted to the range $(0, 1)$ [77]. The logistic model reflects the inverse exponential relationship between detection probability and features D, d, θ, ϕ. We refer to such model as RTS model.

For comparison, the conventional model, where the detection probability is a function of distance between tag and ST, is presented. We refer to this probability detection model as TS model.

$$p(d) = \frac{1}{1 + e^{a_0 + a_1 d}}, \tag{4.7}$$

where d is the distance between tag and ST, a_0 and a_1 are the model coefficients.

4.1.3 Model evaluation

We evaluated the proposed detection probability model by the experiment data obtained from the newly developed PASS simulation framework. PASS is system-level time-domain UHF RFID simulator, which is based on PARIS simulator developed by Dr. Arnitz [61, 66]. In the experiment, the reader antenna is RFMAX S9028PCRJ, which is a circularly polarized panel antenna working at 902-928 MHz frequency band. The power level of reader antenna is set as 30 dBm. Figure 4.3 plots the antenna radiation pattern. The channel type is selected as *"room"* in PASS. The tag model is based on NXP UCODE G2XM tag. The ST model is designed to emulate the specific ST device with dual-antenna implementation.

Figure 4.4 shows the experimental setup. The reader antenna is placed at the origin $(0, 0, 0)$. The position of tag is uniformly distributed over the cuboid area, where $x \in [1, 8]$ m , $y \in [-4, 4]$ m, $z \in [-4, 4]$ m. There are 3000 possible positions for tag, which are obtained by Monte Carlo sampling method and represented by green points. The position of ST is randomly sampled within the sphere, whose globe is at tag position and radius is 2 meters. ST possible positions are represented by

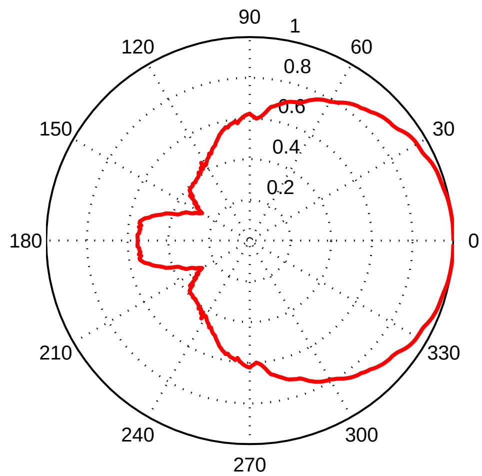

Figure 4.3: Antenna radiation pattern

brown points. The detection y of ST-to-tag among these 3000 measurement samples are recorded.

The cost function for training the logistic model is

$$J(\mathbf{a}) = \frac{1}{m}\sum_{i=1}^{m}[-y^{(i)}log(p_{\mathbf{a}}(D,d,\theta,\phi)^{(i)}) - (1-y^{(i)})log(1-p_{\mathbf{a}}(D,d,\theta,\phi)^{(i)})] \quad (4.8)$$

where m is the size of dataset [78].

We apply gradient descent method to estimate the model coefficient. The estimated values are $a_0 = -1.462$, $a_1 = 0.4941$, $a_2 = 2.506$, $a_3 = 0.0126$ and $a_4 = 0.0523$. Figure 4.5 shows the visualized detection probability model. It is found that distances D and d are much more significant in affecting the detection probability than orientation of the tag with respect to reader antenna. The reason is mainly related to the radiation pattern of panel antenna, as well as the position sampling space of tag and ST in experiment. The experiment setup reflects the real indoor localization

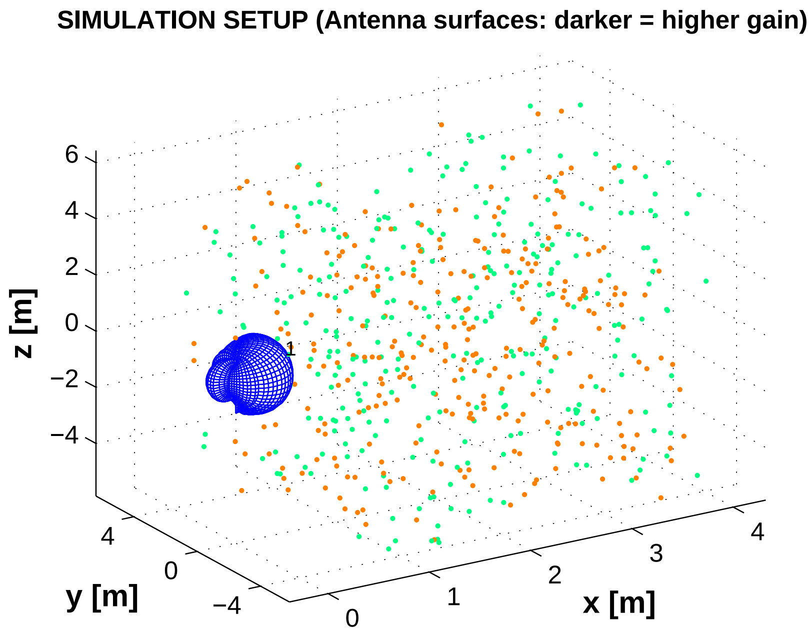

Figure 4.4: Simulation setup

application, in which the panel antenna is usually mounted on the roof while tags and STs on the ground. Following the same manner, we obtain the estimated coefficient values for TS model, where $a_0 = 0.8970$ and $a_1 = 2.4443$. The visualized detection probability is plotted in Figure 4.6.

Figure 4.7 shows the calculated detection probability based on the samples from training dataset. In Figure 4.7(a), the data samples are collected within the region $d \in [0.4, 1]$ m. The detection probability is calculated along the variable D with the interval as 0.3 m shown by the bar chart. The probability curve of RTS and TS model are plotted along the variable D at $d = 0.6$ m. Since the TS model purely depends on the parameter d, the distance between tag and ST, the detection probability is constant over the range of D. In Figure 4.7(b), the data samples are collected with the region $D \in [2, 4]$ m. The detection probability along the variable d with the interval of 0.2 m. The probability curves of RTS and TS model are plotted along the

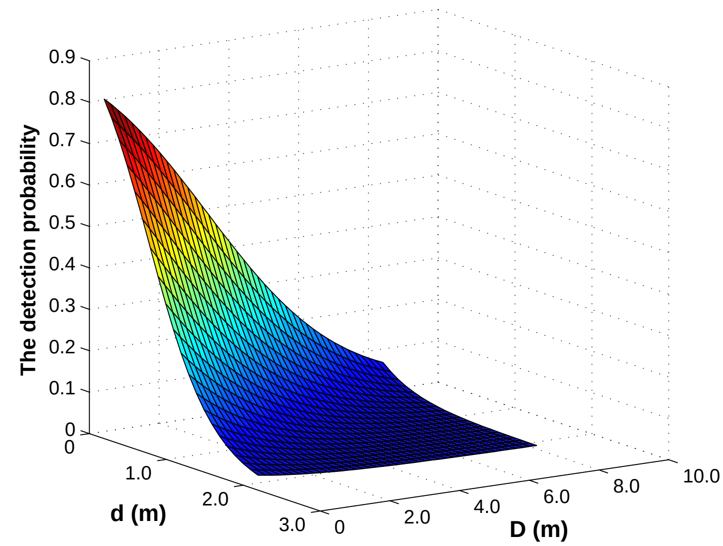

(a)

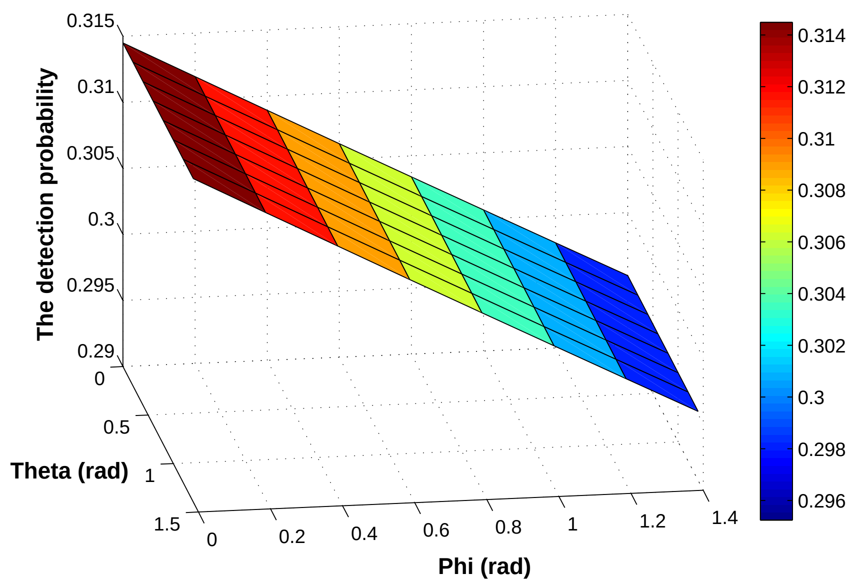

(b)

Figure 4.5: The estimated detection probability versus (a) D and d with $\theta = 0$, $\phi = 0$ (b) θ and ϕ with $D = 2\ m$, $d = 0.5\ m$ for RTS model

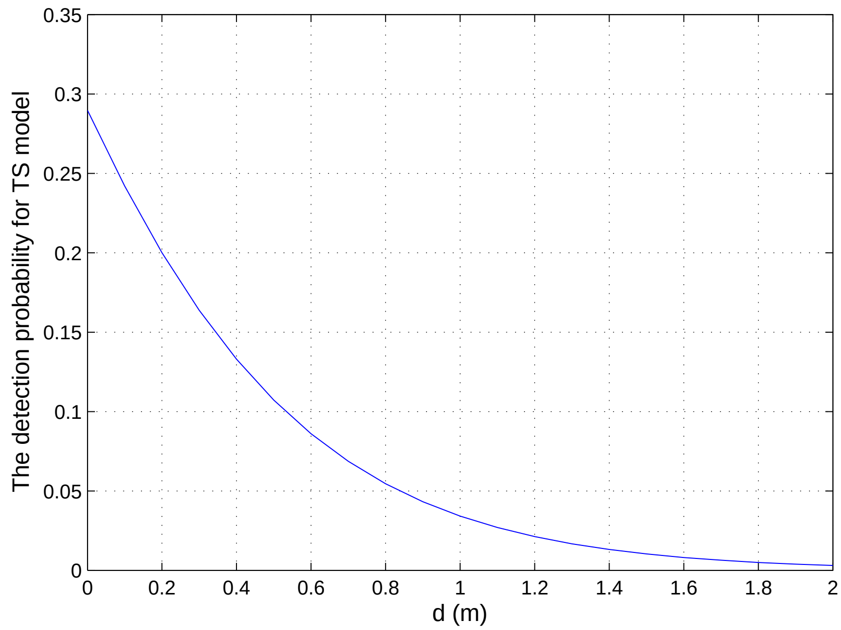

Figure 4.6: The detection probability versus d for TS model

variable d, in which the parameter D of RTS model is set at 3 m. From the Figure 4.7, we can see that probability curve of RTS model agrees with the dataset, while the TS model suffers from the underfitting problem.

Last, we obtain another 1000 measurement samples with the same simulation setup as test dataset. The cost is computed according to Equation 4.8. The cost of RTS model on test dataset is 0.1278, while the cost of TS model is 0.1502. Therefore, we can conclude that RTS model has higher modelling accuracy than the TS model.

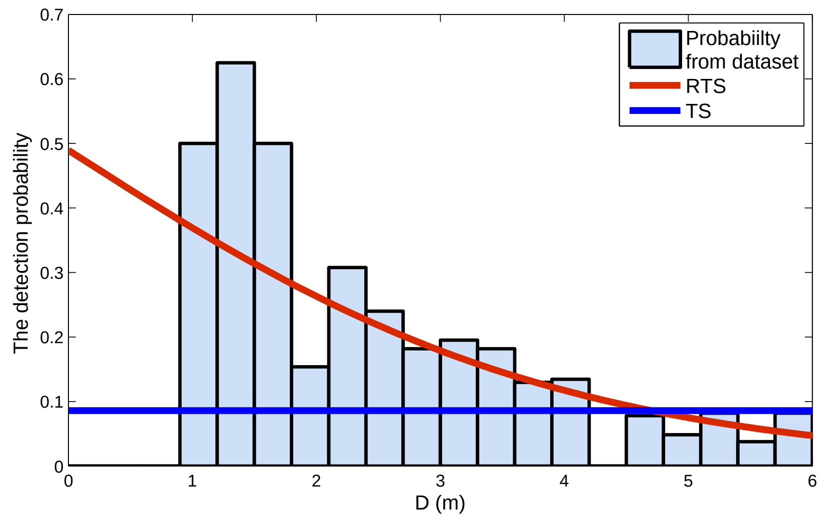

(a)

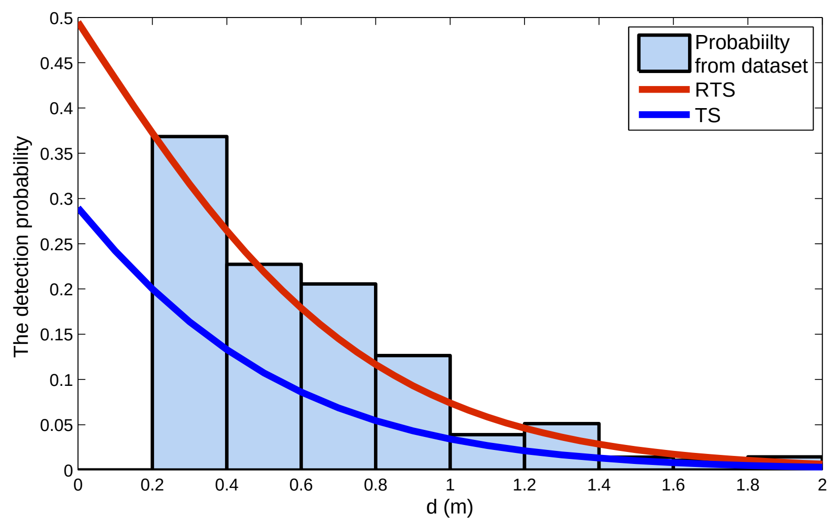

(b)

Figure 4.7: The detection probability versus (a) D with data from region $d \in [0.4, 1]$ (b) d with data from region $D \in [2, 4]$

4.2 Particle filter-based localization method with AURIS

This section addresses the problem of indoor localization of ST-tagged objects in AURIS. The method relies on the binary proximity information of ST-to-tag and the corresponding detection probability model introduced in Section 4.1. As described in Section 2.4.1, ST is a semi-passive UHF RFID component with unique dual functionality, which is augmented to off-the-shelf UHF RFID system. Populated with a large set of passive tags as landmarks, the augmented UHF RFID system could provide fine-grained proximity-based localization service for indoor environment. We propose a novel particle filter method (PF-AA) as inference algorithm for AURIS indoor localization. Some previous works dealing with particle filter-based RFID indoor localization possess strong assumption and constraints on the target state-space model, such as initial pose knowledge, linear target motion model or exteroceptive sensor information [11, 79, 80]. Additionally, according to ST's Gen2-based locator protocol, the host computer controls reader to send out a fixed number of query rounds to reference tags. Then the inference algorithm localizes ST using aggregated binary information reported by ST [5]. Existing inference algorithms possess a false synchronous detection assumption, which considers that the detection measurements are received by ST synchronously [5, 10, 11]. The novel PF-AA introduces current measurements into the state evolution model using a constraint-free auto-regressive (AR) model, and it also addresses the asynchronous measurements with a minor modification of ST locator protocol.

4.2.1 Problem formulation

Figure 4.8 shows a typical deployment case of AURIS for find-grained proximity-based localization. The system is composed of a host server which runs the localization

	Listening (Q_T)	*Responding* (Q_S)
Host server	• Initiate query Q_T • Obtain tags' IDs	• Initiate query Q_S • Obtain ST's EPC payload
ST	• Listen to the reader • Listen to the proximal tags • Store tags' IDs	• Respond to the reader by backscattering its ID and the stored tags' IDs

Table 4.1: ST locator protocol

algorithm, an off-the-shelf RFID reader, a large set of passive tags placed at known locations as landmarks, and a ST attached to mobile target of interest. The ST incorporates a Gen2 compliant locator protocol, which is a two-stage query process as illustrated in Table 4.1.

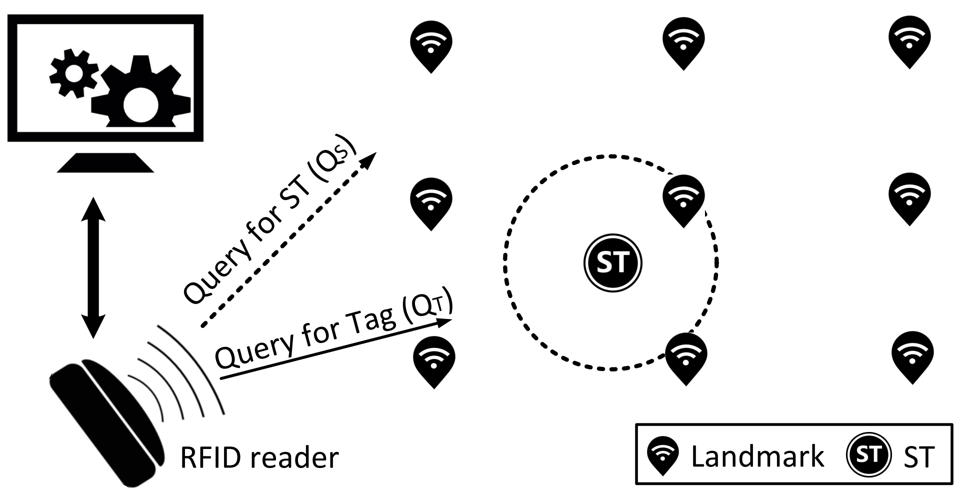

Figure 4.8: The deployment of AURIS

A query of Q_T drives the ST to *Listening* state. In this state, ST does not respond instead listening to backscattering signal of passive tags within its proximity. Upon detecting any backscattering signal, the ST decodes the signal, extracts tag's ID and stores a hash value corresponding to the ID temporally in memory. The query of Q_S

drives ST to *Responding* state. In this state, ST itself works as a standard passive tag, and conveys the information about the detected tags' IDs during Q_T to the RFID reader. As a result of several query rounds, the host server aggregates the associated information and determines the location of ST. For instance, as in Figure 4.8, the detection range of ST is shown by a dotted circle. Thus ST can acquire the ID information of these two tags. Because the location of passive tags are known prior to operation, the host server can determine the location of ST.

In some of our previous works [5, 10, 11], we have studied certain inference algorithms for AURIS localization system. First, we introduce weighted centroid localization (WCL) method, which is commonly used in wireless sensor network localization application [81]. The key idea of WCL method is the weighted average of the detected tags' locations. The WCL method is cheap in computational cost, but yields coarse location estimation. We then propose a general method for continuous localization of ST using particle filtering (PF), by which the localization accuracy is improved but with higher computation cost [11]. Since the computation task is executed on the host server, the increased computation cost draws little concern. However, two fundamental issues, which deteriorate the localization accuracy, are identified in AURIS design itself and PF algorithm. These issues are discussed as following.

False synchronous detection assumption

In AURIS, ST has two operation states *Listening* and *Responding* controlled by RFID reader queries. First, RFID reader sends out N rounds of the query Q_T to address passive tags. Once capturing the backscattering response from passive tag to RFID reader, ST records the tag's ID and the associated read rate out of N. The following query Q_S drives ST to convey the stored information from ST to RFID reader. However, existing localization algorithms treat the detection measurements in N rounds indiscriminately, which assumes that all the measurements are obtained with the same target pose. In other words, It assumes that all the measurement are obtained at the same time instant of Q_S as shown in Figure 4.9. We refer to this situation as false synchronous detection assumption. Such assumption is appropriate when ST is static. But it introduces a significant bias to the estimated ST location when ST is moving, especially when the speed is high.

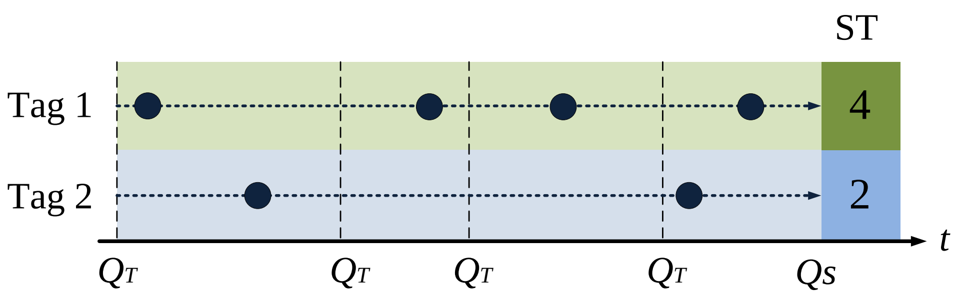

Figure 4.9: Representation of a set of queries Q_T and Q_S with $N = 4$

State evolution model constraints

In PF-like sequential Bayesian estimation algorithm, the state evolution model is used to approximate the current state based on the history [53]. From practical perspective, state evolution model is formulated based on the knowledge of system dynamics. In [11], the state evolution model possesses a strict constraint as shown in Equation 4.9.

$$x_{t+1} = Ax_t + Bu_t \tag{4.9}$$

and

$$A = \begin{pmatrix} 1 & 0 & T_S & 0 \\ 0 & 1 & 0 & T_S \\ 0 & 0 & 1 & 0 \\ 0 & 0 & 0 & 1 \end{pmatrix} \qquad B = \begin{pmatrix} T_S & 0 \\ 0 & T_S \\ 1 & 0 \\ 0 & 1 \end{pmatrix}$$

where $x_t = [x_{1,t}, x_{2,t}, \dot{x}_{1,t}, \dot{x}_{2,t}]^T$ is the state vector at time t. The first two elements of the state vector denote the location of target in the two-dimension Cartesian coordinate system, and the other two elements are the velocity of the target. $u_t = [u_{1,t}, u_{2,t}]^T$ is the process noise with known distribution which accounts for the variation of target speed.

The state evolution model above is a linear model, which has remarkable performance when the dynamic pattern of target is prior known and comparatively linear. However, the performance of the model degenerates severely when dynamic pattern of target is different. Besides that, the model requires the prior knowledge about the initial state of target.

4.2.2 PF-AA algorithm

Our method includes two simple ideas: (1) we estimate the velocity of the moving target based on the estimation state history and current measurement using AR model. The current measurement is introduced into the AR model by WCL method. In [7], the velocity of state evolution model is updated by the time duration of each landmark tag staying in the reader's reading range. The estimation is highly inaccurate and unreliable. To best of our knowledge, our method is the first to use WCL on fusing the current measurement into the state evolution model; (2) we implement a minor modification to ST locator protocol, by which the host server is able to obtain the asynchronous detection information. Based on such information the estimation bias could be computed. With these two ideas, we design PF-AA algorithm for better accuracy and applicability in indoor target localization application.

As mentioned earlier, RFID reader sends out the number of N rounds of Q_T queries for reading the tags in the time interval between $t-1$ and t. In the original ST locator protocol the reader does not record any information about reading, and ST simply accumulates the read rate of passive tags in its proximity. To counter the false synchronous detection assumption, a minor modification is introduced to record the asynchronous detection associated information. Since it is designed to be simple and energy efficient, ST is not a good candidate for the modification to record the detection information. Instead, we propose that RFID reader records the time instant of successive detection associated with the tag ID for each query. In addition, ST reports to the reader the query round number of detections for each detected passive tag rather than merely the read rate out of N. The host server obtains the time instants for each tag detection of ST by fusing the recorded information together. The modified ST locator protocol is still EPCglobal Class1 Gen2 compliant. We denote the detection of the specific passive tag T_k at time t by

$$y_{t,k} = \{n_{t,k}, \tau_{i,k} : n_{t,k} < N, t-1 < \tau_{i,k} < t, i \in \{1, ..., n_{t,k}\}\} \tag{4.10}$$

where $n_{t,k}$ is read rate, $\tau_{i,k}$ is the time instant of ith detection of tag T_k.

The state evolution model characterizes the location state $x_t = [x_{1,t}\ x_{2,t}]$ of the moving target over time. The main purpose of the state evolution model is to predict location state x_t given the most current one x_{t-1}. The implementation of state evolution model depends on the dynamic pattern of the moving target. In this work, we utilize AR model to represent the discrete state evolution model as follows:

$$\mathbf{x}_t = \mathbf{x}_{t-1} + \hat{\mathbf{v}}_t \Delta t + \mathbf{q}_t \tag{4.11}$$

where $\mathbf{x}_t = [x_{1,t}\ x_{2,t}]$ denotes ST location in 2D cartesian coordinate system at time t. $\hat{\mathbf{v}}_t = [\hat{v}_{1,t}\ \hat{v}_{2,t}]$ denotes the ST velocity estimation based on the current measurement and history estimation. $\mathbf{q}_t$ is the noise vector with known Gaussian distribution.

Now we address the velocity estimation given the target location $\hat{\mathbf{x}}_{t-1}$ and velocity $\hat{\mathbf{v}}_{t-1}$ from previous sampling step, as well as the current measurement $\{y_{t,k}, k \in \{1, ..., N_{tag}\}\}$. It is worth noting that $y_{t,k}$ is represented in Equation 4.10.

First, the current target location $\mathbf{x}_t$ is estimated through WCL method:

$$\hat{\mathbf{x}}_t^* = \frac{\sum_{i=1}^{N_{tag}} (n_{t,i} \cdot LT_i)}{\sum_{i=1}^{N_{tag}} n_{t,i}} \tag{4.12}$$

where $\{LT_i, i \in 1, ..., N_{tag}\}$ are the known locations of landmark tags. Then the velocity estimation $\hat{\mathbf{v}}_t^*$ simply based on the current measurements is calculated by

$$\hat{\mathbf{v}}_t^* = \frac{\hat{\mathbf{x}}_t^* - \hat{\mathbf{x}}_{t-1}}{\Delta t} \tag{4.13}$$

The current velocity $\hat{\mathbf{v}}_t$ is estimated by a auto-regressive (AR) model,

$$\hat{\mathbf{v}}_t = b_0 \hat{\mathbf{v}}_t^* + b_1 \hat{\mathbf{v}}_{t-1} \tag{4.14}$$

where b_0 and b_1 are weighting parameters. Note 1-order AR model is reasonable since there is no dynamic pattern constraints and proprioceptive sensor information.

When the RFID reader, landmark tags and ST are deployed as in Figure 4.8, the number of times that the tag is detected by ST is modelled as binomial distribution, that is, the probability of n detections out of the number N query rounds is given by

$$P(n|D, d, \theta, \phi) = \binom{N}{n} p(D, d, \theta, \phi)^n (1 - p(D, d, \theta, \phi))^{N-n} \tag{4.15}$$

where D, θ and ϕ are the distance, azimuth and elevation from reader antenna to tag.

d is the distance from tag to ST. $p(D, d, \theta, \phi)$ is the detection probability of ST-to-tag.

With the state evolution model and measurement model, we are ready to implement particle filter scheme to localize ST. Suppose that at time instant $t-1$, a random measure of size M, $\chi_{t-1} = \{\mathbf{x}_{t-1}^{(m)}, w_{t-1}^{(m)}\}_{m=1}^{M}$ is available, which is used to characterize the posterior distribution of $\mathbf{x}_{t-1}$, where $\mathbf{x}_{t-1}^{(m)}$ are the particles of measure, and $w_{t-1}^{(m)}$ are the corresponding weights indicating the goodness of the particle.

Upon receiving the current measurements $\{y_{t,k}, k \in \{1, ..., N_{tag}\}\}$ at the time instant t, the particles are propagated by using

$$\mathbf{x}_t^{(m)} \sim \pi(\mathbf{x}_t | \mathbf{x}_{t-1}^{(m)}, y_{0:t}) \tag{4.16}$$

where $\pi(\mathbf{x}_t | \mathbf{x}_{t-1}^{(m)}, y_{0:t})$ is the proposal distribution used for generating new particles $\mathbf{x}_t^{(m)}$.

PF-AA utilizes a different method to generate new particles based on current measurement compared with the traditional auxiliary particle filter, which uses current measurement to reweight the particles $\mathbf{x}_{t-1}^{(m)}$ before particle propagation [56]. Current measurement is used to update dynamic input of state evolution model through WCL method. Therefore, the target state at time instant t is predicted by propagating all particles at time $t-1$ according to the importance function $p(\mathbf{x}_t | \mathbf{x}_{t-1}^{(m)})$ based on state evolution model. The weights that are assigned to the particles are given by

$$\begin{aligned} w_t^{(m)} &\propto \frac{p(y_t | \mathbf{x}_t^{(m)}) p(\mathbf{x}_t^{(m)} | \mathbf{x}_{t-1}^{(m)})}{\pi(\mathbf{x}_t | \mathbf{x}_{0:t-1}^{(m)}, y_{0:t})} w_{t-1}^{(m)} \\ &\propto \frac{p(y_t | \mathbf{x}_t^{(m)}) p(\mathbf{x}_t^{(m)} | \mathbf{x}_{t-1}^{(m)})}{p(\mathbf{x}_t | \mathbf{x}_{t-1}^{(m)})} w_{t-1}^{(m)} \\ &\propto p(y_t | \mathbf{x}_t^{(m)}) w_{t-1}^{(m)} \end{aligned} \tag{4.17}$$

where

$$p(y_t|\mathbf{x}_t^{(m)}) = \prod_{i=1}^{N_{tag}}[\binom{N}{n_{t,i}} p_i(\mathbf{x}_t^{(m)})^{n_{t,i}}(1-p_i(\mathbf{x}_t^{(m)}))^{N-n_{t,i}}] \quad (4.18)$$

$$p_i(\mathbf{x}_t^{(m)}) = \frac{1}{1+e^{a_0+a_1 D_i+a_2 d_i^{(m)}+a_3|\theta_i|+a_4|\phi_i|}} \quad (4.19)$$

where D_i, θ_i and ϕ_i are from the geometry relationship between reader and tag T_i, $d_i^{(m)}$ is the distance between particle $\mathbf{x}_t^{(m)}$ and tag T_i.

Then the weight of particles are normalized by

$$w^{(m)} = \frac{w^{(m)}}{\sum_{i=1}^{M} w^{(i)}} \quad (4.20)$$

Once the weights are normalized, we form the random measure for the time instant t, $\chi_t = \{\mathbf{x}_t^{(m)}, w_t^{(m)}\}_{m=1}^{M}$. This random measure is used to estimate $\mathbf{x}_t$ by

$$\hat{\mathbf{x}}_t = \sum_{m=1}^{M} w_t^{(m)}\mathbf{x}_t^{(m)} \quad (4.21)$$

To avoid degeneration of the random measure, the resampling scheme is executed to eliminate particles with small weights and replicate particles with large weights [82]. After resampling the current particles is replaced with the new one and the weights $\{w_t^{(m)}, m = 1, ..., M\}$ are set to $1/M$.

Then we utilize the current target location estimation to update the current velocity estimation,

$$\hat{\mathbf{v}}_t = \frac{\hat{\mathbf{x}}_t - \hat{\mathbf{x}}_{t-1}}{\Delta t} \quad (4.22)$$

An additional step of the algorithm is to characterize the estimation bias from the synchronous detection assumption. When the speed estimation $\hat{\mathbf{v}}_t$ exceeds certain predefined threshold, the following steps are executed. We obtain the time instants of successive detections from the measurement $\{y_{t,k}, k \in \{1, ..., N_{tag}\}\}$, which spread over the range of $(t-1, t)$. We assume the location estimation $\hat{\mathbf{x}}_t$ is at the time instant $\hat{t}$ given by

$$\hat{t} = \frac{\sum_k^{N_{tag}} \sum_i^{n_{t,k}} \tau_{i,k}}{\sum_k^{N_{tag}} n_{t,k}} \tag{4.23}$$

thereby, the final estimate of target at the time instant t is given by

$$\tilde{\mathbf{x}}_t = \hat{\mathbf{x}}_t + (b_0 \hat{\mathbf{v}}_t + b_1 \hat{\mathbf{v}}_{t-1})(t - \hat{t}) \tag{4.24}$$

The PF-AA algorithm takes the above steps in a recursive fashion. A pseudo-code description of this algorithm is given by Algorithm 2.

4.2.3 Performance evaluation

In this section, the simulation is used to evaluate the effectiveness of the proposed algorithm. The simulation setup follows the deployment scenario of AURIS in PASS as shown in Figure 4.10. The area was 4 m $\times$ 3.2 m, and covered by 9 $\times$ 5 UHF RFID landmark tags. RFID reader's panel antenna is placed at center of the area with height as 2 m facing the ground. The PASS simulation framework is configured as in Section 4.1.3. As for simulation parameters, the state evolution noise vector is given as $\mathbf{q}_t = [\mathcal{N}(0, 0.3), \mathcal{N}(0, 0.3)]$. The parameters of measurement models were the ones obtained in Section 4.1.3. In all the simulation, the PF algorithms used 200 particles. The number of query round Q_T was set as 10. The localization performance was measured by average root mean square error (RMSE). The RMSE for one realization

ALGORITHM 2: PF-AA algorithm

```
while t = 1, 2, 3, ... do
    if t == 1 then
        /* Initialization                                                */
        x_1^(m) ~ N(x̂*_1, q_1), w^(m) = 1/M and v̂_1 = 0
            where x̂*_1 is calculated according to (4.12), q_1 is predefined Gaussian
             noise vector.
        /* Weight Update                                                 */
        Update w^(m) according to (4.17) and normalize according to (4.20).
        /* Estimation                                                    */
        Estimate x̂_1 according to (4.21)
    else
        /* Velocity update                                               */
        v̂_t is updated according to (4.14).
        /* Propagation                                                   */
        Generate particles x_t^(m) ~ p(x_t | x_{t-1}^(m)) according to (4.27)
        /* Weight Update                                                 */
        Update w^(m) according to (4.17) and normalize according to (4.20).
        /* Estimation                                                    */
        Estimate x̂_t according to (4.21).
        /* Velocity update                                               */
        v̂_t is updated according to (4.22).
    end
    /* Resampling                                                        */
    Resample M particles from the current measure χ_t = {x_t^(m), w_t^(m)}_{m=1}^M;
    Assign w^(m) = 1/M to each weight of new particle set.
    /* Output                                                            */
    if v̂_t < v_threshold then
        x̃_t = x̂_t
    else
        /* Bias compensation                                             */
        x̃_t is estimated according to (4.24).
    end
end
```

is calculated as $\sqrt{(\tilde{x}_{1,t} - x_{1,t})^2 + (\tilde{x}_{2,t} - x_{2,t})^2}$.

In the first set of experiments, our goal was to obtain the speed threshold used

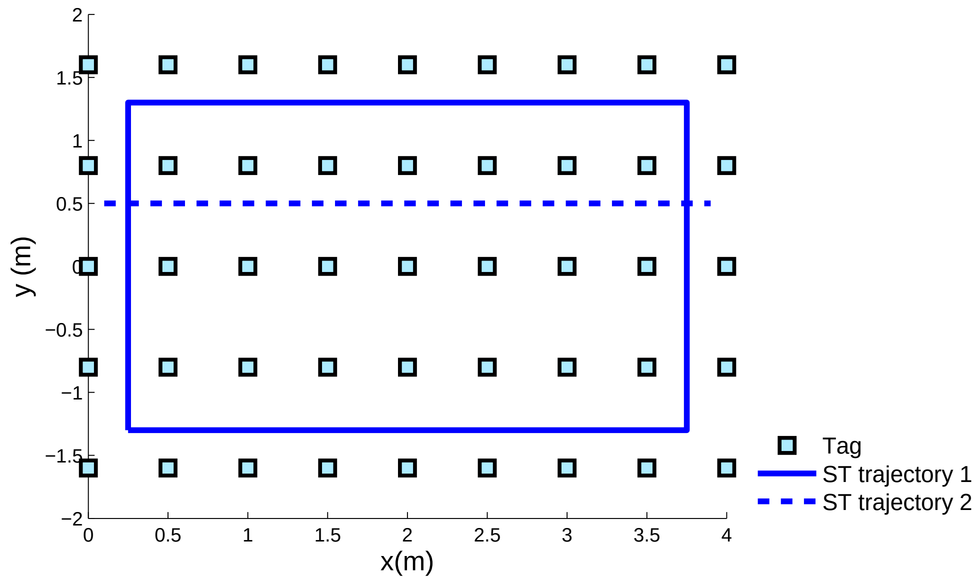

Figure 4.10: Experiment setup with landmark tags deployment, and ST trajectories.

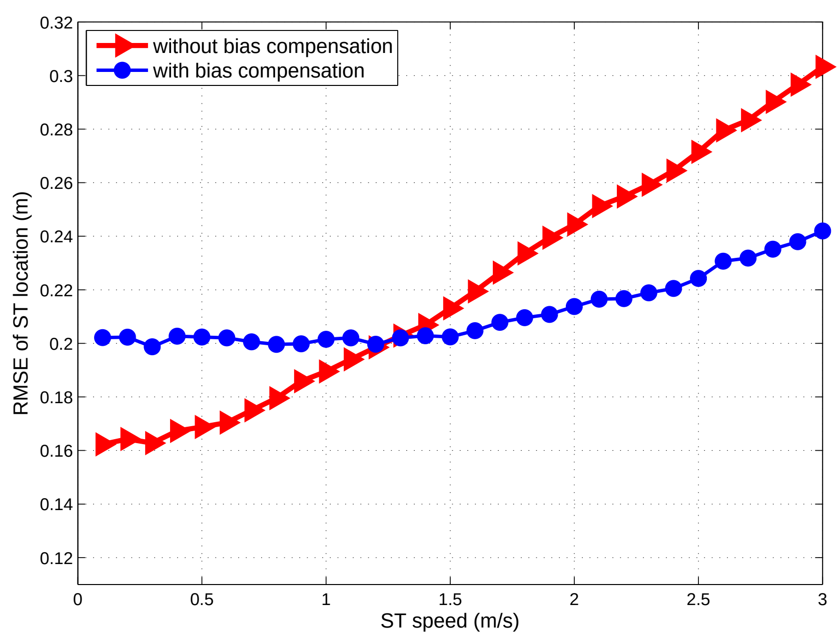

Figure 4.11: The performance of PF-AA bias compensation technique.

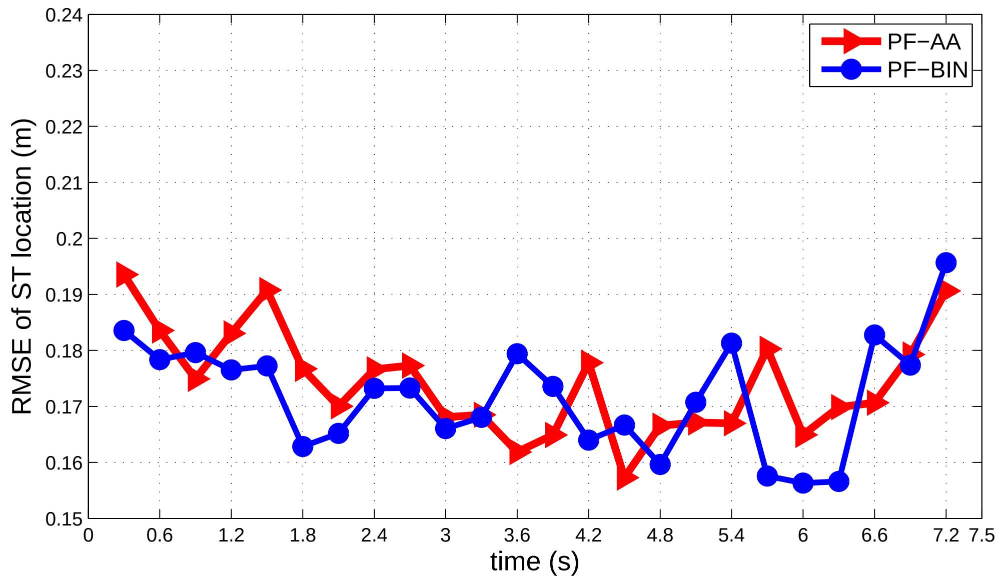

Figure 4.12: The performance of PF-AA and PF-BIN with ST speed 0.5 m/s.

for bias compensation of false synchronous detection assumption. We compared the localization performance of two implementations of PF-AA algorithms over moving speed at the range of $[0.1, 3]$ m/s. One implementation was the original PF-AA without bias compensation at any $\mathbf{v}_t$ by setting $\mathbf{v}_{threshold}$ as 100. The other was the original PF-AA with bias compensation at any $\mathbf{v}_t$ by setting $\mathbf{v}_{threshold}$ as 0. We generated 100 independent realizations for the two implementations following the ST trajectory 1 as shown in Figure 4.10. The query period was set as $T_s = 0.3$ s. The results are shown in Figure 4.11. We can see that these two implementations perform differently for ST with different speed. To be specific, PF-AA without bias compensation performs better than that with bias compensation when the speed of ST is lower than 1.2 m/s. Therefore, it is reasonable to set $\mathbf{v}_{threshold}$ as 1.2 m/s.

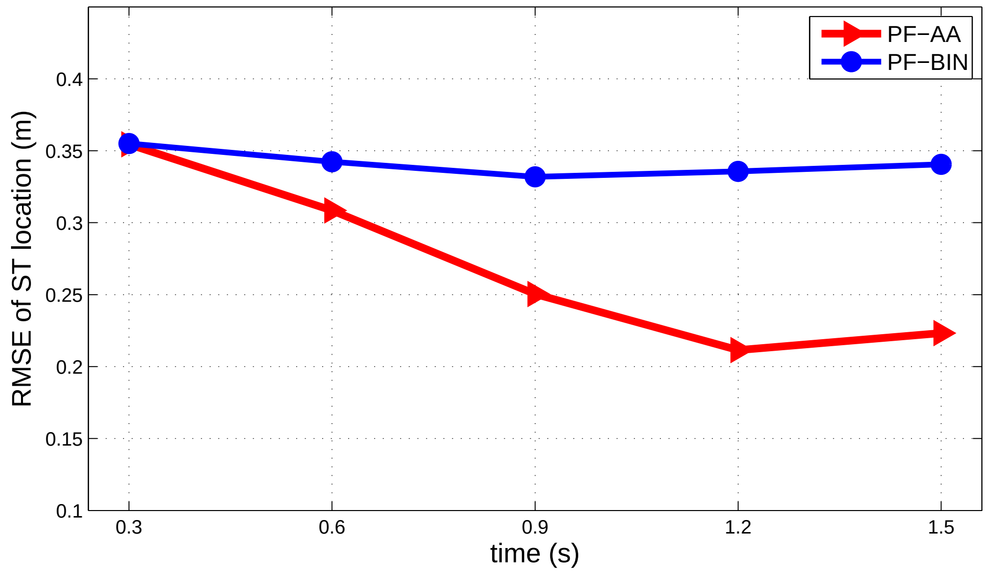

Figure 4.13: The performance of PF-AA and PF-BIN with ST speed 2.5 m/s.

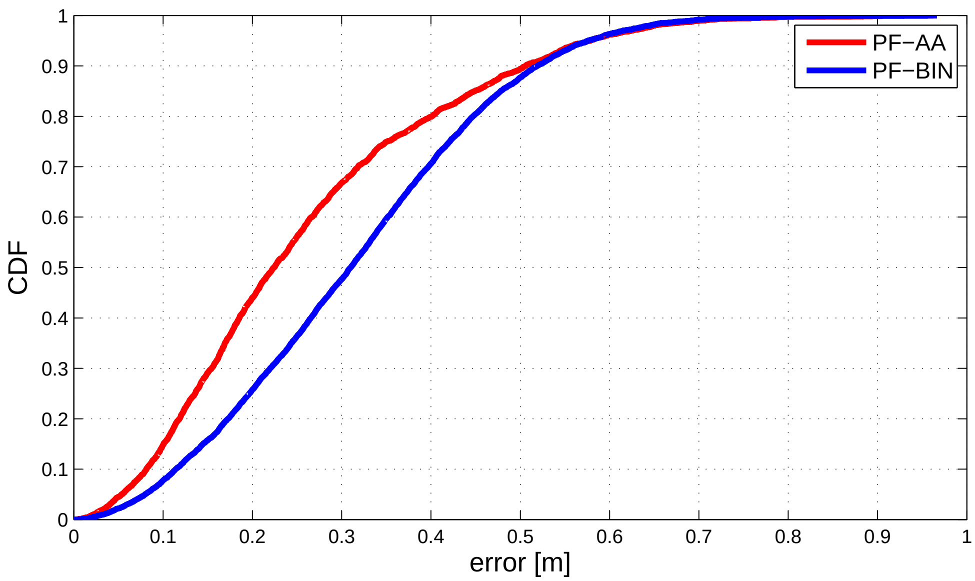

Figure 4.14: The CDFs of position erros of PF-AA and PF-BIN.

In the second set of experiments, we compared the localization performance of different PF algorithms: (a) PF-BIN algorithm in [11]; (b) PF-AA algorithm. For PF-BIN algorithm, it requires prior knowledge of initial state and movement speed. The process covariance matrix of its state evolution model was given by $diag(0.01, 0.01)$. Note the measurement model of PF-BIN is updated to RTS model. First, ST trajectory was set as ST trajectory 2 in Figure 4.10. The speed was 0.5 m/s. We generated 100 independent realizations of the ST trajectory 2. The results are shown in Figure 4.12, where the data is obtained by averaging the RMSEs over time. The overall RMSE of PF-BIN is 0.1681 m, while that of PF-AA is 0.1717 m. In this situation, PF-BIN performs slightly better than PF-AA. Second, ST speed is modified to be 2.5 m/s. We implemented 500 independent realizations of ST trajectory 2. According to Figure 4.13, the PF-AA consistently performs better than PF-BIN. During some initial period, the performance of PF-AA is not desirable due to the setup time for bias compensation. In Figure 4.14, we plot the cumulative distribution functions (CDF) of the errors for PF-AA and PF-BIN. PF-AA performs better than PF-BIN.

Finally, we simulated a scenario with random walk trajectory of ST to compare WCL and PF-AA. The random walk trajectory is implemented as that ST moves straight with a constant speed, whenever it arrives at the area boundary, it bounces back at random angle with random speed. The speed of ST is uniformly distributed over the range of $[0.1, 3]$ m/s. As seen in Figure 4.15, as expected, PF-AA performs better than WCL. As the time goes by 1500 seconds, the cumulated RMSE is reduced by around 36.6%.

4.3 Landmark-based sequential localization and mapping framework using AURIS

In this section, we propose a landmark-based sequential localization and mapping framework (SQLAM) using AURIS, a system that leverages a set of passive landmarks tags to localize ST, and sequentially constructs a geographical map of passive tags

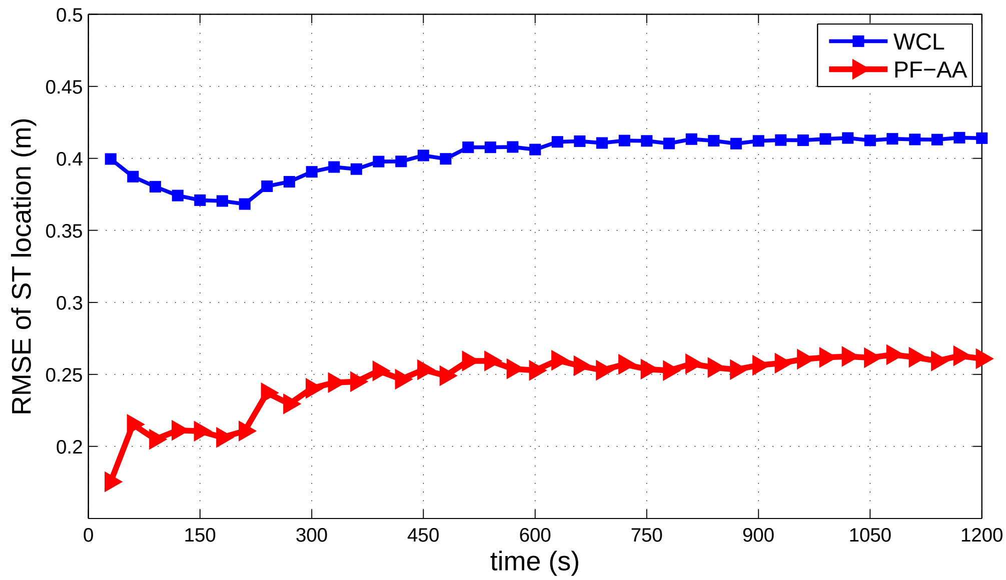

Figure 4.15: The performance of PF-AA and WCL with random walk trajectory.

with unknown locations while ST is moving in the environment. Mapping location-unknown passive tags accurately leads to practical advantages. First, the localization capability of AURIS is not confined to the objects carrying STs. Second, the passive tags with resolved locations could be included into landmark set to localize ST, hence leading to better ST localization accuracy and robustness.

Figure 4.16 shows a typical deployment case of AURIS for fine-grained proximity-based localization. The system is composed of a host server which runs the localization algorithm, an off-the-shelf RFID reader, a large set of standard tags placed at known location as landmarks, a ST attached to mobile target of interest, as well as certain other standard tags with unknown locations. The sensing range of ST is depicted as the dotted circle. In this example there are two landmark tags and one passive tag with unknown location within ST's sensing range. As a result of several query rounds, the host server could utilize the aggregated information to localize ST. Furthermore, the estimation of the passive tag's location is available with the proposed SQLAM

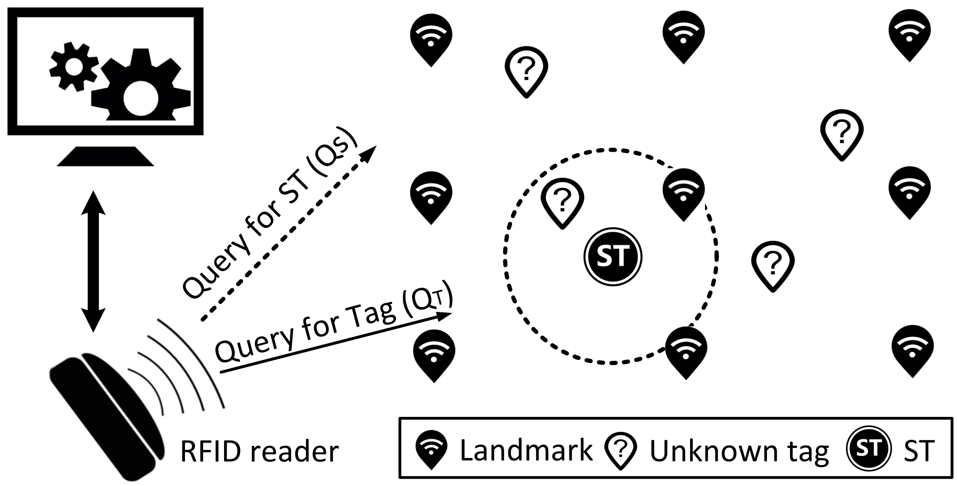

Figure 4.16: The deployment of AURIS with unknown tags

framework in this section.

Compared with the conventional simultaneous localization and mapping (SLAM) method used in robot domain [83], which utilizes various equipped sensors to update a local map of surrounding environment while simultaneously keeping track of the target's position within it, the major difference of SQLAM is that it purely relies on proximity information. In particular, SQLAM uses three critical steps as following:

- First, a large set of passive tags are deployed in the area of interest at known positions as landmarks. According to AURIS's EPCglobal Class1 Gen2-compliant locator protocol, the RFID reader sends out a fixed number of query rounds to the passive tags. Then ST is localized according to a particle filtering-based inference algorithm using aggregated binary measurements reported by ST.

- Second, SQLAM discovers passive tags with unknown locations that already exist in the environment, by a temporal weighted centroid localization approach based on aggregated binary measurements of ST to passive tags as well as ST location estimation. In this way, these passive tags with unknown locations become passive tags with resolved locations. The philosophy behind temporal

WCL is straightforward, in which the most relevant measurements of ST-to-tag are maintained in the observation vector for each passive tag according to the detection rate of ST-to-tag. The observation vector is a vector with pre-defined size, which holds the largest detection rates of ST-to-tag with the number of vector size until the current time instance.

- Third, passive tags with resolved locations are incorporated into the landmark set to replace the landmark tags in case the landmark tags fail or get damaged. Landmark tags will fail to respond to RFID reader due to temporary electromagnetic blockage or permanent hardware failure, which is fatal to proximity-based localization method. SQLAM proposes to compensate the failure of landmark tags by selecting passive tags with resolved locations as substitutes.

4.3.1 Framework overview

The objective of this framework is to design a method to localize ST and map unknown tags accurately. We depict our AURIS system by using Figure 4.16. ST has the capability to capture the backscattering communication between passive landmark tags and RFID reader. The location of ST could be inferred from the aggregated detection information and prior known landmark map. On the other hand, unknown tags are mapped based on the uncertain ST location estimation rather than landmark map, since there is no direct communication link between unknown tag and landmarks. In AURIS system ST is attached to mobile target which is always moving, while passive tags are attached to static objects. Along with more aggregated detection information collected by ST, the mapping accuracy of unknown tags is improved gradually. Unlike conventional simultaneous localization and mapping (SLAM) framework, SQLAM does not include the discovered unknown tags to localize ST till their mapping accuracy surpasses certain threshold. Figure 4.17 shows the

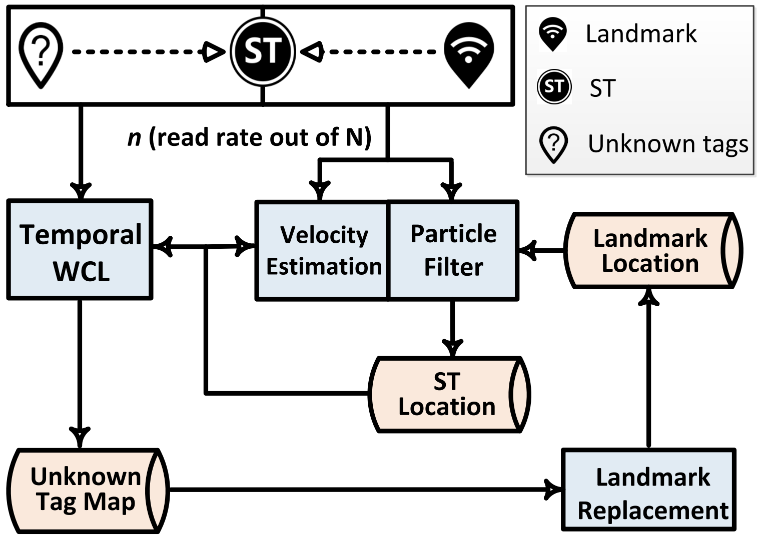

Figure 4.17: The SQLAM framework architecture (the blue box represents the algorithm that will be performed, the light red shape represents the data that will be stored).

SQLAM framework architecture.

Our SQLAM framework includes three main modules.

Particle filter

In particle filter-like approach, two models are defined: first, a model describing the evolution of object's state (the state evolution model); second, a model relating the noisy ST readings (the measurement model) [53].

As the control input the state evolution model, the velocity of the moving ST is not estimated in the particle filter framework but based on the location history and current ST-to-landmark measurements. Incorporating the current velocity estimation as input, the state evolution model of the particle filter is more robust than previous models, which relies on a strong assumption that the motion pattern of the object is relatively stable without sharp maneuver and speed change [11].

Temporal WCL

The weighted centroid localization (WCL) calculates the mobile target's location by weighted average from all the locations of the landmarks in the range of mobile target [49]. However, ST keeps moving while unknown tags are static, which leads conventional WCL unapplicable for localizing unknown tags. To overcome the above issue, we extend WCL in time domain for localizing unknown tags with obtained ST location estimation. Specifically, the current location of unknown tag is estimated by weighted averaging a limited number of most relevant ST location estimations, whose relevance are measured in terms of read rate.

Landmark replacement

The coverage of landmark tags is crucial for proximity-based indoor localization methods. However, certain landmark tags could be compromised due to temporary electromagnetic blockage or permanent hardware failure. We propose landmark replacement algorithm exploiting passive tags with resolved location from previous stage. The replacement algorithm depends on the combination of passive tag location uncertainty and the distance of passive tag to the failed landmark. Additionally, two methods are proposed to include the substitute into the landmark set, which will described in Section 4.3.2.

4.3.2 The SQLAM Framework

The general introduction of SQLAM framework is described in Section 4.3.1. This section explains the details of different modules in the framework.

Table 4.2: Summary of terms and their definitions related to SQLAM

Term	Definition
$\hat{\mathbf{x}}_t$	ST location estimation at time t
$\hat{\mathbf{v}}_t$	ST velocity estimation at time t
$p(D, d, \theta, \phi)$	the detection probability model of ST-to-tag
N_{LT}	the number of landmark tags
LT_k	the prior known location of the kth landmark tag
$n_{t,k}$	the read rate of the kth landmark tag at time t
$\aleph_i$	the read rate vector of the ith unknown tag along the time $1:t$
OV_i	the vector formed by N_{tmp} largest elements in $\aleph_i$
N_{u_i}	the number of aggregated binary measurements for the ith unknown tag along the time $1:t$
N_{UT}	the number of unknown tags
UT_i	the location estimation of the ith unknown tag
RP_k	the unknown tag selected to replace the failed landmark tag k
N^*_{LT}	the number of replacement landmark tags

Velocity Estimation

We first estimate the speed of the moving ST at time t. Let's suppose that $\mathbf{x}_t = [x_{1,t}\ x_{2,t}]$ denotes ST location in 2D cartesian coordinate system at time t. $\mathbf{v}_t = [v_{1,t}\ v_{2,t}]$ denotes the ST velocity. $\hat{\mathbf{x}}_t = [\hat{x}_{1,t}\ \hat{x}_{2,t}]$ denote ST location estimation. $\hat{\mathbf{v}}_t = [\hat{v}_{1,t}\ \hat{v}_{2,t}]$ denotes the ST velocity estimation.

Given the ST location estimation $\hat{\mathbf{x}}_{t-1}$ and velocity estimation $\hat{\mathbf{v}}_{t-1}$ at time $t-1$, as well as the detection rate from N_{LT} landmark tags at time t, $\mathbf{n}_t = \{n_{t,k}, k \in \{1, \ldots, N_{LT}\}\}$, we estimate the current velocity $\hat{\mathbf{v}}_t$. The current ST location is roughly estimated using WCL method:

$$\hat{\mathbf{x}}_t^* = \frac{\sum_{k=1}^{N_{LT}} (n_{t,k}\ LT_k)}{\sum_{k=1}^{N_{LT}} n_{t,k}} \tag{4.25}$$

where $\{LT_k, k \in \{1, \ldots, N_{LT}\}\}$ are the prior known locations of landmark tags. Then the velocity $\hat{\mathbf{v}}_t^*$ simply based on the current measurement is calculated by $\hat{\mathbf{v}}_t^* = (\hat{\mathbf{x}}_t^* - \hat{\mathbf{x}}_{t-1})/\Delta t$. $\hat{\mathbf{v}}_t$ is estimated by a auto-regressive (AR) model to improve the performance [84].

$$\hat{\mathbf{v}}_t = b_0 \hat{\mathbf{v}}_t^* + b_1 \hat{\mathbf{v}}_{t-1} \tag{4.26}$$

where b_0 and b_1 are weighting parameters.

ST Tracking with Particle Filter

In this subsection, we solve the ST tracking problem through particle filter approach. The state evolution model characteristics state sequence of ST location, $\mathbf{x}_t = [x_{1,t}\ x_{2,t}]$. We have the discrete state evolution model as follows:

$$\mathbf{x}_t \quad = \quad \mathbf{x}_{t-1} + \hat{\mathbf{v}}_t \Delta t + \mathbf{q}_t \tag{4.27}$$

where $\mathbf{q}_t$ is the noise vector with a known Gaussian distribution.

The detection rate from passive tag to ST is modeled as a binomial distribution, that is, the probability of n detections in N query rounds is given as follows:

$$P(n|D, d, \theta, \phi) = \binom{N}{n} p(D, d, \theta, \phi)^n (1 - p(D, d, \theta, \phi))^{N-n} \tag{4.28}$$

Upon receiving the current measurement $\mathbf{n}_t$, the particles are propagated for generating new particles $\mathbf{x}_t^{(m)}$ according to state evolution model Equation (4.27). The weights that are assigned to the new particles are given.

$$w_t^{(m)} \quad \propto \quad p(\mathbf{n}_t|\mathbf{x}_t^{(m)})w_{t-1}^{(m)} \tag{4.29}$$

where $p(\mathbf{n}_t|\mathbf{x}_t^{(m)})$ is formulated by the measurement model.

$$p(\mathbf{n}_t|\mathbf{x}_t^{(m)}) = \prod_{k=1}^{N_{LT}}[\binom{N}{n_{t,k}}p_k(\mathbf{x}_t^{(m)})^{n_{t,k}}(1-p_k(\mathbf{x}_t^{(m)}))^{N-n_{t,k}}] \tag{4.30}$$

$$p_k(\mathbf{x}_t^{(m)}) = \frac{1}{1+e^{a_0+a_1D_k+a_2d_k^{(m)}+a_3|\theta_k|+a_4|\phi_k|}} \tag{4.31}$$

D_k, θ_k and ϕ_k are from the geometry relationship between reader and landmark tag k, $d_k^{(m)}$ is the Euclidean distance between particle $\mathbf{x}_t^{(m)}$ and landmark tag k.

Once the weights of particles are computed according to Equation (4.29), we normalize the weights and form a new random measure, $\chi_t = \{\mathbf{x}_t^{(m)}, w_t^{(m)}\}_{m=1}^M$. This random measure then is used to estimate $\mathbf{x}_t$ by

$$\hat{\mathbf{x}}_t = \sum_{m=1}^{M} w_t^{(m)}\mathbf{x}_t^{(m)} \tag{4.32}$$

To avoid a degeneration of the random measure, we execute resampling on $\chi_t = \{\mathbf{x}_t^{(m)}, w_t^{(m)}\}_{m=1}^M$, by drawing M particles from $\mathbf{x}_t^{(m)}$ with probability proportional to the corresponding weight $w_t^{(m)}$. An additional step of the algorithm, is to update the estimation of current velocity $\hat{\mathbf{v}}_t$ by $(\hat{\mathbf{x}}_t - \hat{\mathbf{x}}_{t-1})/\Delta t$, which could be used in velocity estimation at time $t+1$.

The algorithm is specified below in Algorithm 3.

ALGORITHM 3: ST tracking with particle filter

```
while t = 1, 2, 3, ... do
    if t == 1 then
        /* Initialization                                                    */
        x_1^(m) ~ N(x̂_1^*, q_1), w_0^(m) = 1/M and v_1 = 0;
            x̂_1^* is calculated according to Eq. (4.25), q_1 is predefined Gaussian
            noise vector.
        /* Weight Update                                                     */
        Update w_1^(m) according to Eq. (4.29) and normalization;
        /* Estimation                                                        */
        Estimate x̂_1 according to Eq. (4.32);
    else
        /* Evolution Model Update                                            */
        v̂_t is updated by v̂_t = b_0 v̂_t^* + b_1 v_{t-1};
            v̂_t^* = (x̂_t^* - x̂_{t-1})/Δt, x̂_t^* from Eq. (4.25).
        /* Propagation                                                       */
        Generate the new particles according to Eq. (4.27);
        /* Weight Update                                                     */
        Update w_t^(m) according to Eq. (4.29) and normalization;
        /* Estimation                                                        */
        Estimate x̂_t according to Eq. (4.32), evolution model is updated by
        v_t = (x̂_t - x̂_{t-1})/Δt.
    end
    /* Resampling                                                            */
    Resample M particles from the current measure χ_t = {x_t^(m), w_t^(m)}_{m=1}^M;
    Assign w_t^(m) = 1/M to each weight of new particle set.
end
```

Unknown Tag mapping with Temporal WCL

As mentioned in previous subsection, ST is localized accurately using particle filter based on the aggregated binary measurements with landmark tags. Meanwhile, ST also gathers the aggregated binary measurements with unknown tags as it moves in the environment. The task of localizing unknown tags is rooted in analyzing the aggregated binary measurements. We propose a WCL-like method, in which the conventional WCL is extended in time domain.

ALGORITHM 4: Tag mapping with temporal WCL

```
while t = 1, 2, 3, ... do
    for i = 1,..., N_UT do
        /* Update OV_i                                  */
        if Nu_i < N_tmp then
            OV_i = ℵ_i;
        else
            OV_i = MAX(ℵ_i, N_tmp);
        end
        /* Location estimation                          */
        UT_i is calculated according to Eq. (4.33).
    end
end
```

The detections of ST-to-unknown tag are accumulated to form a vector with read rates as elements. One major limitation of WCL method is that it is easily affected by outliers [85]. To resolve this issue, we iteratively update the vector so that it includes only the limited number of the most relevant observations by comparing the read rate.

For unknown tag i the aggregated binary measurements are represented as $\aleph_i = \{n_{i,t_j}, j \in \{1, \ldots, Nu_i\}\}$, and the location estimation of ST at time t_j is $\hat{\mathbf{x}}_{t_j}$. The number of unknown tags is represented by N_{UT}. We form the vector OV_i of unknown tag i by selecting N_{tmp} largest read rate in $\aleph_i$. It could be written in the form of $OV_i = MAX(\aleph_i, N_{tmp})$, in which the observation set is $\{n_{i,t_j^*}, j \in \{1, \ldots, N_{tmp}\}\}$.

The location of unknown tag i is estimated according to the following equation:

$$UT_i = \frac{\sum_{j=1}^{N_{tmp}} (n_{i,t_j^*} \; \hat{\mathbf{x}}_{t_j^*})}{\sum_{j=1}^{N_{tmp}} n_{i,t_j^*}} \quad (4.33)$$

The algorithm is specified below in Algorithm 4.

Replacement Algorithm with Resolved Unknown Tags

Our next objective is to exploit the estimated location of unknown tags to assist in localization of the STs in case some of the landmark tags are not available. To realize this objective, our strategy is to select unknown tags with resolved locations as substitutes for dysfunctional landmarks. If it is detected that a landmark tag is failed, the neighboring unknown tag with resolved location is selected to replace it. Otherwise, certain part of the environment will not be covered by the landmarks.

From previous subsection, for unknown tag i we obtain the location estimation UT_i and the corresponding $OV_i = \{n_{i,t_j^*}, j \in \{1, \ldots, N_{tmp}\}\}$. The variance of the observations is

$$s_i^2 = \frac{1}{\sum_{j=1}^{N_{tmp}} n_{i,t_j^*} - 1} \sum_{j=1}^{N_{tmp}} (n_{i,t_j^*} \ ||\hat{\mathbf{x}}_{t_j^*} - UT_i||_2^2) \tag{4.34}$$

where $|| \bullet ||_2$ is ℓ^2-norm operation.

Considering the distance to the failed landmark and the variance of observations, the unknown tags with resolved locations are selected under the following constraints:

- *Constraint 1*: the distance from the unknown tag with resolved location to the failed landmark should be closer than the distance to any other landmarks.
- *Constraint 2*: $s_i^2 < S_{threshold}$, the variance of observations s_i^2 reflects the estimation precision of observation mean UT_i. $S_{threshold}$ is a predefined parameter.
- *Constraint 2**: $sum(OV_i) > \alpha N_{tmp}$, the alternative constraint for *Constraint 2* to evaluate the quality of observations collected by ST. The summation of OV_i reflects the estimation accuracy of the observations to the unknown tags, since higher read rate means closer distance between ST-to-tag. α is the scaling parameter.

From the previous constrains, a set of potential substitutes for failed landmark k is formed. Among the substitutes , the one with the smallest distance to the failed landmark k is selected as replacement RP_k. The read rate vector of RP_k is $OV_{RP_k} = \{n_{t_j^*,k}, j \in \{1, \ldots, N_{tmp}\}\}$.

To incorporate the substitute landmark into particle filter method, this paper proposes two methods that we refer to as parametric and Monte Carlo-based method.

a. Parametric method

The unknown tag i with resolved location substitutes the failed landmark tag assuming that the location of unknown tag is UT_i without considering the uncertainty of location estimation. Therefore, the likelihood probability $p(\mathbf{n}_t|\mathbf{x}_t^{(m)})$ is updated as

$$\begin{aligned} p(\mathbf{n}_t|\mathbf{x}_t^{(m)}) = & \prod_{k=1}^{N_{LT}-N_{LT}^*} [\binom{N}{n_{t,k}} p_k(\mathbf{x}_t^{(m)})^{n_{t,k}} (1 - p_k(\mathbf{x}_t^{(m)}))^{N-n_{t,k}}] * \\ & \prod_{k=1}^{N_{LT}^*} [\binom{N}{n_{t,k}^*} p_k^*(\mathbf{x}_t^{(m)})^{n_{t,k}^*} (1 - p_k^*(\mathbf{x}_t^{(m)}))^{N-n_{t,k}^*}] \end{aligned} \tag{4.35}$$

where N_{LT} is the number of landmarks, N_{LT}^* is the number of substitutes. $n_{t,k}$ and $n_{t,k}^*$ are the read rate of ST to landmark and substitute tag respectively. $p_k(\mathbf{x}_t^{(m)})$ and $p_k^*(\mathbf{x}_t^{(m)})$ are the detection probability from ST sampling particle $\mathbf{x}_t^{(m)}$ to landmark and substitute respectively following Equation (4.31).

b. Monte Carlo-based method

In Monte Carlo-based method, the distribution of substitute location is approximated by a set of samples. Take the substitute RP_k for instance, the sampling particles of substitute location distribution is represented by $\{\hat{\mathbf{x}}_{t_j^*,k}, n_{t_j^*,k}\}_{j=1}^{N_{tmp}}$ according to the read rate vector $OV_{RP_k} = \{n_{t_j^*,k}, j \in \{1, \ldots, N_{tmp}\}\}$. The detection probability $p_k^*(\mathbf{x}_t^{(m)})$ from ST sampling particle to substitute is represented in terms of conditional

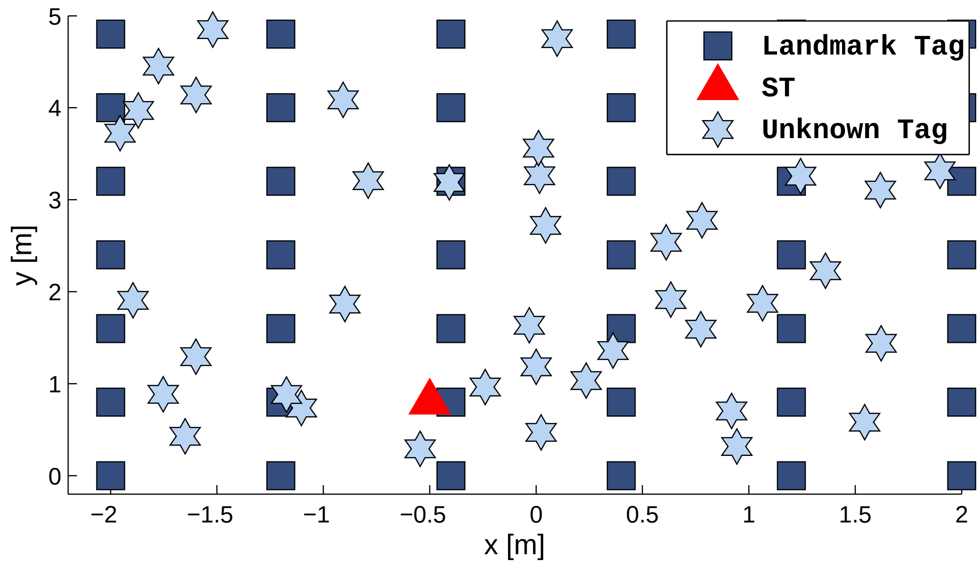

Figure 4.18: Experiment setup with landmark tag, unknown tag and ST.

probability:

$$p_k^*(\mathbf{x}_t^{(m)}) = \frac{1}{\sum_{j=1}^{N_{tmp}} n_{t_j^*,k}} \sum_{j=1}^{N_{tmp}} n_{t_j^*,k}\; p_k^*(\mathbf{x}_t^{(m)}, \hat{\mathbf{x}}_{t_j^*,k}) \tag{4.36}$$

$p_k^*(\mathbf{x}_t^{(m)}, \hat{\mathbf{x}}_{t_j^*,k})$ is the detection probability from ST sampling particle $\mathbf{x}_t^{(m)}$ to substitute sampling particle $\hat{\mathbf{x}}_{t_j^*,k}$. The form of $p_k^*(\mathbf{x}_t^{(m)}, \hat{\mathbf{x}}_{t_j^*,k})$ follows Equation (4.31), where D_k, θ_k and ϕ_k are from the geometry relationship between reader and replacement tag particle $\hat{\mathbf{x}}_{t_j^*,k}$, $d_k^{(m)}$ is the Euclidean distance between ST particle $\mathbf{x}_t^{(m)}$ and substitute sampling particle $\hat{\mathbf{x}}_{t_j^*,k}$. After obtaining $p_k^*(\mathbf{x}_t^{(m)})$, the likelihood probability is calculated as in the form of Equation (4.35).

4.3.3 Performance Evaluation

To evaluate the validity of the proposed SQLAM framework, a number of experiments have been carried out. The simulation setup follows the deployment scenario as shown in Figure 4.18. The PASS simulation framework is configured as in Section 4.1.3. The area is 5 $m \times 4$ m, and is covered by 7×6 UHF RFID landmark tags. Unknown tags are randomly distributed in the area. RFID reader's panel antenna is mounted at the center of the area at 2 m height facing the ground. The number of Q_T in each query round is set to 10. The localization performance is measured by average root mean square error (RMSE), which is ℓ^2-norm operation of the difference between estimation and true location.

In the first set of experiments, we simulate a scenario with random walk trajectory of ST to evaluate the localization performance of ST with particle filter comparing with conventional WCL method. The random walk trajectory is implemented as that ST moves along a straight line with constant speed. Whenever it arrives at the area boundary, ST bounces back at random angle with random speed. The speed is uniformly distributed over the range of $[0.1, 3]$ m/s. As for simulation parameters, the state evolution noise vector is given as $\mathbf{q}_t = [\mathcal{N}(0, 0.3), \mathcal{N}(0, 0.3)]$. The weighting parameter of speed approximation are $b_0 = 0.8$ and $b_1 = 0.2$. The particle filter uses 200 particles, $M = 200$. The reader sends out query round every 0.3 second. The time duration of query rounds is assumed to be proportional to the population of tags in the environment [86]. We conduct the simulations of 100 random tracks of ST. As seen in Figure 4.19, particle filter method performs better than WCL in terms of localization accuracy of ST. The overall RMSE of ST location is reduced by around 41.9% for the duration of 500 seconds.

The second set of experiments is to explore the temporal WCL for unknown tags based on the obtained ST location estimations. Our goal is to get the parameter N_{tmp} for the size of the observation set. The reader and landmark tags are deployed as in Figure 4.18. The ST moves along the random walk trajectory as described in

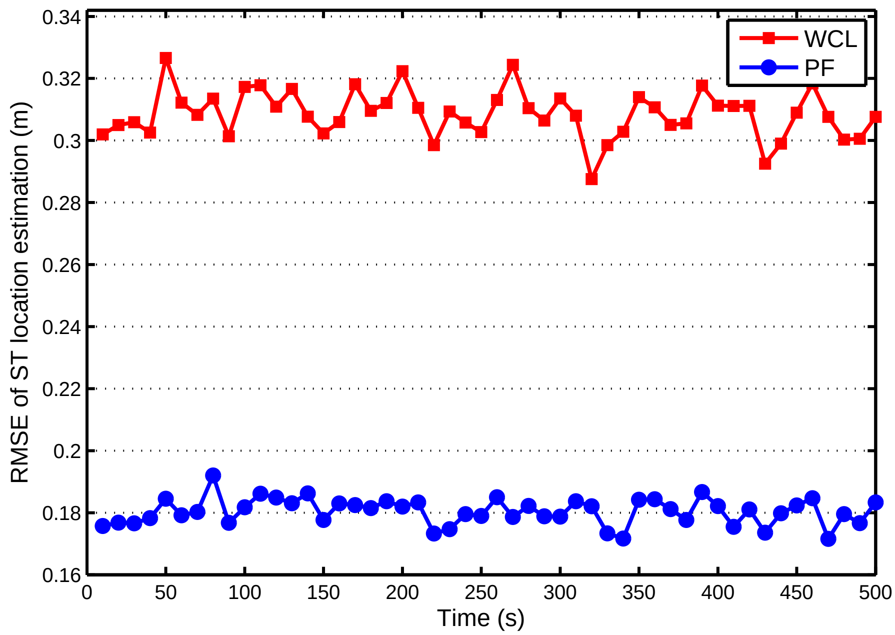

Figure 4.19: The performance of PF and WCL with random walk trajectory (the RMSE of ST location estimation against time).

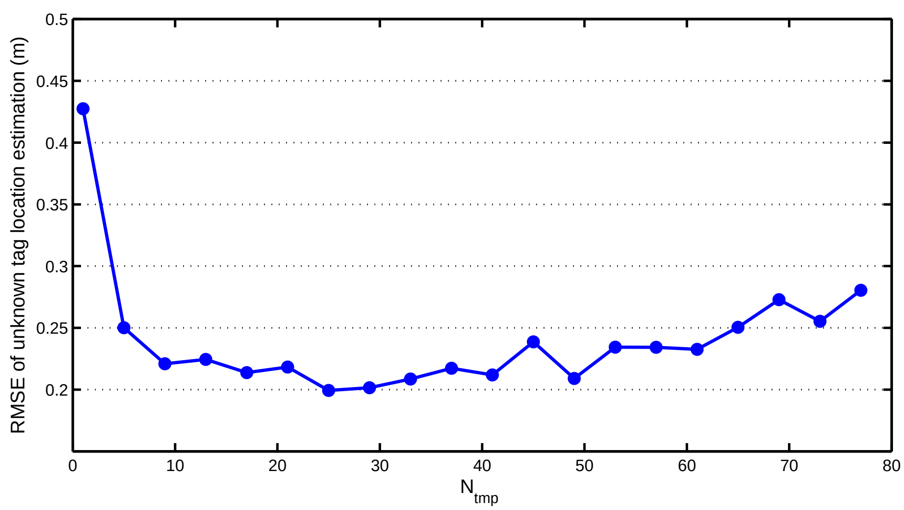

Figure 4.20: The performance of temporal WCL with different N_{tmp} (the RMSE of unknown tag location estimation against the number of N_{tmp}).

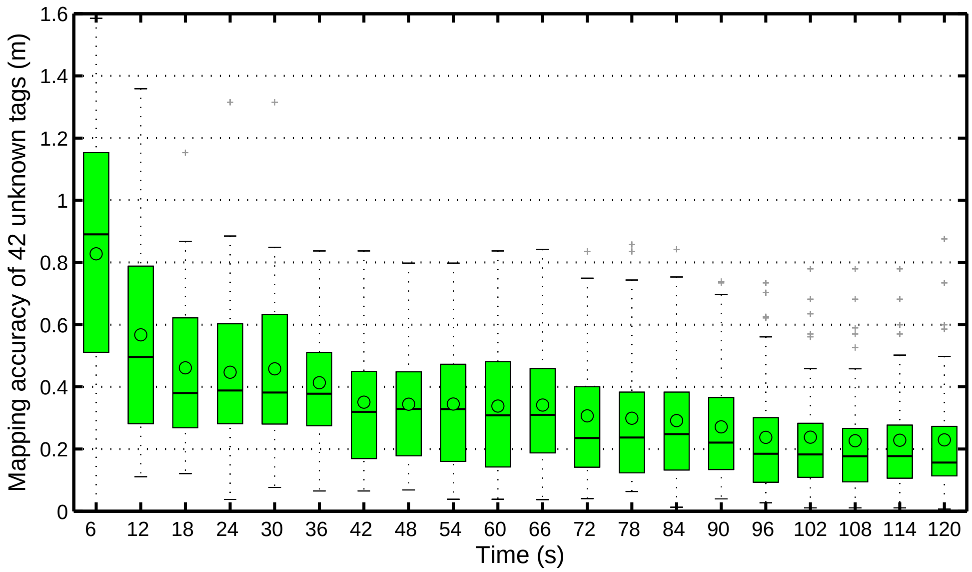

Figure 4.21: The performance of temporal WCL for 42 unknown tags (the mapping accuracy of 42 unknown tags against time).

the first set of experiments. An unknown tag is randomly placed in the environment, which is mapped by temporal WCL method. We repeat the simulation for 300 times with difference unknown tag placements. The results are shown in Figure 4.20 as the RMSE of the unknown tag location estimation versus different value of N_{tmp}. The temporal WCL algorithm achieves the highest mapping accuracy of unknown tag at $N_{tmp} = 25$.

The third set of experiments is to investigate the mapping accuracy of temporal WCL with $N_{tmp} = 25$. We conduct the simulation with 42 unknown tags randomly deployed in the scenario as in Figure 4.18. Figure 4.21 shows the mapping error distribution of these 42 unknown tags over time with box-and-whisker plot. In the plot, the central rectangular spans the first quartile to the third quartile. A segment inside the rectangular shows the median. The circle represents the mean. The "whiskers" above and below the box show the locations of the minimum and maximum. The crosses above the maximum whisker are the outliers. As time goes, there are more

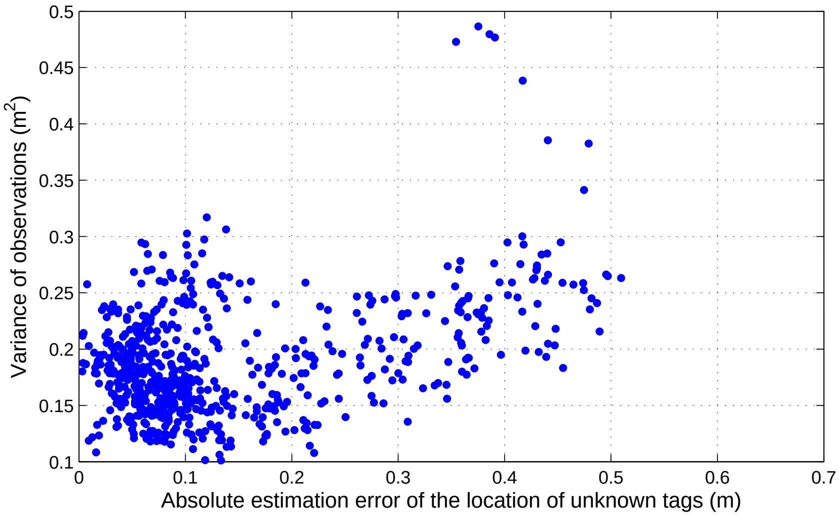

(a)

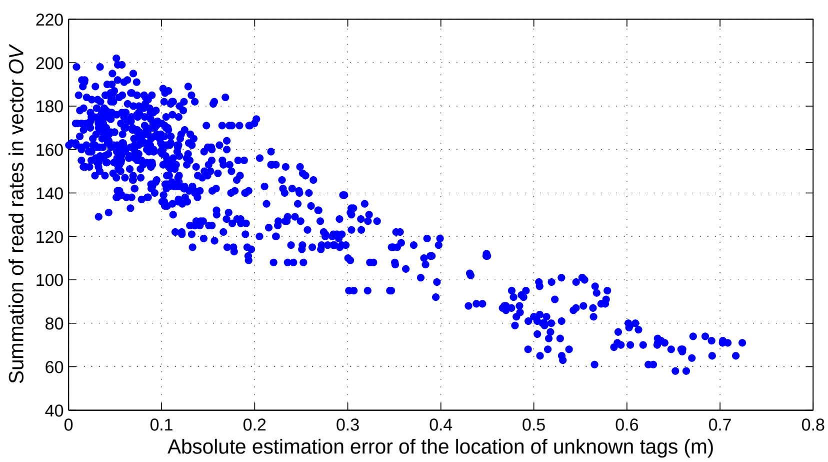

(b)

Figure 4.22: The estimation error of unknown tag versus (a) variance of observations in *Constraint* 2 (b) summation of read rates in vector OV in *Constraint* 2^*.

observations of unknown tags are collected by ST, thus the mapping accuracy is improved. It is found that the outliers at the time 120 s are the tags with limited amount of available observations.

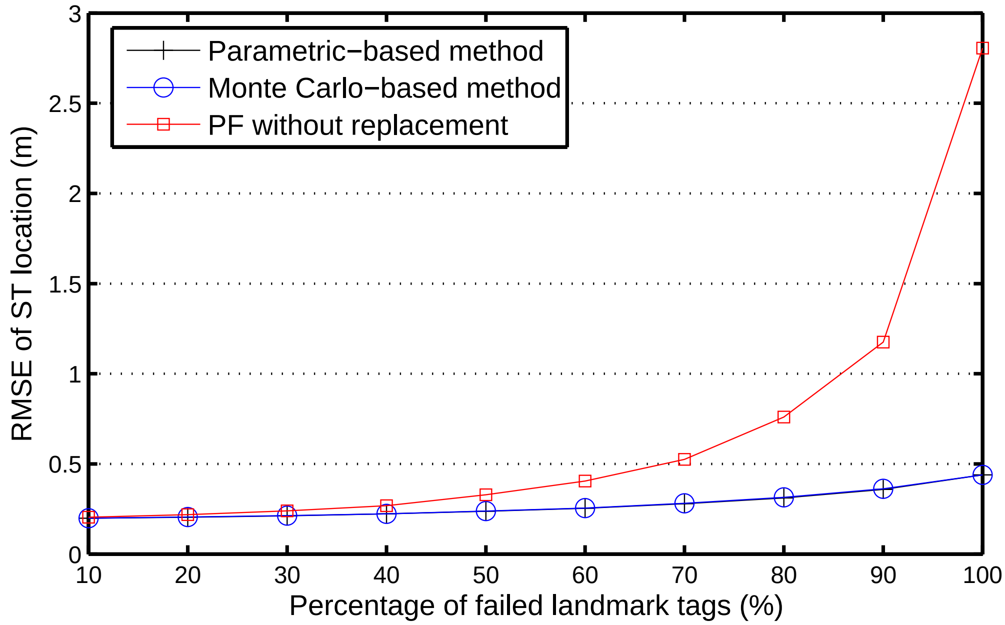

Figure 4.23: ST Localization performance with three methods: parametric-based method, Monte Carlo-based method and PF without replacement method.

We continue the simulation for another 300 s and obtain 2100 unknown tag estimations, as well as the corresponding read rate vectors. Based on the read rate vectors, the metrics in *Constraint 2* and *2** are calculated. Figure 4.22 shows the scatter plot of variance of observation and summation of read rate vector along with the estimation error of unknown tags. The correlation coefficient of estimation error of unknown tags versus variance of observation and summation of read rate vector is 0.4787 and -0.8939 respectively. Therefore, the summation of read rate vector is a more accurate linear indicator for estimation error of unknown tags. The *Constraint 2** is selected and the scaling parameter α is set as 7.

Last, the experiment is to evaluate the overall performance of SQLAM framework. The simulation setup is as shown in Figure 4.18. There are 60 unknown tags randomly

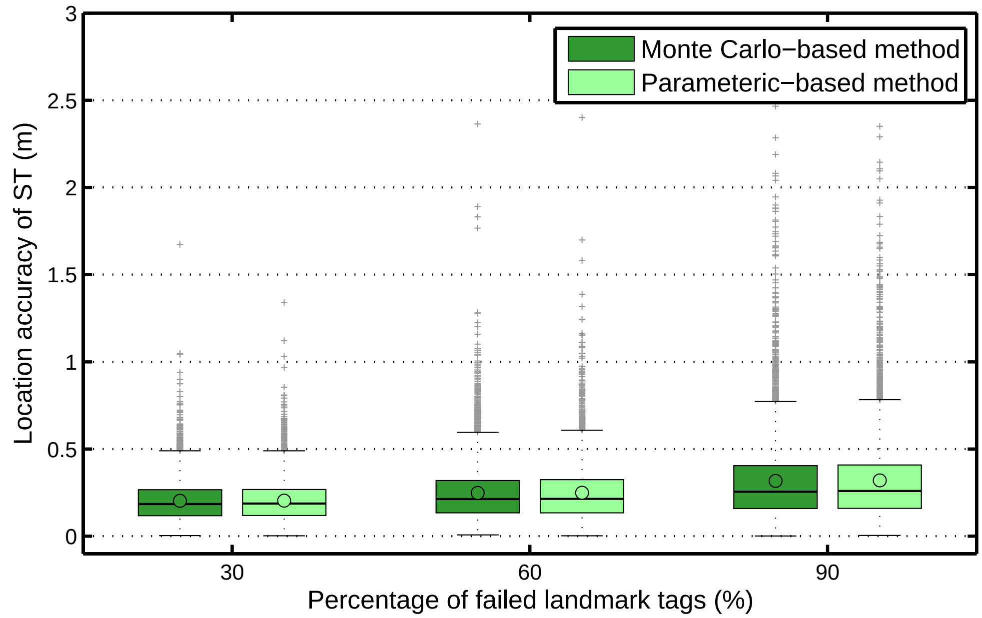

Figure 4.24: ST localization accuracy for different percentage of failed landmark tags (ST localization accuracy is measured by ℓ^2-norm operation of the difference between estimation and true location).

distributed in the environment. The ST moves along the random trajectory as described in the first set of experiments. We compare three methods: the particle filter localization method without replacement, SQLAM with parametric replacement and SQLAM with Monte Carlo-based replacement. The simulation time is 4500 seconds, during which certain amount of landmark tags are removed after 1500 s. The removed landmark tags stand for the failed landmarks, which are randomly picked from the whole population of landmark tags. The results are shown in Figure 4.23. We can see that the new proposed algorithms outperform the other method without replacement. To be specific, for instance, the RMSE of ST location estimation is improved by 2.3 meters when the percentage of failed landmark tags is 100%. For the particle filter method without replacement, the location of ST is estimated as origin of the area, since there is no available measurements. The parametric-based method performs as good as the Monte Carlo-based method in terms of RMSE of ST location estimation, notwithstanding the former method possesses significantly higher computation cost. Then we compare the distribution of ST location estimation with box-and-whisker plot for parametric-based and Monte Carlo-based method. We pick the percentage of failed landmark tags as 30%, 60% and 90%. As shown in Figure 4.24, the distributions of location estimation for these two methods have minor difference. Therefore, the parametric-based method is selected over the Monte Carlo-based method due to lower computation cost.

Simulation in research lab application

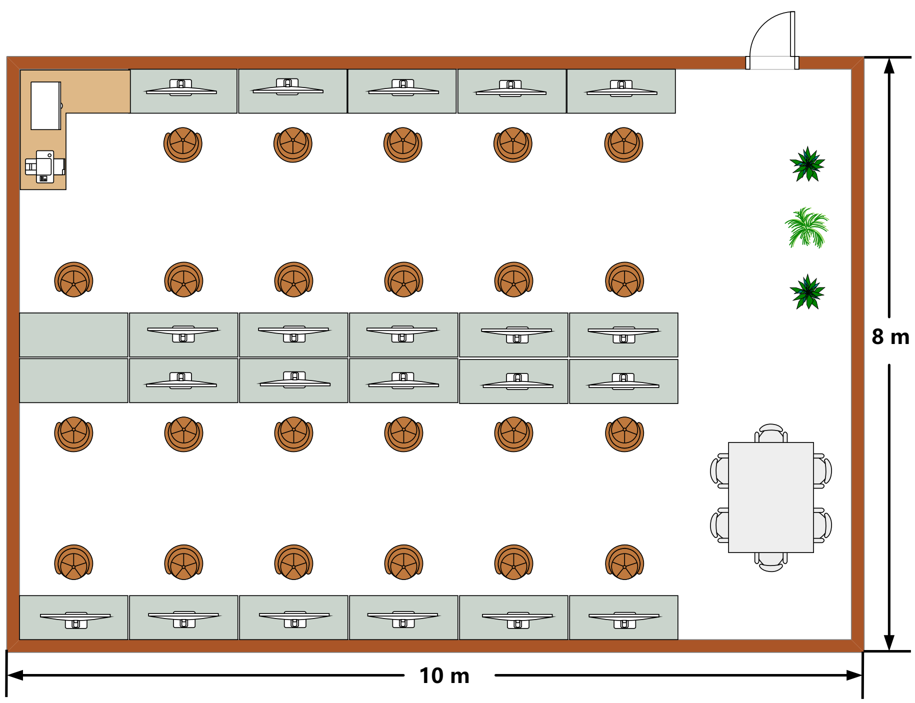

Figure 4.25: The floor plan of uOttawa SITE 5130 research lab.

The second proof-of-concept simulation for the above-mentioned SQLAM framework has been conducted in the scenario of uOttawa SITE 5130 research lab. A floor plan of the room can be found in Figure 4.25. Let's envisage that in lab environment the grid of landmark tags are embedded into the carpet or floor during the deployment phase. Afterwards, the lab is filled with furniture, equipments and other objects that UHF RFID tags are attached to. Empowering by SQLAM framework, the system could construct a geographical map of these UHF RFID tags, while a mobile object with ST is traversing in the area. The UHF RFID tags with resolved locations could assist in the localization of ST, when certain landmark tags are not available due to temporal electromagnetic blockage or permanent hardware failure.

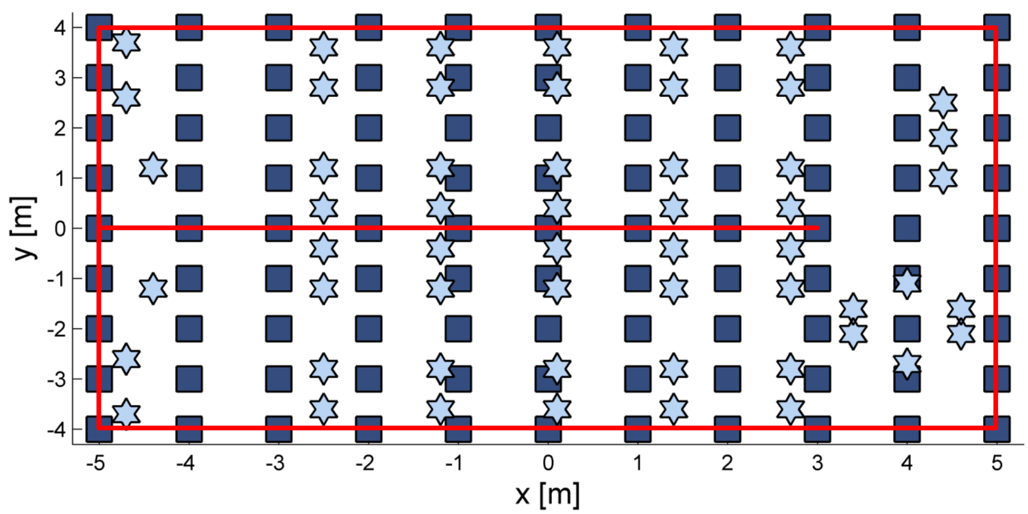

Figure 4.26: Simulation setup following the deployment scenario in SITE 5130 (the square represents landmark tag, the hexagon represents unknown tag, and the red line represents the boundary).

The simulation setup follows the deployment scenario of Figure 4.25, which is shown in Figure 4.26. The area is 10 $m \times 8$ m, and is covered by 11×9 UHF R-FID landmark tags. Unknown tags are attached to the monitors, the printer, the microwave, the pots of plants and the chairs. We use one RFID reader with four panel antennas placed at the coordinates $(-2.5\ m, -2\ m, 2\ m)$, $(2.5\ m, -2\ m, 2\ m)$, $(-2.5\ m, 2\ m, 2\ m)$ and $(2.5\ m, 2\ m, 2\ m)$. The panel antennas face the ground. The

RFID reader activates the antenna whose distance is closer to the location estimation of ST in the simulation. The ST follows a random walk trajectory within the boundary of the area. The random walk trajectory is implemented as the ST moves along a straight line with constant speed. Whenever it arrives at area boundary, ST bounces back at random angle with random speed. The speed is uniformly distributed over the range of $[0.1, 3]$ m/s. The angle is uniformly distributed in $[-\pi, \pi]$. The SQLAM framework uses the same configuration parameters as described in the previous subsection. The localization and mapping error is measured by ℓ^2-norm operation of the difference between estimation and true location.

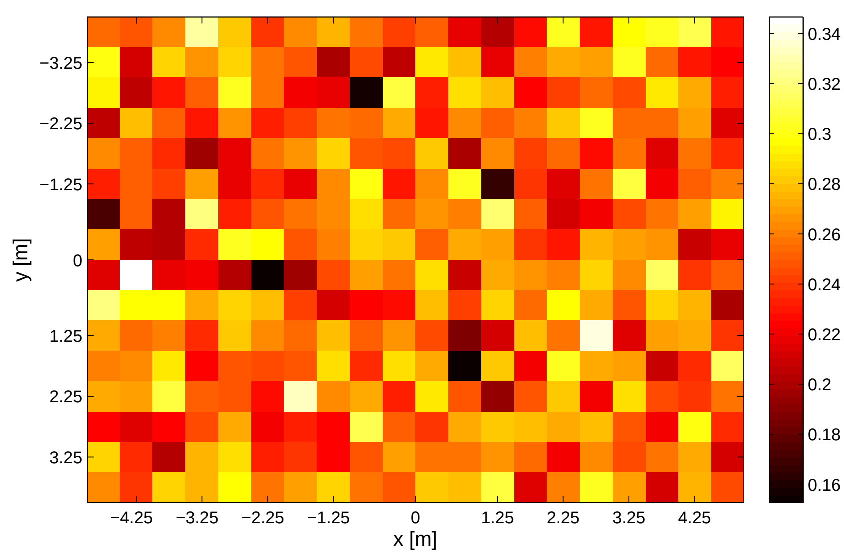

Figure 4.27: The heat map of location estimation error associated with coordinates when all landmark tags are available (each block is $0.5\ m \times 0.5\ m$).

In the scenario of research lab, we conduct the simulation to evaluate the localization performance of ST. ST travels along the random walk trajectory for 10000 s. We collect the data of true ST location and location estimation error along the trajectory. The average RMSE of ST location estimation is 0.2560 m. Figure 4.27 shows the heat map of location estimation error associated with coordinates. Each block of heat map is 0.5 $m \times 0.5$ m, whose value is determined by the average RMSE of location estimation while ST resides within the block.

As the ST travels in the area, the unknown tags are mapped. Figure 4.29 shows the mapping error of unknown tags over time with box-and-whisker plot.

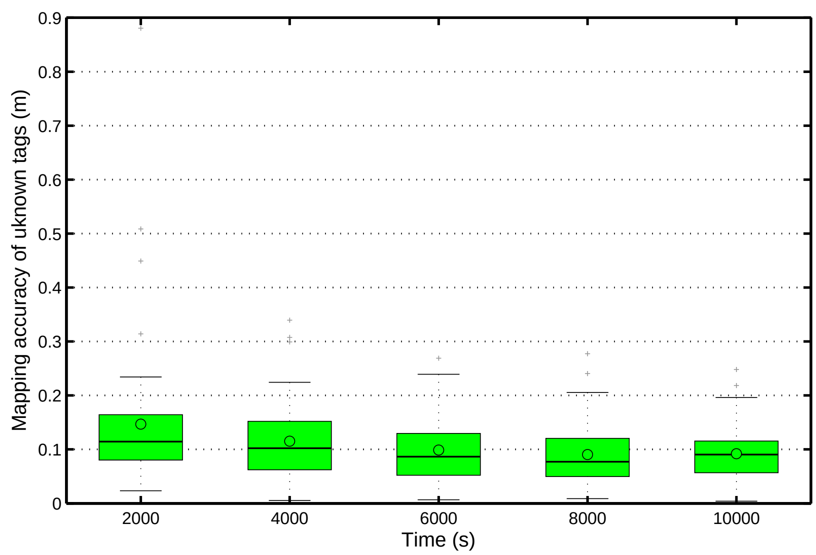

Figure 4.28: The mapping accuracy of 55 unknown tags in research lab scenario against time.

Last, at the time instance of 10000 s we remove all the landmark tags. According to the SQLAM framework, 14 unknown tags with resolved locations are selected as the substitutes for landmark tags. The average RMSE of ST location estimation is 1.1945 m. Figure 4.30 shows the heat map of location estimation error associated with coordinates. Since the localization algorithm without replacement could not locate target with ST, it is a significant advantage for SQLAM. In addition, it is reasonable to anticipate that the localization accuracy of ST would be improved with more objects in the lab, that are attached by UHF RFID tags, such as books or cups.

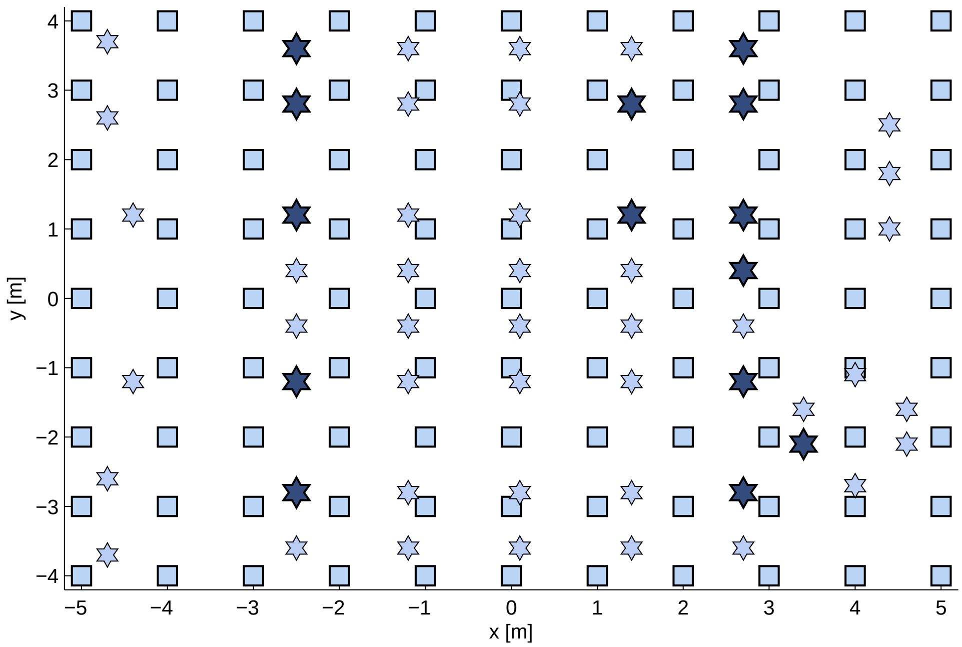

Figure 4.29: Simulation setup (the 14 darker passive tags are landmarks).

4.4 Summary

In this chapter, we address the problem of indoor localization of ST-tagged objects in AURIS system. A more realistic parametric model of the detection probability of ST-to-tag is proposed, which is a function of the distance between ST to tag, and also the distance and angle of the tag with respect to the reader. Furthermore, we propose a particle filter-based inference algorithm to localize ST based on the aggregated binary measurements of landmark tags reported by ST. The proposed PF-AA algorithm addresses the problems as false synchronous detection assumption and state evolution model constraint. Last, we propose a landmark-based sequential localization and mapping (SQLAM) framework, so that we could construct the geographical map of passive tags with unknown locations in the environment. The mapping of unknown tags assist in the localization of ST in future stage. We demonstrate the performance

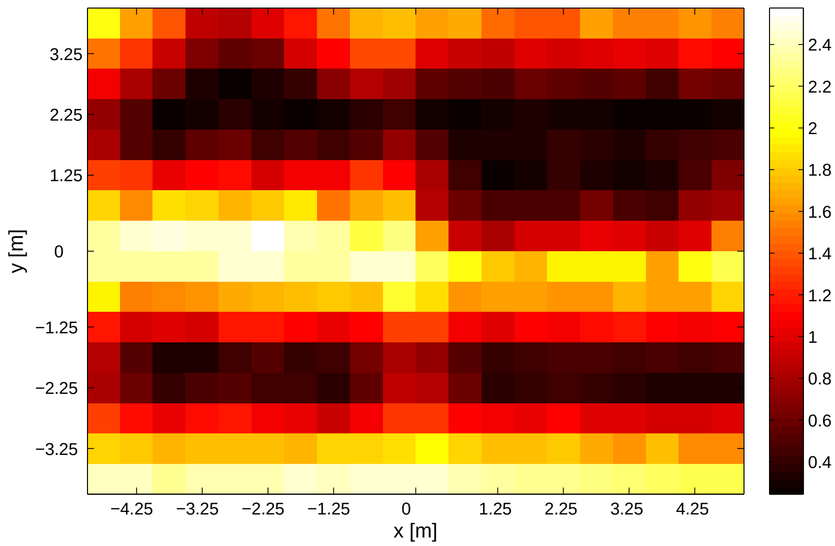

Figure 4.30: The heat map of location estimation error associated with coordinates when all landmark tags are not available, and 14 passive tags with resolved locations are used as substitutes of landmarks (each block is $0.5\ m \times 0.5\ m$).

of the proposed algorithms by extensive computer simulations.

Chapter 5

Research directions and future work

This chapter contains some research directions for future work related to ST-to-ST backscattering network. In addition, it describes future work related to AURIS system described in Chapter 3 and 4.

5.1 ST-to-ST backscattering network

The key ingredient of AURIS is that ST uses backscatter modulator to convey data and passive envelope detector to receive passive tag's backscattering signal. With such capability it is natural to consider that STs have the potential to communicate among themselves without the coordination of RFID reader. Incorporating ad-hoc communication protocol would enable multihop network of STs. One direction of the advancement is that ST could be augmented by low power sensors, have smaller form-factor and become battery-less [74]. In this way, a multihop network of STs will bring the vision of IoT closer to reality. In this section, we emphasize on the benefits for localization brought by ST-to-ST backscattering network.

In AURIS, passive tags and STs are inexpensive while RFID readers are rather expensive. Apparently, the cost of RFID reader raises scalability issue when one envisages a world-wide infrastructure for localization in the IoT [3]. One benefit of

ST-to-ST backscattering network is that STs are capable to communicate among themselves within the presence of the simple and inexpensive RF exciter rather than RFID reader. RF exciter simply feeds CW with zero intelligence. RF exciter is low cost compared with RFID reader, and can be simply integrated into the infrastructure. Another benefit of ST-to-ST backscattering network is that single RF exciter can cover larger area compared with RFID reader since there is no reverse link from ST to RF exciter.

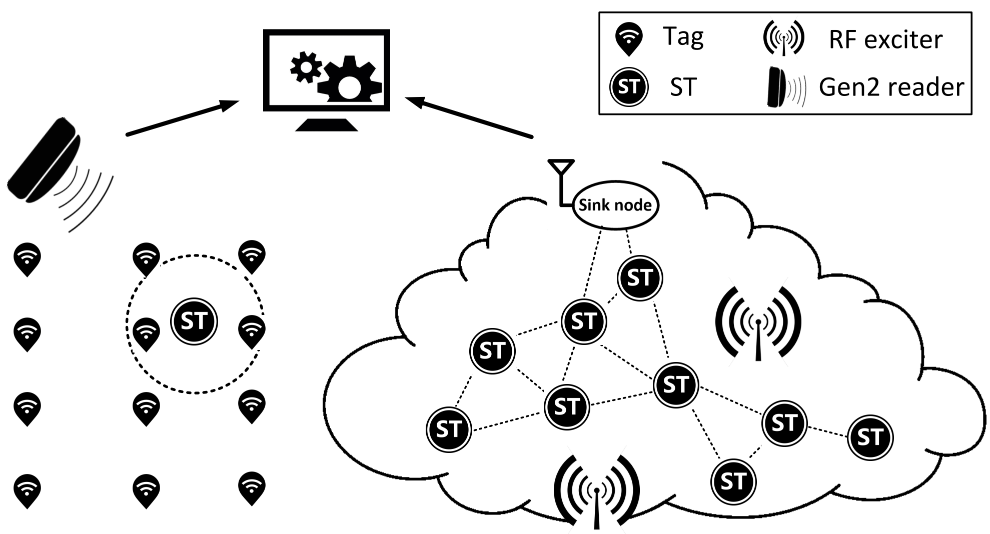

Figure 5.1: The infrastructure of AURIS on the left and ST-to-ST backscattering network on the right.

A pictorial description of one implementation of the proposed localization infrastructure is shown in Figure 5.1. In ST-to-ST backscattering network, STs backscatter the incoming CW generated by RF exciters. STs can broadcast their connectivity information to neighboring STs through backscattering communication, and eventually forward the information to server through the sink node. The localization algorithms in multihop wireless sensor network could be borrowed into the research [87, 88].

There are some open issues for realizing ST-to-ST backscattering network for

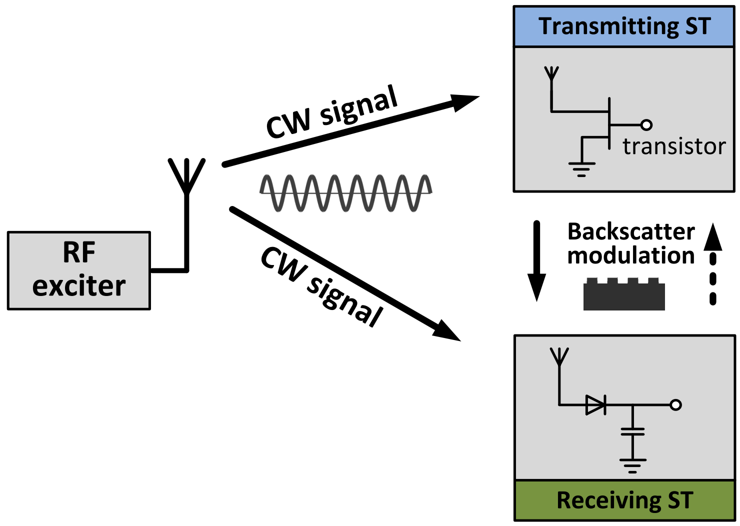

Figure 5.2: Schematic depiction of ST-to-ST backscatter link

localization.

- Phase cancellation effect is also a problem in ST-to-ST backscattering network. Figure 5.2 depicts the scheme of ST-to-ST backscattering communication link wherein the CW signal is provided by RF exciter. The signal at the receiving ST antenna is the superposition of the backscattering signal of the transmitting ST and CW of RF exciter. In next section, we briefly describe a technique to counter phase cancellation effect with dual antenna implementation in ST-to-ST backscattering network, which has been done as the initial work of incorporating ST-to-ST link in AURIS. Inspired by our work, in [89] the author proposes that a tag sends one bit of information twice using ASK and PSK modulation respectively to counter the phase cancellation effect. The method is simple and efficient in term of countering phase cancellation effect. However, the method does not make the best of the valuable communication resource in the link. Since the ST-to-ST backscattering network is at the research stage and communication standards have not been developed, the modulation scheme in

ST-to-ST backscattering communication link possesses more flexibility. Therefore, the main emphasis of the design is on the modulation and encoding scheme of ST-to-ST backscattering communication by exploiting multiple phase diversity. The new design should have higher communication capacity, and is also invulnerable to phase cancellation effect.

- In ST-to-ST backscattering network, it is preferable to implement the localization algorithm in a distributed fashion rather than on a central unit as shown in Figure 5.1. The distributed localization can be found in the area of wireless sensor network [90]. However, compared with wireless sensors ST has simple hardware in terms of limited memory space and computational capability. The sensing information of ST is merely binary detection. Therefore, it is challenging to implement simple localization algorithm in ST while achieving high localization accuracy.

- To realize ST-to-ST backscattering network, interference control and routing algorithm should be studied. Without the presence of RFID reader, ST-to-ST backscattering network must rely on distributed and asynchronous schemes for multiple access and interference control. The routing algorithm of ST-to-ST backscattering network is similar to those of wireless sensor network. However, the ST-to-ST backscattering communication link is more prone to failure. Therefore, the routing algorithm should act fast to the link failure. In [91, 92] the communication protocols for tag-to-tag backscattering network have been studied. However, these works are mainly feasibility studies and need prototype system or comprehensive simulator to evaluate the proposed protocols.

5.2 Reducing phase cancellation effect in ST-to-ST backscattering network

Phase cancellation effect is also a problem in ST-to-ST backscattering network. Dual-antenna based receiving path selection technique is feasible to combat the phase cancellation effect in this scenario. However, due to the ad hoc fashion of the network, the power consumption would be a major issue for ST compared with that of Gen2 reader-based system. In AURIS, receiving path technique performs simple selection algorithm on two co-operating receiving paths, all the workload of countering phase cancellation effect lies at at ST's two receiving paths.

In ST-to-ST backscattering network such technique leads to unnecessary power consumption. Unlike standard passive tags, with simple modification the transmitting ST would acquire the capability of informing the occurrence of phase cancellation to the receiving ST. This work proposes to inject an ASK-PSK modulated stamp to the pilot tone of ST's backscattering signal. The receiving ST decides on activating one of the two receiving paths in digital section based on the captured stamp. Adopting this technique allows only one receiving path of ST's digital section to operate for each communication round.

In off-the-shelf UHF RFID systems, the backscatter link employs either ASK or PSK backscatter generated by a two-state modulation of impedance presented to the transponder's antenna [22]. Employing multiple FET switches along with multiple load impedances, passive RFID components could perform M-ary modulation, such as arbitrary QAM [93]. Thus as shown in Figure 5.3 with three FET switches and two impedances, ST could conduct ASK and PSK modulation in the backscattering communication link. Each impedance value Z_1 and Z_2 must be designed around a given antenna impedance Z_a and center frequency 915 MHz. With the design the refection coefficients for two states in ASK and PSK are as Figure 5.4. The

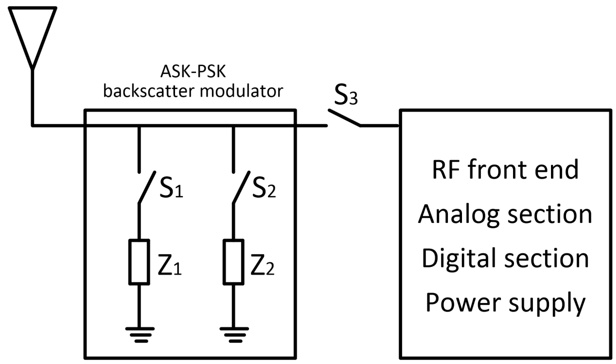

Figure 5.3: Backscatter modulator scheme

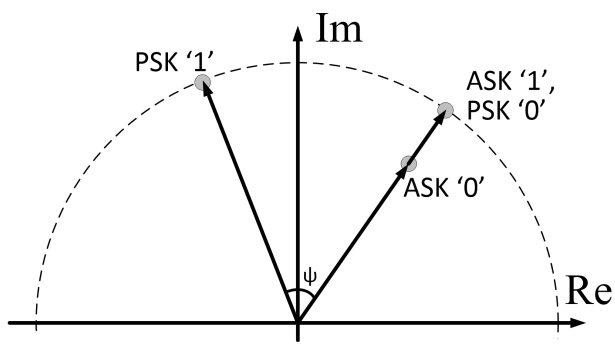

Figure 5.4: Model of ST reflection coefficients

probability of phase cancellation occurring for two types of modulation in the same frame is minimal. Therefore, in ST-to-ST communication link a ASK-PSK modulated stamp in the pilot tone could be used as the signature of phase cancellation effect.

The model for the ASK-PSK modulated backscatter signal is as following. Let A_R denote the amplitude of external RF exciter's CW signal received at the receiving ST antenna SA_2. Let A_{S1} and A_{S2} be the amplitude of the transmitting ST backscatter in two states of ASK modulation measured at the receiving ST antenna. The amplitude of the signal backscattered by the transmitting ST in PSK modulation remains the same as A_{S1}, while ψ is the phase difference of backscatter signal in two states. Let θ be the phase difference between the RF exciter signal and the transmitting ST signal

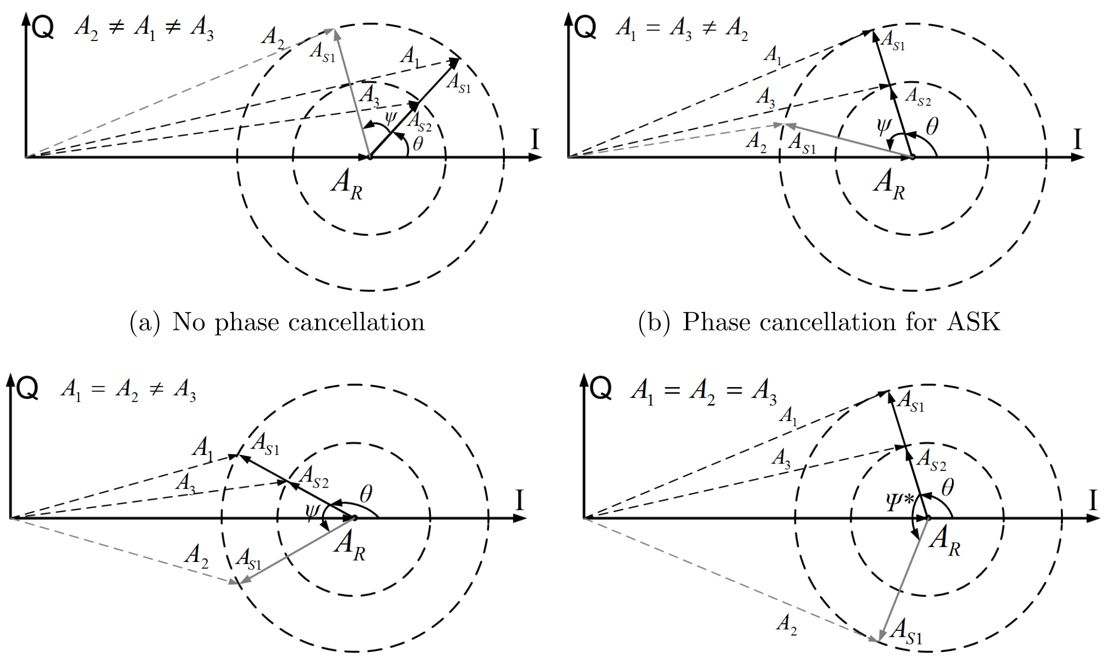

(a) No phase cancellation (b) Phase cancellation for ASK

(c) Phase cancellation for PSK (d) Phase cancellation for ASK-PSK

Figure 5.5: Phasor diagram that shows superimposed signals at receiving ST antenna for ASK-PSK backscatter modulation

in one of three states as measured at the receiving ST antenna.

Figure 5.5 shows the phasor diagram of the superimposed signal at receiving ST antenna. The dotted circles represent the locus of A_{S1}, A_{S2} with varying θ. Figure 5.5(a) depicts an example with no phase cancellation for either ASK or PSK. The envelope amplitude A_1 and A_3, A_1 and A_2 are not equal, thus the receiving ST could detect two types of modulation. Figure 5.5(b) and Figure 5.5(c) depict the example with phase cancellation for one type of modulation schemes ASK and PSK respectively. The examples above apply one set of ASK-PSK modulated signal parameters A_{S1}, A_{S2} and ψ. Figure 5.5(d) depicts one example with phase cancellation for both ASK and PSK modulation with a different set of signal parameters A_{S1}, A_{S2} and $\psi*$.

Theoretically, the phase cancellation condition for both modulation schemes could

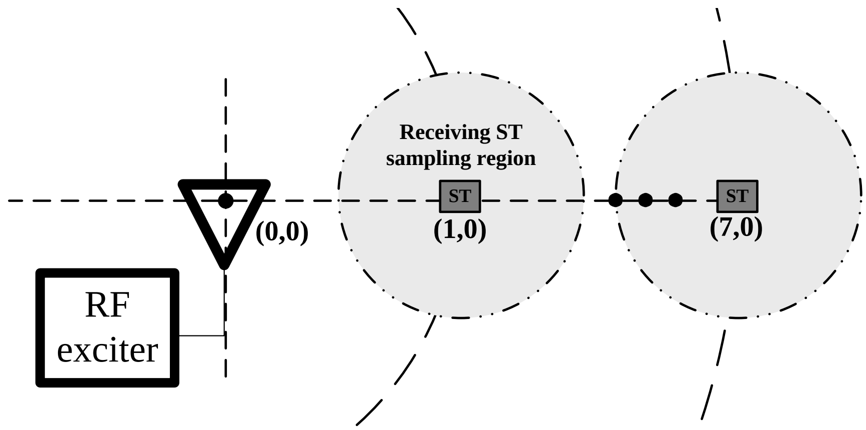

Figure 5.6: Experiment setup for ASK-PSK modulated stamp technique.

be avoided with certain backscatter modulation design, e.g. $\psi = \pi$. However, the RCS of passive backscatter modulator is highly frequency-dependent, nonlinear and fast time variant [61]. Therefore, the probability of phase cancellation for both modulation schemes could not be eliminated, but the likelihood of the occurrence of such type phase cancellation would be extremely low. Thus a ASK-PSK modulated stamp in pilot tone could serve as the signature of phase cancellation for receiving ST. Once detecting the occurrence of phase cancellation for ASK modulation in stamp, ST could switch to the alternative receiving path. It is reasonable to assume the phase cancellation effect would be lessened.

We evaluate the proposed ASK-PSK stamp-based technique in PASS simulator. The RF exciter antenna is placed at the origin (0,0) of the area. The trajectory of the transmitting ST is along x-axis from (1,0) to (7,0) in the increment of 0.5 m. The position of receiving ST is uniformly distributed over the circle centering at the transmitting ST and with the radius of 0.5 m. An instance of the experiment for one transmitting ST and its associated receiving ST's sampling positions is referred as a cell. In a cell there are 300 possible positions for receiving ST which are sampled by Monte Carlo method based on uniform distribution. The experiment scenario is

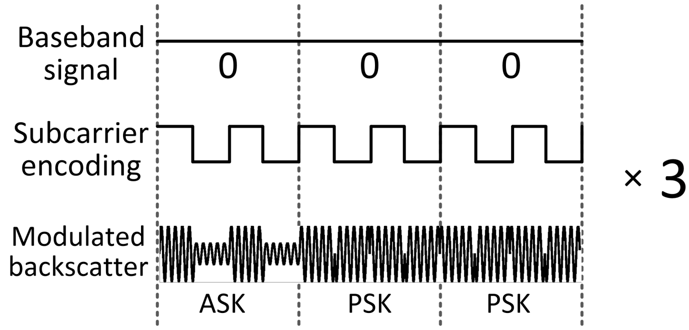

Figure 5.7: The format of ASK-PSK modulated stamp in test.

established in PASS simulation framework.

The test stamp frame used in simulation is shown in Figure 5.7, followed by the data frame as 10 bits '0' in Miller 2 modulated by ASK. The phase difference of two PSK states are separated by the ideal 180°. In the receiving ST, the output of decoded module of one receiving path is '-' when phase cancellation occurs. As the decoded stamp matches the phase cancellation pattern, the selection algorithm activates the switch procedure to activate the other receiving path. Noteworthily, the communication protocol used in the simulation is simple, in which the transmitting ST merely send data frame with ASK-PSK stamp to the receiving ST.

In the simulation, we explored the anti-phase cancellation performance of ASK-PSK modulated stamp based dual-antenna selection technique, and compared with the single antenna implementation and original receiving path selection technique. The output of ST's envelope detector for ASK modulated 10-bits data serves as the indicator of anti-phase cancellation performance of ASK-PSK stamp based technique. As in the simulation setup in Figure 5.6, we conducted experiment through 3900 sampling positions in 13 cells. We repeated the experiments three times with different Monte Carlo sampling. In Figure 5.8, the probability of phase cancellation for three techniques is presented. The performance of two dual-antenna based techniques are at the same level. The difference of overall probability for these two techniques is below

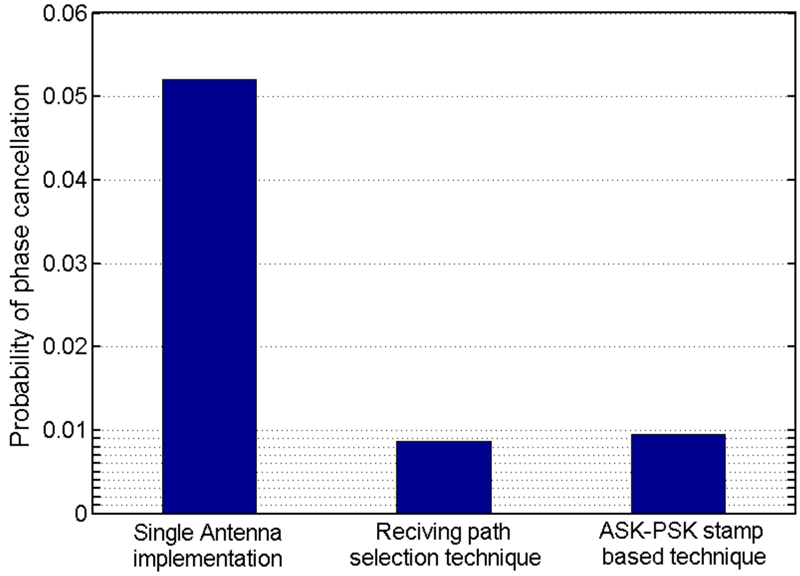

Figure 5.8: Anti-phase cancellation performance.

0.1%. Last, we roughly estimate power consumption of current FPGA Spartan-3 embedded implementations in Xilinx Power Estimator (XPE), the dynamic power consumption of one operating receiving path implementation is 79 mW, while that of two co-operating receiving paths is 94 mW. Thus ASK-PSK stamp based technique is promising in increasing the power efficiency.

5.3 Future directions related to AURIS

In this section, we will return back to RFID reader based systems and look at future directions related to AURIS.

Indoor localization using tag-to-tag backscattering communication link was in its infancy at the beginning of this thesis project. Even though it has definitely grown in the meantime, it is still immature. As a consequence, the research will be promoted by new technologies and applications. The following are suggested topics that can be considered in future research.

Optimizing landmark delopment did not receive a lot of attention during the work on this thesis. We simply deploy the landmark tags in a square pattern, and the distance among neighboring landmark tags is constant. However, it is beneficial to investigate the relationship between localization accuracy and the density of landmark tags, as well as the deployment pattern. In the reader-based method [7], the spacing of landmark tags was 0.27 m. The reading range of the reader was 0.3 m. The achieved localization error was 0.062 m on average. Such solution achieves high localization accuracy with densely deployed landmarks and fine-tuned reader read range. In AURIS, we could anticipate that the localization accuracy depends on the combination of the read range of ST-to-tag and the density of landmark tags.

Through this work, landmark tags are considered as homogeneous. However, in reality it is highly possible that the backscattering capability and sensitivity of landmarks are different from other other. Therefore, the heterogeneity of landmark tags should be investigated.

In the thesis, we studied the localization of single ST with a set of landmark tags. The localization method could be easily extended to localize multiple STs, since we could localize each of these STs independently.

In SQLAM framework, we assume that unknown tags in the environment are stationary, which is not always the case. The future work needs to identify the dynamic pattern of the movement of unknown tags, which could depend on additional information, such as RSSI or phase of arrival, that can be obtained at the RFID reader from unknown tags other than the aggregated binary measurements of ST-to-unknown tags. Besides that, this work only considers the localization of one ST. However, it can be easily extended to more than one since STs collect aggregated binary measurements of neighboring tags independently.

The most important research direction is to realize the proposed ST improvement and localization algorithms. The real system would evaluate the proposed improvements and algorithms against certain factors, which are not considered in the simulation. These factors include the cross-talk between dual antennas, and human or metal shielding.

Another interesting direction to proceed is to develop the tag-to-tag backscattering using WiFi signal. In [30] the WiFi backscatter is presented, which bridges the WiFi-powered tag with the WiFi model. The proposed method enables the reader-to-tag like backscattering communication link. This is an encouraging start for the tag-to-tag backscattering using WiFi signal. The research on tag-to-tag backscattering using WiFi signal will benefit in the proximity-based localization solutions facing the consumer electronic sector, since WiFi deployment is popular in various scenarios. The research problems answered in this thesis would be a good starting point for backscatter-based localization in WiFi network. However, it is reasonable to anticipate that the problems encountered in tag-to-tag backscattering using WiFi signal would be more challenging. For example, in UHF RFID system RFID reader transmits a single-tone CW as the medium for tag to backscatter, but for WiFi there are 60 OFDM subcarriers over 20 MHz [30].

Chapter 6

Conclusion

In recent publications on proximity-based UHF RFID indoor localization solutions [5, 7, 8, 11, 12, 45, 46], proximity-based localization using tag-to-tag backscattering communication becomes a promising technology for locating items indoors in IoT paradigm. However, certain critical issues are left unanswered or open to explore, such as phase cancellation, the mathematical models and location inference algorithms. This dissertation attempts to address the challenging issues of proximity-based indoor localization using tag-to-tag backscattering communication in AURIS.

First, in Chapter 3 we investigated a unique phase cancellation effect that occurs in the tag-to-tag backscattering communication link. The essence of tag-to-tag backscattering communication is the adoption of backscatter modulator and envelope detection on both communication participants. In AURIS, during the communication between UHF tag and ST, the RFID reader must transmit CW for the tag to backscatter. Consequently, the signal at the ST's antenna is the superposition of tag's backscattering signal and RFID reader's CW. Unfortunately, due to the random phase difference between these two signals, the baseband information from UHF tag that contained in the envelope of the superimposed signal could be significantly attenuated, or even cancelled out. We modelled the phase cancellation effect for both ASK and PSK modulation. We proposed to counter such phase cancellation effect by exploiting the spatial diversity of dual antennas.

We have proposed a new and realistic probability detection model of ST-to-tag, which is better suited to ST-to-tag communication link. The probability detection model of ST-to-tag is modelled as a function of the distance and relative angle between tag and RFID reader antenna in addition to the distance between tag to ST. The modelling accuracy of RTS model is improved compared with TS model in terms of cross-entropy cost function. We further proposed a particle filter-based location inference algorithm for AURIS. To this end, we identify two technical roadblocks of AURIS and existing localization algorithm as false synchronous detection assumption and state evolution model constraints. Our method to overcome such roadblocks includes two simple ideas. Firstly, we estimate the velocity of ST based on the estimation state history and current measurement using AR model. The current measurement is introduced into the AR model by WCL method. Second, we implemented a minor modification to ST locator protocol, which is still Gen2 protocol compliant. Through such modification, the host server is able to obtain the asynchronous detection information. With these two ideas, we designed PF-AA algorithm for better accuracy and applicability in indoor localization application. Compared with PF-BIN algorithm, the localization capability of PF-AA is enhanced to handle the sharp maneuver and speed change of target.

We have also proposed a landmark-based sequential localization and mapping (SQLAM) framework for AURIS. The SQLAM framework includes three critical parts, such as ST tracking with particle filter, unknown tag mapping with temporal WCL and replacement algorithm with resolved unknown tags. The framework extends the localization capability to unknown tags other than ST. Furthermore, the unknown tags with resolved locations could be utilized to localize ST. The extensive computer simulation demonstrates that unknown tags could be mapped accurately according to SQLAM. In addition, when certain landmarks are not available, the higher localization accuracy is achieved by including unknown tags with resolved locations into localization procedure.

List of References

[1] "Gen 2 EPC protocol approved as ISO 18000-6C." http://www.rfidjournal.com/articles/view?2481. Accessed: 2016-09-30.

[2] Z. Zou, *Impulse radio UWB for the internet-of-things: a study on UHF/UWB hybrid solution*. PhD thesis, Royal Institute of Technology (KTH), Stockholm, Sweden, 2011.

[3] L. Geng, *Indoor localization and tracking using binary information*. PhD thesis, Stony Brook University (SBU), Stony Brook, USA, 2015.

[4] M. Bolic, D. Simplot-Ryl, and I. Stojmenovic, *RFID systems: research trends and challenges*. John Wiley and Sons, 2010.

[5] A. Athalye, V. Savic, M. Bolic, and P. Djuric, "Novel semi-passive RFID system for indoor localization," *IEEE Sensors Journal*, vol. 13, no. 2, pp. 528–537, 2013.

[6] P. Yang and W. Wu, "Efficient particle filter localization algorithm in dense passive RFID tag environment," *IEEE Transactions on Industrial Electronics*, vol. 61, no. 10, pp. 5641–5651, 2014.

[7] L. Yang, J. Cao, W. Zhu, and S. Tang, "Accurate and efficient object tracking based on passive RFID," *IEEE Transactions on Mobile Computing*, vol. 14, no. 11, pp. 2188–2200, 2015.

[8] L. Geng, M. Bugallo, A. Athalye, and P. Djuric, "Indoor tracking with RFID systems," *IEEE Journal of Selected Topics in Signal Processing*, vol. 8, no. 1, pp. 96–105, 2014.

[9] "Handhold UHF RFID readers." https://www.atlasrfidstore.com/fixed-rfid-readers/. Accessed: 2016-12-13.

[10] M. Bolic, M. Rostamian, and P. Djuric, "Proximity detection with RFID: A step toward the internet of things," *IEEE Pervasive Computing*, vol. 14, no. 2, pp. 70–76, 2015.

[11] V. Savic, A. Athalye, M. Bolic, and P. Djuric, "Particle filtering for indoor RFID tag tracking," in *IEEE Statistical Signal Processing Workshop (SSP)*, pp. 193–196, 2011.

[12] L. Geng, M. Bugallo, A. Athalye, and P. Djuric, "Real time indoor tracking of tagged objects with a network of RFID readers," in *IEEE European Signal Processing Conference (EUSIPCO)*, pp. 205–209, 2012.

[13] M. Vemula, M. Bugallo, and P. Djuric, "Sensor self-localization with beacon position uncertainty," *Signal Processing*, vol. 89, no. 6, pp. 1144–1154, 2009.

[14] M. Sun, L. Yang, and K. Ho, "Accurate sequential self-localization of sensor nodes in closed-form," *Signal Processing*, vol. 92, no. 12, pp. 2940–2951, 2012.

[15] M. Rostamian, "Localization and proximity detection in the internet of things based on an augmented UHF RFID system," Master's thesis, University of Ottawa (uOttawa), Ottawa, Canada, 2014.

[16] D. Arnitz, *Tag localization in passive UHF RFID*. PhD thesis, Graz University of Technology (TU Graz), Graz, Austria, 2011.

[17] Z. Zhang, *Networked RFID Systems for the Internet of Things*. PhD thesis, Royal Institute of Technology (KTH), Stockholm, Sweden, 2013.

[18] R. Mautz, *Indoor Positioning Technologies*. PhD thesis, Swiss Federal Institute of Technology in Zurich (ETH Zurich), Zurich, Swiss, 2012.

[19] E. Fleisch, "What is the internet of things? an economic perspective," *Economics, Management, and Financial Markets*, no. 2, pp. 125–157, 2010.

[20] L. Atzori, A. Iera, and G. Morabito, "The internet of things: A survey," *Computer Networks*, vol. 54, no. 15, pp. 2787 – 2805, 2010.

[21] SRI Consulting Business Intelligence, "Distruptive Technologies: Global Trends 2025, Appendix F: The Interenet of Things," 2008.

[22] D. Dobkin, *The RF in RFID: Passive UHF RFID in Practice*. Elsevier Science, 2007.

[23] C. Tellkamp, T. Wiechert, F. Thiesse, and E. Fleisch, *The Adoption of RFID-based Self-Check-Out-Systems at the Point-of-Sale*, pp. 153–165. Springer, 2006.

[24] G. Jayendra, S. Kumarawadu, and L. Meegahapola, "RFID-based anti-theft auto security system with an immobilizer," in *IEEE International Conference on Industrial and Information Systems (ICIIS)*, pp. 441–446, 2007.

[25] R. Angeles, "RFID technologies: supply-chain applications and implementation issues," *Information systems management*, vol. 22, no. 1, pp. 51–65, 2005.

[26] M. L. Ng, K. S. Leong, D. M. Hall, and P. H. Cole, "A small passive UHF RFID tag for livestock identification," in *IEEE International Symposium on Microwave, Antenna, Propagation and EMC Technologies for Wireless Communications (MAPE)*, vol. 1, pp. 67–70, IEEE, 2005.

[27] S. Zhou, W. Ling, and Z. Peng, "An RFID-based remote monitoring system for enterprise internal production management," *The International Journal of Advanced Manufacturing Technology*, vol. 33, no. 7-8, pp. 837–844, 2007.

[28] K. Finkenzeller, *RFID Handbook: Fundamentals and Applications in Contactless Smart Cards and Identification*. John Wiley and Sons, 2 ed., 2003.

[29] V. Liu, A. Parks, V. Talla, S. Gollakota, D. Wetherall, and J. R. Smith, "Ambient backscatter: Wireless communication out of thin air," in *ACM Conference on SIGCOMM (SIGCOMM)*, pp. 39–50, 2013.

[30] B. Kellogg, A. Parks, S. Gollakota, J. Smith, and D. Wetherall, "Wi-fi backscatter: Internet connectivity for RF-powered devices," in *ACM Conference on SIGCOMM (SIGCOMM)*, pp. 607–618, 2014.

[31] J. Ensworth and M. Reynolds, "Every smart phone is a backscatter reader: Modulated backscatter compatibility with bluetooth 4.0 low energy (BLE) devices," in *IEEE International Conference on RFID (RFID)*, pp. 78–85, IEEE, 2015.

[32] E. Lun, *An accurate and robust indoor localization system*. PhD thesis, The Hong Kong Polytechnic University (HKPU), Hong Kong, China, 2010.

[33] S. Azzouzi, M. Cremer, U. Dettmar, T. Knie, and R. Kronberger, "Improved AoA based localization of UHF RFID tags using spatial diversity," in *IEEE International Conference on RFID-Technologies and Applications (RFID-TA)*, pp. 174–180, September 2011.

[34] A. Povalac, *Spatial Identification Methods and Systems for RFID Tags.* PhD thesis, Brno University of Technology (BUT), Brno, Czech Republic, 2012.

[35] R. Kronberger, T. Knie, R. Leonardi, U. Dettmar, M. Cremer, and S. Azzouzi, "UHF RFID localization system based on a phased array antenna," in *IEEE International Symposium on Antennas and Propagation (APSURSI)*, pp. 525–528, 2011.

[36] S. Azzouzi, M. Cremer, U. Dettmar, R. Kronberger, and T. Knie, "New measurement results for the localization of UHF RFID transponders using an angle of arrival (AoA) approach," in *IEEE International Conference on RFID (RFID)*, pp. 91–97, April 2011.

[37] H. Liu, H. Darabi, P. Banerjee, and J. Liu, "Survey of wireless indoor positioning techniques and systems," *IEEE Transactions on Systems, Man, and Cybernetics Part C (Applications and Reviews)*, vol. 37, no. 6, pp. 1067–1080, 2007.

[38] T. Xiong, J. Liu, Y. Yang, X. Tan, and H. Min, "Design and implementation of a passive UHF RFID-based real time location system," in *IEEE International Symposium on VLSI Design Automation and Test (VLSI-DAT)*, pp. 95–98, 2010.

[39] T. Nick, G. Smietanka, and J. Gotze, "RSS-based channel measurements and their influence on localization in RFID applications," in *IEEE International Symposium on Consumer Electronics (ISCE)*, pp. 71–72, June 2013.

[40] A. H. Sayed, A. Tarighat, and N. Khajehnouri, "Network-based wireless location: challenges faced in developing techniques for accurate wireless location information," *IEEE signal processing magazine*, vol. 22, no. 4, pp. 24–40, 2005.

[41] Z. Zhang, Z. Lu, V. Saakian, X. Qin, Q. Chen, and L.-R. Zheng, "Item-level indoor localization with passive UHF RFID based on tag interaction analysis," *IEEE Transactions on Industrial Electronics*, vol. 61, no. 4, pp. 2122–2135, 2014.

[42] C. Bishop, *Pattern recognition and machine learning.* Springer, 2006.

[43] L. M. Ni, D. Zhang, and M. R. Souryal, "RFID-based localization and tracking technologies," *IEEE Wireless Communications*, vol. 18, pp. 45–51, April 2011.

[44] A. Athalye, V. Savic, M. Bolic, and P. Djuric, "A radio frequency identification system for accurate indoor localization," in *IEEE International Conference on Acoustics, Speech and Signal Processing (ICASSP)*, pp. 1777–1780, 2011.

[45] E. DiGiampaolo, “A passive-RFID based indoor navigation system for visually impaired people,” in *IEEE International Symposium on Applied Sciences in Biomedical and Communication Technologies (ISABEL)*, pp. 1–5, 2010.

[46] E. DiGiampaolo and F. Martinelli, “A passive UHF-RFID system for the localization of an indoor autonomous vehicle,” *IEEE Transactions on Industrial Electronics*, vol. 59, no. 10, pp. 3961–3970, 2012.

[47] P. Yang and W. Wu, “Efficient particle filter localization algorithm in dense passive RFID tag environment,” *IEEE Transactions on Industrial Electronics*, vol. 61, no. 10, pp. 5641–5651, 2014.

[48] T. He, C. Huang, B. M. Blum, J. A. Stankovic, and T. Abdelzaher, “Range-free localization schemes for large scale sensor networks,” in *ACM Annual International Conference on Mobile computing and networking (MobiCom)*, pp. 81–95, 2003.

[49] L. Yang, J. Cao, W. Zhu, and S. Tang, “Accurate and efficient object tracking based on passive RFID,” *IEEE Transactions on Mobile Computing*, vol. 14, no. 11, pp. 2188–2200, 2015.

[50] M. Arulampalam, S. Maskell, N. Gordon, and T. Clapp, “A tutorial on particle filters for online nonlinear/non-gaussian bayesian tracking,” *IEEE Transactions on signal processing*, vol. 50, no. 2, pp. 174–188, 2002.

[51] G. Welch and G. Bishop, “An introduction to the Kalman filter,” tech. rep., Chapel Hill, NC, USA, 1995.

[52] J. Curn, *Correlated Estimation Problems and the Ensemble Kalman Filter*. PhD thesis, Trinity College, Dublin, 2014.

[53] P. Djuric, J. Kotecha, J. Zhang, Y. Huang, T. Ghirmai, M. Bugallo, and J. Miguez, “Particle filtering,” *IEEE Signal Processing Magazine*, vol. 20, no. 5, pp. 19–38, 2003.

[54] A. Doucet and A. Johansen, “A tutorial on particle filtering and smoothing: fifteen years later,” in *Oxford Handbook Of Nonlinear Filtering*, 2011.

[55] F. Gustafsson, F. Gunnarsson, N. Bergman, U. Forssell, J. Jansson, R. Karlsson, and P. Nordlund, “Particle filters for positioning, navigation, and tracking,” *IEEE Transactions on signal processing*, vol. 50, no. 2, pp. 425–437, 2002.

[56] X. Chen, A. Edelstein, Y. Li, M. Coates, M. Rabbat, and A. Men, "Sequential monte carlo for simultaneous passive device-free tracking and sensor localization using received signal strength measurements," in *IEEE International Conference on Information Processing in Sensor Networks (IPSN)*, pp. 342–353, April 2011.

[57] M. K. Pitt and N. Shephard, "Filtering via simulation: Auxiliary particle filters," *Journal of the American statistical association*, vol. 94, no. 446, pp. 590–599, 1999.

[58] H. Durrant-Whyte and T. Bailey, "Simultaneous localization and mapping: part i," *IEEE robotics and automation magazine*, vol. 13, no. 2, pp. 99–110, 2006.

[59] L. Geng, M. Bugallo, and P. Djuric, "Tracking with asynchronous binary readings and layout information in RFID systems with sense-a-tags," in *IEEE European Signal Processing Conference (EUSIPCO)*, pp. 1–5, 2013.

[60] P. Yang, W. Wu, M. Moniri, and C. Chibelushi, "Efficient object localization using sparsely distributed passive RFID tags," *IEEE Transactions on Industrial Electronics*, vol. 60, no. 12, pp. 5914–5924, 2013.

[61] D. Arnitz, U. Muehlmann, T. Gigl, and K. Witrisal, "Wideband system-level simulator for passive UHF RFID," in *IEEE International Conference on RFID (RFID)*, pp. 28–33, April 2009.

[62] D. Arnitz, U. Muehlmann, T. Gigl, and K. Witrisal, "Wideband system-level simulator for passive UHF RFID," in *IEEE International Conference on RFID (RFID)*, pp. 28–33, 2009.

[63] J. D. Griffin, *High-frequency modulated-backscatter communication using multiple antennas*. PhD thesis, Georgia Institute of Technology (Georgia Tech), Atlanta, USA, 2009.

[64] G. Marrocco and S. Caizzone, "Electromagnetic models for passive tag-to-tag communications," *IEEE Transactions on Antennas and Propagation*, vol. 60, no. 11, pp. 5381–5389, 2012.

[65] D. Arnitz, U. Muehlmann, and K. Witrisal, "Characterization and modeling of UHF RFID channels for ranging and localization," *IEEE Transactions on Antennas and Propagation*, vol. 60, no. 5, pp. 2491–2501, 2012.

[66] J. Wang and M. Bolic, "Reducing the phase cancellation effect in augmented RFID system," *International Journal of Parallel, Emergent and Distributed Systems*, vol. 30, no. 6, pp. 494–514, 2015.

[67] J. Mietzner, R. Schober, L. Lampe, W. Gerstacker, and P. Hoeher, "Multiple-antenna techniques for wireless communications-a comprehensive literature survey," *IEEE Communications Surveys and Tutorials*, vol. 11, no. 2, pp. 87–105, 2009.

[68] H. T. Friis, "A note on a simple transmission formula," *Proceedings of the IRE*, vol. 34, no. 5, pp. 254–256, 1946.

[69] N. Metropolis and S. Ulam, "The Monte Carlo method," *Journal of the American statistical association*, vol. 44, no. 247, pp. 335–341, 1949.

[70] Y. Kim and S. Kim, "Optimum selection combining for m-ary signals in fading channels," in *IEEE Global Telecommunications Conference (GLOBECOM)*, vol. 2, pp. 1234–1238, 2002.

[71] L. Geng, M. Bugallo, A. Athalye, and P. Djuric, "Real-time self-tracking in the internet of things," in *IEEE International Conference on Acoustics, Speech and Signal Processing (ICASSP)*, pp. 5510–5514, April 2015.

[72] P. Nikitin, S. Ramamurthy, R. Martinez, and K. Rao, "Passive tag-to-tag communication," in *IEEE International Conference on RFID (RFID)*, pp. 177–184, IEEE, 2012.

[73] G. Marrocco and S. Caizzone, "Electromagnetic models for passive tag-to-tag communications," *IEEE Transactions on Antennas and Propagation*, vol. 60, no. 11, pp. 5381–5389, 2012.

[74] K. Finkenzeller, *RFID Handbook: Fundamentals and Applications in Contactless Smart Cards and Identification.* John Wiley and Sons, 2003.

[75] P. Nikitin, K. Rao, S. Lam, V. Pillai, R. Martinez, and H. Heinrich, "Power reflection coefficient analysis for complex impedances in RFID tag design," *IEEE Transactions on Microwave Theory and Techniques*, vol. 53, no. 9, pp. 2721–2725, 2005.

[76] P. Nikitin, K. Rao, and R. Martinez, "Differential RCS of RFID tag," *Electronics letters*, vol. 43, no. 8, pp. 431–432, 2007.

[77] C. H. Lee, "Learning to combine discriminative classifiers: confidence based," in *ACM international conference on knowledge discovery and data mining (KDD)*, pp. 743–752, 2010.

[78] J. Friedman, T. Hastie, and R. Tibshirani, *The elements of statistical learning*, vol. 1. Springer, 2001.

[79] L. Geng, M. Bugallo, A. Athalye, and P. Djuric, “Indoor tracking with RFID systems,” *IEEE Journal of Selected Topics in Signal Processing*, vol. 8, no. 1, pp. 96–105, 2014.

[80] E. DiGiampaolo and F. Martinelli, “Mobile robot localization using the phase of passive UHF RFID signals,” *IEEE Transactions on Industrial Electronics*, vol. 61, no. 1, pp. 365–376, 2014.

[81] G. Zodi, G. Hancke, G. Hancke, and A. Bagula, “Enhanced centroid localization of wireless sensor nodes using linear and neighbor weighting mechanisms,” in *ACM International Conference on Ubiquitous Information Management and Communication (IMCOM)*, p. 43, 2015.

[82] M. Bolic, P. Djuric, and S. Hong, “Resampling algorithms and architectures for distributed particle filters,” *IEEE Transactions on Signal Processing*, vol. 53, pp. 2442–2450, July 2005.

[83] A. Errington, B. Daku, and A. Prugger, “Initial position estimation using RFID tags: A least-squares approach,” *IEEE Transactions on Instrumentation and Measurement*, vol. 59, no. 11, pp. 2863–2869, 2010.

[84] M. H. Ghaeminia, A. H. Shabani, and S. B. Shokouhi, “Adaptive motion model for human tracking using particle filter,” in *IEEE International Conference on Pattern Recognition (ICPR)*, pp. 2073–2076, 2010.

[85] M. Rostamian, J. Wang, and M. Bolic, “An accurate passive RFID indoor localization system based on sense-a-tag and zoning algorithm,” in *EAI International Conference on Ad Hoc Networking (AdHocNets)*, pp. 1–12, 2016.

[86] J. Park, M. Y. Chung, and T.-J. Lee, “Identification of RFID tags in framed-slotted ALOHA with robust estimation and binary selection,” *IEEE Communications Letters*, vol. 11, no. 5, pp. 452–454, 2007.

[87] Y. Shang, W. Rumi, Y. Zhang, and M. Fromherz, “Localization from connectivity in sensor network,” *IEEE Transcations on Parallel and Distributed Systems*, vol. 15, no. 11, pp. 961–974, 2004.

[88] L. Doherty and L. ElGhaoui, “Convex position estimation in wireless sensor networks,” in *IEEE Annual Joint Conference of Computer and Communication Societies (INFOCOM)*, pp. 1655–1663, 2001.

[89] Z. Shen, A. Athalye, and P. Djuric, “Phase cancellation in backscatter-based tag-to-tag communication systems,” *IEEE Internet of Things Journal*, vol. PP, no. 99, pp. 1–10, 2016.

[90] K. Langendoen and N. Reijers, “Distributed localization in wireless sensor networks: a quantitative comparison,” *Computer Networks*, vol. 43, no. 4, pp. 499–518, 2003.

[91] H. Niu and S. Jagannathan, “A cross layer routing scheme for passive RFID tag-to-tag communication,” in *IEEE Conference on Local Computer Networks (LCN)*, pp. 438–441, September 2014.

[92] M. Buettner, *Backscatter protocols and energy-efficient computing for RF-powered devices.* PhD thesis, University of Washington (UW Seatle), Seatle, USA, 2012.

[93] S. Thomas and M. S. Reynolds, “QAM backscatter for passive UHF RFID tags,” in *IEEE International Conference on RFID (RFID)*, pp. 210–214, 2010.

Appendix A

The PASS Simulation Framework

Figure A.1 shows the signal flow implemented in the simulator, which reflects the communication between reader and tag, reader and ST, as well as tag and ST. The PASS framework supports multiple readers, tags and STs. Each reader, tag and ST interfaces with the channel.

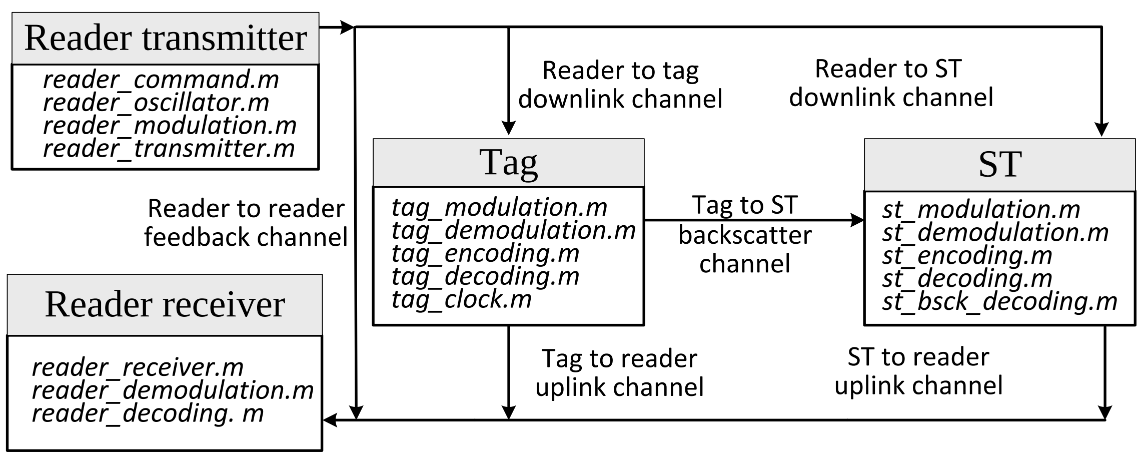

Figure A.1: Signal flow and component model graph for the simulator

A.1 Component models

(1) Reader model

The reader in PASS simulation framework is a generic powerful device, with impressive analog and digital processing capabilities. The model of reader does not reflect any specific types of readers.

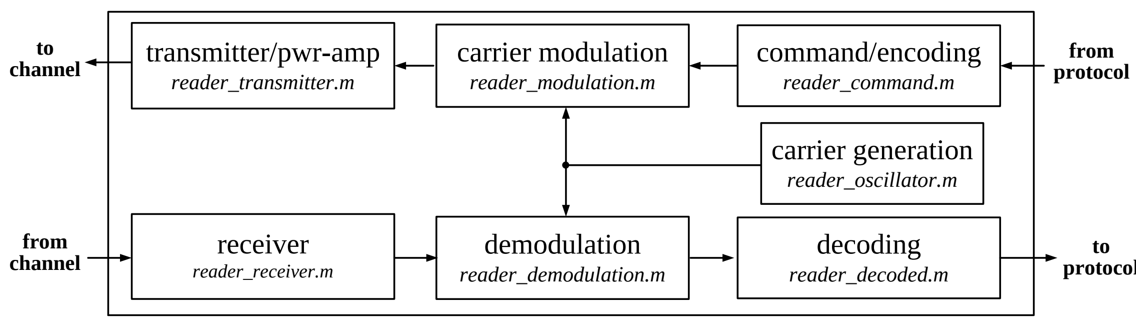

Figure A.2: Basic structure and functions of reader model

The main reader function, *reader_main.m*, provides an interpreter interface to control the functions in Figure A.2. The reader structure implements a standard communication transceiver. Fist a command/encoding block *reader_command.m* encodes the query command and then send to the carrier modulator *reader_modulation.m*, which in turn modulates the carrier signal provided by carrier generation block *reader_oscillator.m*. The modulated signal is fed into the transmitter *reader_transmitter.m*, through which it enters into the channel. The receiving path includes receiver *reader_receiver.m*, I/Q demodulator *reader_demodulation.m*, and decoding block *reader_decoding.m*.

(2) Tag model

In the PASS simulation framework the tag model is based on a NXP UCODE G2XM passive UHF RFID tag. The structure of tag model is shown in Figure A.3.

On the transmitting path, the encoding block *tag_encoding.m* sends the encoded data to the backscatter modulator *tag_modulation.m*. On the receiving path the imping wireless signal is send over the backscatter modulator *tag_modulation.m* to determine the portion of reflection and absorbtion by the tag's modulator circuity. And according to the absorbed imping power tag calculates whether the on-board is powered up. Subsequently, the signal is sent to the demodulator block *tag_demodulation.m*. Finally, it is decoded in the *tag_decoding.m*.

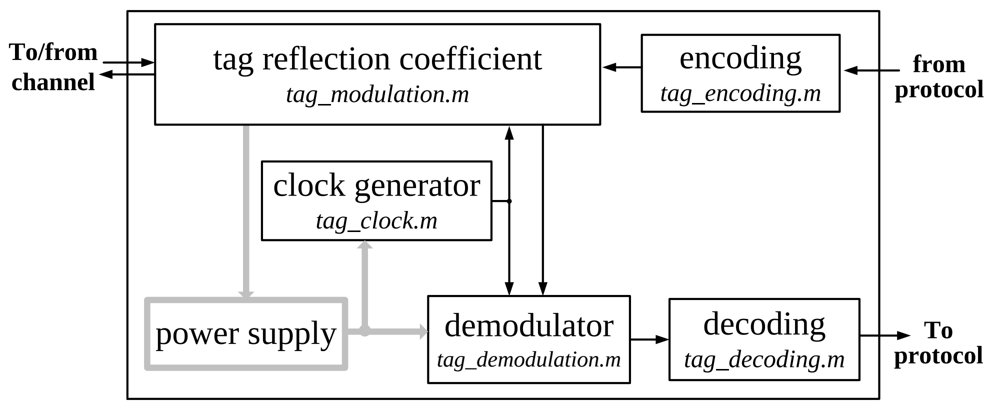

Figure A.3: The structure and functions of tag

(3) ST model

The ST model is designed to emulate the specific ST device. The basic structure and functions of ST is shown in Figure A.4.

The reflection coefficients of ST is determinant for communication process modelling, since it is the physical parameter bridging ST with tag and reader. The reflection coefficient is frequency-dependent highly non-linear and time-variant, which is provided by *st_modulation.m*. On the receiving side some portion of incident signal is captured by the antenna and RF front end of ST according to the reflection coefficient over frequency and power level of the incident signal. Afterward, the captured signal

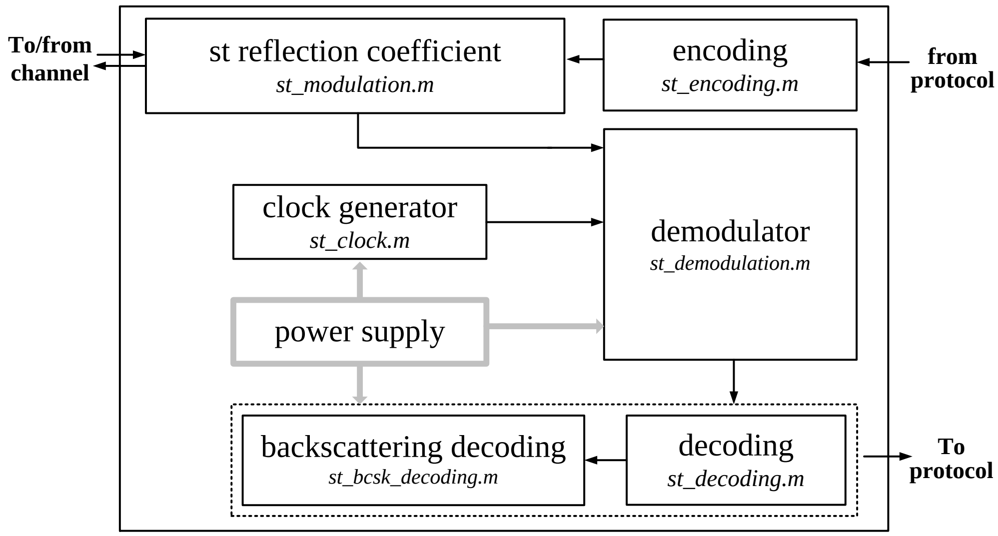

Figure A.4: The structure and functions of ST

is amplitude-demodulated by the envelope detector and resampled to the ST clock by the demodulator block *st_demodulation.m*. Decoding block for reader's command signal is implemented in *st_bcsk_decoding.m*. The backscatter decoding block obtains certain parameters of tag's backscattering modulation from the decoding block. Both of the blocks strictly comply with ISO 18000-6C. On the transmitting side the encoding block *st_encoding.m* sends the encoded data directly to modulate the ST's reflection state in *st_modulation.m*. The locator protocol of ST is provided in the behavior description script, where the *Listening* and *Responding* query rounds are performed.

(4) Channel model

The channel model of PASS simulation framework is optimized for UHF RFID-typical application. The structure and functions of channel model are shown in Figure A.5. This model combines large-scale path loss, antenna gain pattern, a deterministic small-scale model consisting of surfaces and virtual transmitters, and a stochastic small-scale model.

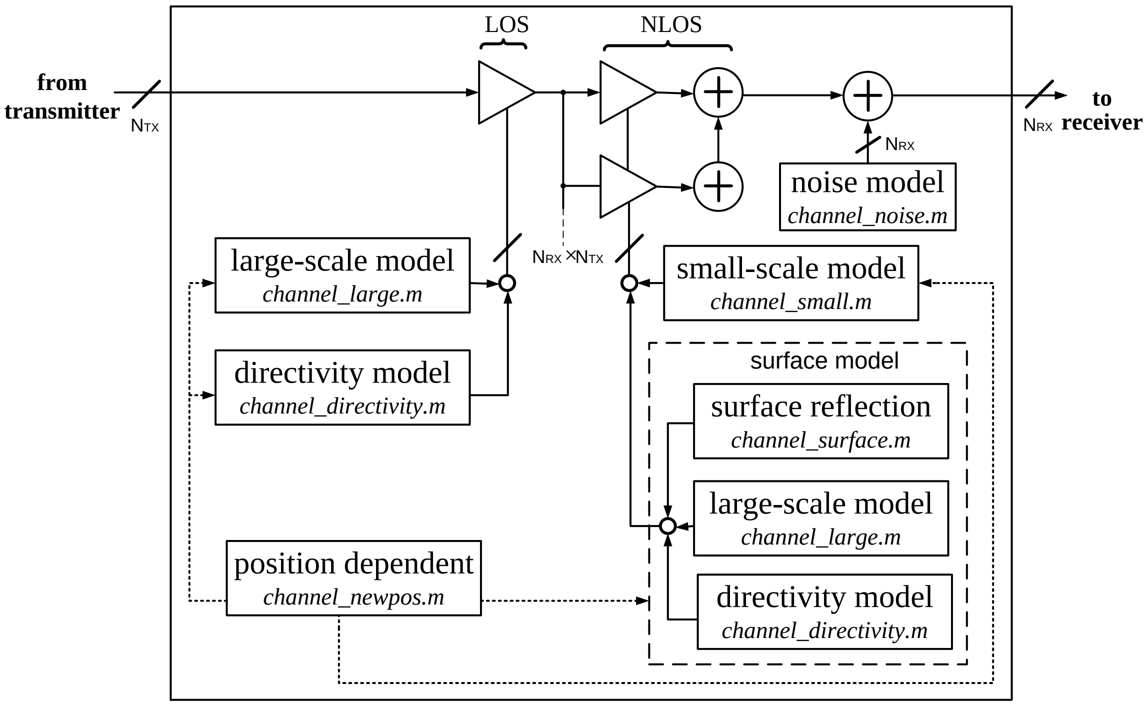

Figure A.5: The structure and functions of channel model

In PASS simulation framework the channel model does not provide a script interface, but merely calculate the output signal for the given input signals and channel settings. The model can handle arbitrary number of transmitters and receivers, N_{TX} and N_{RX}. The channel impulse response between a transmitter and a receiver is formed by a piecewise assembly fashion. The LoS component is created by large-scale propagation model *channel_large.m* and transmission again *channel_directivity.* The LoS component power gain is calculated via Friis equation (log-distance model) and transmission gain using lookup table. The large-scale propagation delay is calculated based on the speed of light and sampling frequency.

The NLoS part of the channel impulse response is created by deterministic reflection in surfaces and a stochastic small-scale model. The virtual transmitters are employed to model reflection from surfaces. The virtual transmitters are created by mirroring the transmitters by surfaces. Like normal transmitters, the channel between the virtual transmitter and the receiver contains a "direct" path (*channel_large.m*, *channel_directivity.m*), a stochastic small-scale part, as well as reflections in surfaces *channel_surface.m*. The stochastic small-scale components are created by *channel_small* implementing via a sampled version of an exponentially decaying short-range indoor wireless average power-delay-profile (APDP).

Position-dependent model *channel_newpos.m* provides the geometric setting, such as distance, directivity pattern angle, distance-dependent small-scale parameters, etc. The background noise is modeled as additive Gaussian noise (AWGN) *channel_noise.m*.

A detail description of tag backscatter modulator and channel model can be found in [61].